University of Camerino
International School of Advanced Studies

Ph.D. course in Chemical and Pharmaceutical Sciences and Biotechnology

Curriculum in Pharmaceutical, Nutraceutical and Food Sciences
XXXVI cycle

Advancements In Excipient Characterization For The Optimization of Oral Solid Dosage Forms: From Characterization To Formulation.

Doctoral Thesis

Ph.D. Candidate

Beatrice Sabbatini

Supervisors

Prof. Giulia Bonacucina

Prof. Marco Cespi

AA.YY. 2020/2024

Table of Contents

1. Introduction on Oral Solid Dosage (OSD) forms

Oral solid dosage (OSD) forms are the most widely used forms to deliver pharmaceuticals. In the 2010-2019 decade, the oral administration represented the dominant route among the New Molecular Entities (NMEs) approved by Food and Drug Administration (FDA) [1]. According to the recently published report of FDA's new drug approvals in 2023, 55 drugs were authorized for the market and, among these, 24 drugs required an oral administration (44%); the remaining part was represented by other administration routes (intravenous, pulmonary, ocular and topical) [2]. In particular, Tablets represented the 27% of all new drugs approved, followed by capsules (13%) with a total percentage of OSD of almost 40% only in 2023's new drugs approved. Therefore, this report confirms the primary role that oral solid dosage (OSD) forms still play in the pharmaceutical industry. Despite minor fluctuations over the last few years, OSD remains the primary formulation choice.

OSD forms have several advantages in terms of cost-effectiveness, convenience of manufacturing, well-established production processes, ease of administration and high compliance among patients. Their chemical and physical stability is enhanced by the solid-state form and also storage and transport are simpler than that of other dosage forms. In essence, the advantages of OSDs provide a strong impetus to their market, encouraging continued and increased usage. Estimates suggest that the profits generated with OSDs will reach 1.03 trillion USD in 2032, compared to the current 524.6 billion. [3].

OSDs include tablets, capsule, powders, granules and most of these are also easily handled to obtain controlled release pharmaceutical forms (i.e., enteric coated capsules and tablets). Besides these, new formulations approved by FDA could offer significant advances in the OSD field, such as chewable tablets and capsules [2] or fast dissolving tablets [4], both suitable for paediatric, dysphagic and bed-ridden patients.

OSDs are commonly well accepted by patients, but there are some categories of them to which a solid oral therapy cannot be prescribed and administered, specifically the paediatric population, patients who are in a state of unconsciousness and dysphagic patients. Regarding the first, despite an increasing interest about the paediatric drugs and appropriate formulations, there is still a lack of age-appropriate medications in the market [5]. To solve this problem, manipulation of the medicines has become a common practice,

together with the tailored formulation of paediatric drugs in galenic laboratories. New formulations approved to overcome this problem have been developed, such as oral-soluble tablets, oral films and sublingual dosage forms [5], but there is still room for improvement to guarantee an appropriate therapy for these patients. These improvements would as well be suitable for dysphagic patients, a group of population affected by difficulties or inability in swallowing. This is not a marginal issue because it is estimated that the incidence of dysphagia in patients over 65 years old ranges from 7% to 13% [6] and this number is expected to increase with the awaited increase of the average lifespan. Caregivers of dysphagic patients are often in need of a proper formulation that could be administered to them and, as a result of the lack of appropriate dosage forms, they manipulate the drugs in order to obtain a suitable dosage form. These manipulations include the solubilization of tablets, opening of capsules and tablet splitting. However, this process is not only risky because it is an "off-label" use of the medicine, but the splitting of medicines that were originally in the form of capsules or tablets has been correlated to the appearance of adverse effects [7]. Hopefully, in the next future more efforts will be taken to guarantee age-appropriate formulations available in the market.

The formulation of an OSD form presents several challenges to the formulation scientists, first of all the choice of the excipients. The excipients in a formulation could have different roles, for instance they could be necessary to carry out the production without process disruptions or they could just have an aesthetic role. While the former role may seem the most important aspect of the manufacturing process, the aesthetic role also plays a fundamental role in patients' compliance. In fact, several studies demonstrated that different colours help in the identification of the products, especially for patients in polytherapy, and it was also demonstrated how the colour has a psychological impact [8]. Amawi and Murdoch [9] proved that the colour of the pills has a notable impact on the efficacy perceived by patients and they also showed how different colours are more impactful for a disease than another. For instance, the blue and white was the most chosen among patients in need for a sedative medicine, red pills were the most chosen among stimulants and both yellow and red were the most chosen for the hallucinogenic category. Table 1 displays some of the widely used classes of excipients for OSDs, together with a few examples for each class and their role in the formulation [10] [11].

Table 1 List of the classes of excipients commonly used in OSD formulations.

Class	Examples	Amount (%)	Role
Diluents	Lactose, MCC, Dibasic Calcium Phosphate, Sorbitol, starches for DC	10-90	To make up an adequate mass to produce the pharmaceutical form
Lubricants	Magnesium Stearate, talc, Sodium Stearyl Fumarate	1-5	To reduce the friction between the materials and the tools used to manufacture (e.g., die wall and punches)
Disintegrant / Superdisintegrant	Croscarmellose Sodium, Sodium starch glycolate	0.5-2	To facilitate the disintegration of the OSD once it is in contact with the body fluids
Binders	PVP, Carboxymethyl cellulose, starch	-	To give cohesive qualities to the formulation
Glidants	Silica, corn starch	3-10	To improve the blend's flowability
Sweeteners	Saccharin, Mannitol	-	To convey a sweet taste (e.g., to mask unpleasant tastes of chewable tablets)
Colourants	Ferric oxide	-	To impart a colour to the dosage forms, helping the product identification
Coating materials	HPMC, synthetic polymers (Eudragit®), ethyl cellulose	-	To protect the OSD from humidity, mask unpleasant tastes, control the drug release
Plasticizers	Diethyl phthalate, glycerine, polyethylene glycol	-	To convey elasticity, resistance and flexibility to the coating materials
Wetting agents	Sodium Lauryl Sulphate (or other surfactants)	-	To promote the interaction of between hydrophobic solids and water, reducing the interfacial tension

In this chapter, OSD forms will be discussed both from a technological and formulative point of view, to explain the process robustness and the challenges that the formulator has to face in the daily practice. First, a general introduction to the manufacturing methods of tablets will be provided, followed by an overview of the properties of bulk solids that

directly influence the formulation and selection of manufacturing methods. Moreover, a general introduction on the OSDs (mainly tablets and capsules) coating will be reported.

2. Tablets: manufacturing and formulation challenges

Tablets are the most popular drug delivery systems among all the pharmaceutical forms. They are usually made through the compression of a mixture containing the Active Pharmaceutical Ingredient (API) and one or more excipients, which are materials that are required to manufacture the tablets but with no therapeutical effect. Even if the most common way to obtain a tablet is by compression, the selection of the most appropriate manufacturing process to employ is non-trivial and requires good knowledges of OSD formulation and a complete characterization of the tablet's components [12]. The production process usually involves the use of a tableting machine, even though in the last years other methods have been developed (e.g., 3D-Printed tablets). There are three main processes to produce tablets:

- Direct compression (DC)
- Wet Granulation (WG)
- Dry Granulation (DG).

Direct Compression represents the simplest type of compression process in which the API-excipient mixture undergoes direct compression, without further handling. DC needs some requirements that the mixture must meet, such as an appropriate flowability and tabletability of the materials. The mixture must flow enough to go through the tableting machine parts, fill the die properly ensuring a reproducible weight and content in the tablets and it must have appropriate mechanical features that allow the formation of the tablets.

If the materials have insufficient flow, it is possible to enhance this property by adding some excipients in the formulation, such as silica, which is one of the most used glidants. On the other hand, if the materials don't meet the compressibility requirements in terms of physical and mechanical properties, the WG or DG should be performed in order to obtain an optimized material to be compressed.

Wet granulation (WG) is a bottom-up process that allows the conversion of powdered materials into granules with an improved flowability, as a result of the bigger particle size and more spherical morphology of the granules. This process requires expensive equipments and more excipients for the technological operations, it's a longer and more costly process and it's also unsuitable for several materials (e.g., water-sensitive

materials). The WG is commonly performed using the high shear granulator, the fluidized bed or a microwave dryer.

WG has several advantages: higher content uniformity for low dosage drugs, better mechanical properties of the tablets (higher tensile strenght) and lower friability of the granules (mainly due to the binder added in the formulation).

Similarly to WG, the Dry Granulation (DG) is a process that generates granules from powders, with the exception that this is achieved without the addition of solvents. Granules are commonly obtained by roller compaction of the powders and then by fragmentation of the obtained ribbons. The granules produced through this process have better flow and compaction properties than the original powders but they are less performant than the granules obtained via WG, because they are less round-shaped and more friable. Despite this, modern continuous roller compactors require less steps and are less expensive than the WG process.

The choice of the compression process depends on the powder's characteristics, such as their flowability and tabletability. For this reason, an in-depth discussion of these properties is provided in the following paragraphs, since they directly affect the final product.

2.1 Flowability

Flowability of materials is a fundamental parameter to study since this property is not only interesting for the pharmaceutical industry, but also in many other fields, such as the food processing, the manufacturing and building industry.

In general, flowability is described as the ability of a material to flow under gravity or external forces, but this simple definition does not embrace the complexity of this property. In fact, Prescott and Barnum proposed a more complex definition stating that flowability is “a multidimensional problem that is the result of the combination of material physical properties and the equipment used for handling, storing, and/or processing the material” [13]. Flowability is affected by many fundamental and derived bulk solid properties, such as density, particle size distribution (PSD), morphology, moisture content and electrostatic interaction. These properties affect the flow behavior of bulk solids in various ways, and the extent of each one's contribution to altering the flow is still partially unknown. As said before, flowability is one of the main parameters that have a crucial influence on the quality of a tablet. Regarding the compression process, an appropriate flowability is necessary to achieve a homogeneous filling of the die [14]

and subsequent content uniformity. This is primary requirement that is necessary to meet the quality standard set by regulatory agencies.

Bulk solids, such as powders, granules and pellets exhibit unique flow characteristics that differ significantly from those of liquids or gases, since they possess solid-like properties, including cohesion, friction, and interparticle forces, which influence their flow behaviour. These characteristics can give rise to challenges such as bridging, arching, ratholing, segregation, and erratic flow, which can impede material flow and disrupt production processes. Thus, the characterization of the flowability is a mandatory analysis to be performed in order to run a DC trial.

Understanding the interplay between the factors that affects flowability is crucial in designing equipment, storage silos, and handling systems that promote reliable and efficient flow.

Some authors do not consider flowability as an inherent material property of powders, as it is influenced by many other powder characteristics and physical properties [13]. Although many efforts, there is a clear statement in literature about flowability: it can't be adequately described by a single measurement or instrument.

Flowability is directly affected by numerous powder properties that will be now listed, in order to better understand the theoretical foundation on which the present project is based.

- *Particle size distribution (PSD)* allows the formulator to understand the size distribution of particles in the bulk solid. PSD is not a single value, but it describes a frequency distribution. Typically, the full distribution is presented to describe the PSD of a powder population. Alternatively, to simplify the presentation of data, D10 (i.e., 10% of the particles have a particle size smaller than this value), D50 and D90 (50% and 90% of the particles have a particle size smaller than these values, respectively) are presented and/or the 'SPAN', which is the measure of how widely spread is the distribution of the particle size. It is well-known that bulk solids composed by small size particles are poorly flowing because of the higher surface energy, while a coarser powder flows better.
- *Bulk (BD) and Tapped density (TD)* are fundamental parameters to be considered when studying flowability of powders. The BD is the ratio of the mass (g) over the volume (mL) occupied by the powder poured into a graduated cylinder; the TD is evaluated by measuring again the volume after a certain number of tapping. Knowing BD and TD also allows to calculate two of the most easily measurable

flow indexes, Hausner Ratio (HR) and Carr's Index, with the following equations (1) and (2), respectively.

Eq. 1 $$HR = \frac{\rho \text{ tapped}}{\rho \text{ bulk}}$$

Eq. 2 $$Carr's\ Index = \left(\frac{\rho \text{ tapped} - \rho \text{ bulk}}{\rho \text{ tapped}}\right) x\ 100$$

- *Particle shape* strongly affects powder's flow: the more irregular the particles, the poorer will be the flow. This is because with higher surface roughness or irregular shape, the particles tend to reduce the flow on each other's surface, and this results in a poorer flowability.
- *Moisture content* can increase the interparticle adhesive forces, resulting in a decreased flowability because of the formation of liquid bridges between particles.

An additional challenge, beside the difficulty in defining flowability, is measuring it. We should consider the flowability as a multidimensional property that could be imagined as a 3D-shaped object. There are several methods available to estimate the flowability of a bulk solid, some of them can define one or more sides but none of them gives a comprehensive description of the flowability.

Angle of Repose (AOR), Hausner Ratio (HR) and Carr's Index (CI), Flow rate through an orifice and shear cell measurement are the most commonly used methods to estimate the flowability of bulk solids. Among these methods, some consider the so-called static flow and some others the dynamic flow. The choice of the best flow indicator is then made based on the aim of the project. The static flow is defined as the behaviour of bulk solids at rest or in a stationary phase. Here the particles are in equilibrium and the flow properties are mainly affected by the interparticle cohesion and friction. On the contrary, the dynamic flow it's described as the movement of bulk solids under external forces, such as gravity, shear forces or others. This kind of flow is influenced mostly by the wall friction, the interparticle cohesion, the material and the shape of the equipment that contains the bulk solid.

The widely used flow indexes and their flow classification scale will be now briefly described in order to have a general overview of all the existing methods to evaluate the flow of bulk solids:

- The determination of the **angle of repose** is an experiment based on the powder's resistance to movement between the particles. It is the angle formed between a

platform and the cone of powder that flows from a hopper through a flask. The higher the cone of powder (resulting in a higher angle of repose), the lower the flowability. This is a simple and significative test, however it is also highly dependent on the testing conditions and the operator who runs the experiment, so it's not considered a robust flow indicator [15]. In addition, highly cohesive materials do not generate a regular cone, so that the measurement is inaccurate.

- **Hausner Ratio** and **Carr's Index** are both calculated from bulk and tapped density and they're considered as predictors of powder's flowability more than a flow measurement [16]. HR and CI are measurements of the static flow, so they mostly consider the interparticle interactions, neglecting almost completely the dynamic of bulk solids' movement. Therefore, they're usually coupled with other flow descriptor, in order to obtain a better understanding of the bulk solid's flow properties. The scale of flowability according to the Hausner Ratio and Carr's index is reported in Table 2, together with the angle of repose classification:

Table 2 Flowability classification based on the measurement of the Angle of Repose, Carr's Index and Hausner Ratio [from Agarwal et al. http://dx.doi.org/10.26717/BJSTR.2018.05.001237].

Angle of Repose	Carr's Index	Hausner's Ratio	Flow Properties
25-30	<10	1.00-1.11	Excellent
31-35	11-15	1.12-1.18	Good
36-40	16-20	1.19-1.25	Fair
41-45	21-25	1.26-1.34	Passable
46-55	26-31	1.35-1.45	Poor
56-65	32-37	1.46-1.59	Very Poor
>66	>38	>1.60	Very Very Poor

- The **Mass Flow (MF) through an orifice**, measured with the GranuFlow, is one of the most significant dynamic flow indicators when considering a direct compression (DC) process perspective. It is considered as the measurement of dynamic flow because in this test the powder flows through orifices of different diameters and the mass over time is automatically registered thanks to a balance connected to a computer. Several pharmaceutical processes utilize gravimetric filling, such as matrix filling during the tabletting process. That's why this measurement is highly significant in describing the powder's flow. The outcome of this test is a measure of MF expressed in mass over seconds and the result of the subsequent measurement at different orifices diameter is represented as a curve which equation is described by the Beverloo law (eq. 3):

Eq. 3 $$F\ (D) = F\min + C\ (\sqrt{g}\ (D - D\ min)$$

Unfortunately, the major weakness of the GranuFlow is that it's possible to perform the test only for medium to free-flowing bulk solids because poorly flowing and very cohesive powders won't flow through, even when using orifices up to 28mm.

- The **shear cell measurement** is probably the most used to describe the flowability of bulk solids. With this instrument several analyses can be performed, in particular the Wall friction and the Flow Function Coefficient (ffc) [17]. During the ffc measurement, the powder is poured into the cell and it is consolidated under a certain stress (e.g., 4kPa); this phase is called 'preshear phase'. Subsequently, a shear force is applied to the sample to a point at which the powder starts flowing (yield limit). This is the 'shear to failure phase' (fig. 1).

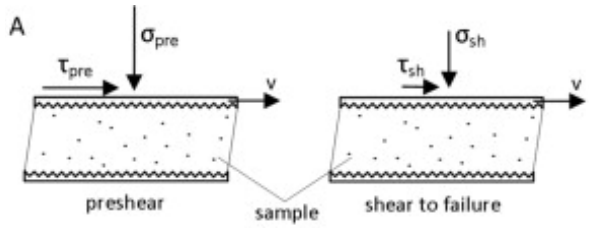

Figure 1 Phases of the flow function coefficient with the Schulze shear cell.

Ffc is the ratio of the consolidation pressure (σ_1) to the unconfined yield strength (σ_c):

Eq. 4 $$ffc = \frac{Consolidation\ pressure(\sigma 1)}{Unconfined\ yield\ strenght\ (\sigma c)}$$

Jenike proposed a classification of powder flow based on ffc and it is here reported (fig. 2):

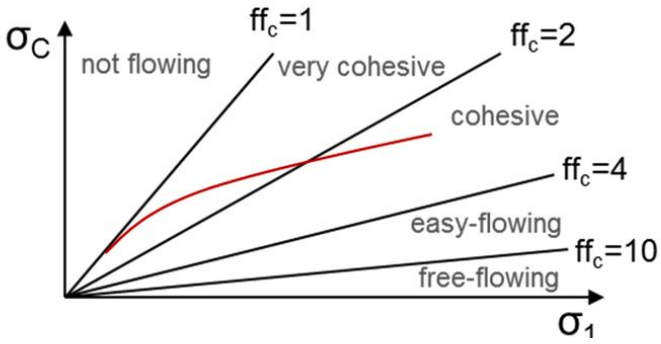

Figure 2 Classification of ffc from 0 to 10, according to Jenike.

This experiment is likely the most generally accepted as measurement of bulk solids' flowability even if it has some downsides. The measurement requires quite long times, quite a waste of material and the classification only comprehends values from

0 to 10 and excludes higher values of ffc. However, this does not represent a huge limitation, because bulk solids with an ffc higher than 10 don't represent a formulation challenge, at least not for processes in which flowability is a critical parameter. Moreover, the test is dependent on the operator, since the preparation of the sample should be done carefully and always following the same procedure.

As previously mentioned, it is essential to estimate the flowability of the formulation before tablet manufacturing to prevent process interruptions and ensure adequate quality of the final product. However, there is currently no pre-determined protocol to determine which method is more suitable to characterize flowability. In order to choose a proper measurement, the formulator should evaluate what is the aim of the analysis and which kind of flow (static or dynamic) is involved in the process. For example, if the flowability measurement has to be done as a preliminary analysis to run a direct compression process, the use of a dynamic flow index such as the HR/CI and the MF through an orifice would be recommended because they simulate the process of die filling during the DC. Undoubtedly, the choice of the method to use is also dependent on the bulk solid features because some flow indexes may have limitations in measuring the flowability of cohesive powders (e.g., GranuFlow), or they couldn't be able to discriminate among samples with very good flow properties.

In case of insufficient flowability, there are different potential solutions, such as including one or more materials with good flow properties in the formulation, so that they could compensate the poor flowability that quite always the APIs have. In this regard, there are currently several grades of fillers (e.g., lactose, microcrystalline cellulose, dibasic calcium phosphate) that undergo physical modifications and agglomeration that give these excipients improved flow properties. To provide an example, lactose is one of the most widely used filler for the formulation of tablets and even if the milled lactose is the cheapest grade, it doesn't offer exceptional properties in terms of flow and compression. This is because its properties are not entirely suitable for a direct compression process. Therefore, most excipient industries that supply lactose for direct compression have developed other grades, particularly granulated or spray-dried lactose, which are more suitable for this purpose (e.g., SuperTab® 30GR or SuperTab® 11SD respectively, both manufactured by DFE Pharma, DE). These grades consist of coarser, more spherical particles, which proved to be more functional in direct compression [18]. Furthermore, their high porosity could also be helpful to obtain a better blending of different powders.

Another useful approach to improve the formulation's flowability could be the use of glidants, a class of excipients that reduces the cohesive forces among the material's particles in order to improve their flowability [19]. Several glidants are available on the market, in particular the most used are colloidal silicon dioxide, starch and talc.
In essence, flowability of bulk solids is a property that severely affects most of the pharmaceutical manufacturing processes used to produce OSDs. The optimization of a formulation in terms of flowability is a fundamental step in the manufacturing process. This ensures the production of high good quality products in a timely and cost-effective manner.

2.2 Tabletability

Tabletability is one of the material's fundamental properties that affect the manufacturing of tablets, together with the aforementioned flowability. Tabletability is defined as the ability of a material to form a tablet at a given compaction force. The excipients intended for compression should be evaluated based on their physical and mechanical properties and in particular it is necessary to study their mechanism of deformation when a certain pression in applied, same as it happens during the compression process.
There are different ways in which a material can be deformed under pressure:

- Elastic deformation: it is a reversible deformation in which the material deforms under pression but when it is unloaded it returns to the original condition, without a permanent modification.
- Plastic deformation: it is an irreversible deformation. Once applied the load, the material is subjected to elastic deformation (with the unloading, the sample could still return to the original state) and at higher stress the deformation of the material becomes irreversible, plastic.

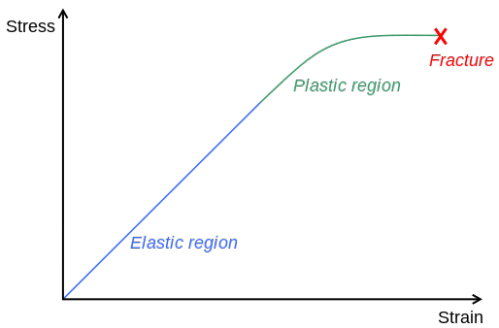

Figure 3 *Diagram of the deformation regions of a ductile material where the stress represents the force applied and the stain represents the deformation.*

- Fragmentation: for some materials (such as lactose) as the force is applied to the sample, it undergoes a fragmentation and rearrangement of the particles.

To provide an example, the mechanism of deformation for lactose has been studied by Shi et al. and the results showed how lactose particles, as brittle material, undergo fragmentation and consolidation at a certain applied force (fig. 3). This deformation results in a reduced mechanical strenght of lactose tablets, hence why it is frequently used a mixture of lactose and MCC as filler for tablets in DC. This combination ensures that MCC's plastic behavior compensates for the brittle properties of lactose, and the good flowability of lactose can counteract the poor flow of MCC [20].

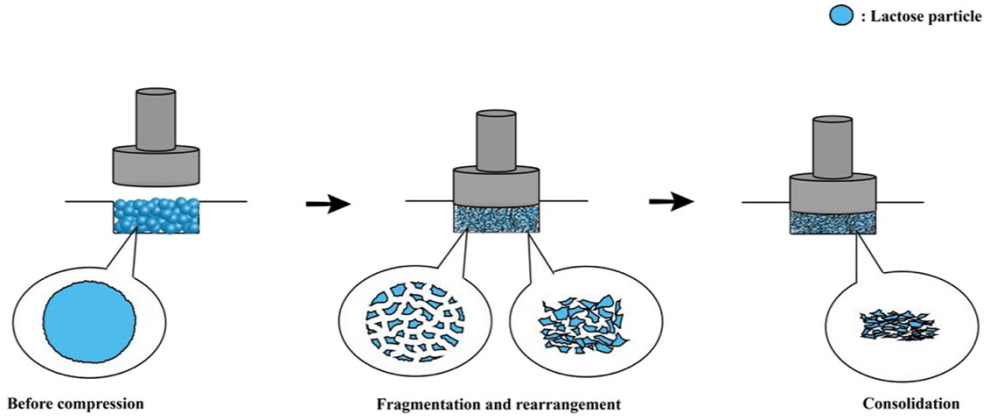

Figure 4 Mechanism of deformation of Lactose particles [20]

The tabletability of a material is usually determined by manufacturing tablets with an increasing compaction force and performing a full characterization of them. For each tablet the calculation of the Tensile Strength is necessary to study the material's tabletability. The Tensile Strength (TS) is defined as the maximum force or external stress applied, beyond which a material loses its resistance and it is calculated as follows (eq. 5) [21][22]:

Eq. 5 $$TS = \frac{2 \cdot Hardness}{\pi \cdot Thickness \cdot Diameter}$$

By plotting the TS (MPa) over the Compaction Pressure (MPa) it is possible to obtain the graphical representation of the material's tabletability. This plot is particularly noteworthy when two materials must be compared based on their tabletability, as showed in Fig. 5. MCC is commonly used to demonstrate how to estimate the tabletability of materials, hence why the comparison of this material with others (e.g., lactose) will be shown in this section.

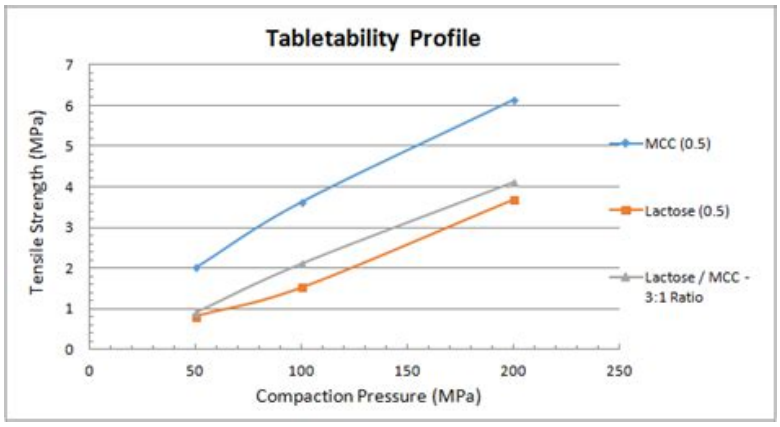

Figure 5 Comparison of the tabletability profile for Lactose, MCC and a binary mixture of Lactose-MCC

The material's tabletability increases with the steepness of the curve, that's because less compaction pressure is required to obtain tablets with higher mechanical strength.

Tabletability and compactability are related properties and sometimes they are both evaluated during the characterization of a material intended for DC, but they are not synonymous. In fact, compactability is graphically represented by the plot of the TS (MPa) over the tablet's Solid Fraction (SF), as shown in Fig. 6. The SF describes how much of the tablet's volume corresponds to solid material and it is calculated as follows (Eq. 6):

Eq. 6 $$Solid\ Fraction = \frac{Tablet\ Density}{True\ Density}$$

where the tablet density can be measured using its weight and volume.

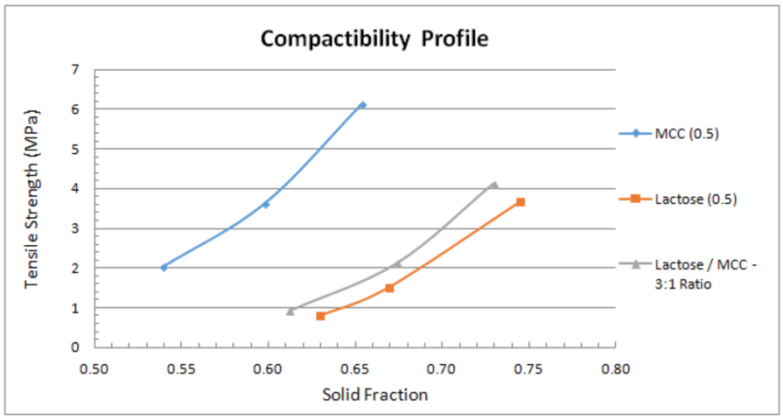

Figure 6 Comparison of the compactability profile for Lactose, MCC and a binary mixture of Lactose and MCC

MCC has the best tabletability and it maintains the primacy even in the compactability profile, despite the lowest solid fraction among the tested samples.

The analysis of the compression properties for the active pharmaceutical ingredients (APIs) and excipients used in tablet formulation is crucial for the formulator. It provides insight into the mechanical properties of these materials, upon which the tablet formulation will be developed. There are some classes of excipients useful to enhance the

mechanical strength of materials that originally provide poor tabletability. Binders represent a class of excipients used to improve the cohesion of the blend's particles in tablets and they operate at low level addition. Moreover, filler-binders have been developed in the last decades in order to promote the use of DC instead of facing longer and more expensive processes with granulation. The final aim should be to prepare a mixture of API with a filler-binder, a disintegrant, a lubricant and manufacture it into tablets [23]. By definition, they have good properties in terms of flowability and tabletability and, to provide an example, MCC is widely used in DC because it has all the features necessary to serve as tablet matrix and as particles binder. Another solution to poor tabletability is offered by the DC grade excipients. These excipients undergo physical transformations to achieve good flow and compression properties, enabling their inclusion in direct compression (DC) formulations. The processes they undergo are usually a modification of the size and shape, often by granulation or spray-drying. By using these methods, the material obtained will have a coarser size (improved flowability) and the compactability of the agglomerates will be higher than that of the original crystals. In addition to these examples, a supplementary class of excipients that has been developed more recently (in the late 1980s) is represented by the co-processed materials. It was found that a material composed by two different starting materials had boosted properties than the simple blending of them. A very common association is that of Lactose with MCC because, when combined together, these materials offer a synergistic effect that results in an exceptional excipient for DC (e.g., MicroceLac® 100 manufactured by Meggle) [20]. Not only fillers and binders are processed together, but also fillers and lubricants; an example of this combination is LubriTose™ SD, which is a combination of spray-dried lactose (96%) and Glyceryl Monostearate (4%). In this co-processed the addition of glyceryl monostearate as a lubricant is a possible solution to the well-known high ejection force caused by the use of lactose in DC.

2.3 OSDs film coating

Among various processes for tablets manufacturing, film coating of a tablet or a capsule is a widely employed process that could have an aesthetic or a functional role in the final pharmaceutical form. Different coatings methods are available, notably sugar coating, film coating and press coating, however the most widely used is the film coating, also thanks to the advancement in the development of polymers with suitable properties to

obtain a film with the required features [24]. The reasons to perform a film coating are the more various and will be briefly discussed:

- *Masking unpleasant taste and odour*: in some cases, APIs may have a bitter taste or unpleasant odour, so that a film coating act as a barrier to make the dosage form more palatable, therefore increasing the patient's compliance.
- *Protecting the API*: some active ingredients (e.g., peptides) are not stable at very low pH so these would be chemically damaged during the transit of the pharmaceutical form in the stomach, especially in a fasted state where the pH is expected to be approximately 1.5.
- *Stomach protection*: some APIs (e.g., NSAIDs) contemplate among their side effects the stomach bleeding and ulceration. The use of a film coating is one of the possible solutions because, by preventing the disintegration of the OSD in the stomach, the side effect is also prevented.
- *Enhancing the stability*: some pharmaceutical excipients and APIs may be unstable at certain conditions of temperature, humidity and light, so the coating could improve their stability by shielding the OSD from the environmental factors.
- *Reducing the interactions*: the film coating may be useful to separate the incompatible components (e.g., API and excipient) within a formulation, minimizing potential interactions that could affect the stability or efficacy of the product.
- *Controlled release*: if there is the necessity to control the API release, a film coating with appropriate polymers is the optimal choice. There are several polymers available in the market to achieve a controlled release, such as polymers with a pH-dependent dissolution (e.g., Eudragit® S) or polymers that undergo a slowly erosion so the disintegration and dissolution of the coated dosage form is slow and gradual (e.g., HPMC).
- *Improving the aesthetic*: the OSDs coating could have an aesthetic role, meaning that it is useful to give a colour to the tablet or mask unpleasant colours of the different component included in the formulation.

Film coating solutions or suspensions are composed by several excipients which are necessary in the formulation to obtain for the final film the desired properties and functionalities. The main components of a film coating formulation are:

1. *Film-forming polymers*: Hydroxypropyl methylcellulose (HPMC), Hydroxypropyl cellulose (HPC), Methacrylic acid copolymers (Eudragit®), Polyvinyl alcohol (PVA).
2. *Plasticizers*: The primary function is to enhance flexibility and elasticity, ensuring that the coating fits the tablet's shape without cracking. Plasticizers can also improve the adhesion of the film coating to the tablet surface. Some examples are Triethyl citrate (TEC), Polyethylene glycol (PEG) and Propylene glycol.
3. *Opacifying agents*: included in the formulation to provide opacity, enhancing the visual appearance of the dosage form and protecting light-sensitive active ingredients from degradation (some examples are Titanium dioxide and iron oxides).
4. *Colorants* (pigments approved by the regulatory agencies)
5. *Anti-adherents*: they inhibit the agglomeration of the substrate during the coating and drying phases (e.g., talc or glyceryl monostearate).
6. *Solvents*: they are required to prepare the coating solution/suspension. In the past organic solvents were frequently used (such as Isopropyl alcohol and Isopropanol) but nowadays their use is very limited and the use of water as solvent is preferred.

The film coating of tablets and capsules is a well optimized industrial process and there are two main categories of equipment used to run a coating procedure: the coating pan and the fluid bed system.

The conventional rotating pan method is the easiest and quickest because it involves introducing tablets into a rotating pan equipped with a spray nozzle, allowing the coating solution to be applied. During the rotation of the tablets, the coating solution is deposited on their entire surface, so that a uniform coating is obtained. Subsequently, a stream of hot air is used to allow the solvent to dry. Despite the simplicity of this methods, there are some drawbacks, such as cracking of the film during the drying phase, clogging of the nozzle with the coating suspension and roughness of the coated surface. To avoid these issues, a deep optimization of the process and its variables is required [25]. The conventional pan has also been modified during the last decades pushed by the evolution of formulations, in which the organic solvents have been gradually reduced because of the possible toxicity of their residues after drying. Therefore, perforated pans with optimized air flow were created to improve the solvent drying by adding several different small gaps in the drum that allow the air to flow through the tablets bed [26].

Fluid bed equipments consist of an airflow that moves in a cylindrical chamber the substrate to be coated and in the meantime the coating solution is sprayed from the top or from the bottom. The coated tablets gain weight and, thanks to the gravity, they fall on the bottom where the final forms are collected. By means of the airflow, the coating is regular and all the sides of the tablets are homogeneously covered by the sprayed solution and immediately dried. Several modifications have been made for this instrument, but there are some critical parameters that directly affect the final quality of the coating, such as the air flow, the coating solution droplets size, the position of the nozzle through which the solution is atomized and the atomization pressure.

References:

[1] D. G. Brown and H. J. Wobst, 'A Decade of FDA-Approved Drugs (2010–2019): Trends and Future Directions', *J. Med. Chem.*, vol. 64, no. 5, pp. 2312–2338, Mar. 2021, doi: 10.1021/acs.jmedchem.0c01516.

[2] FDA, 'New Drug Therapy Approvals 2023', 2023.

[3] Fact.MR, 'Oral Solid Dosage Pharmaceutical Market Outlook (2022-2032)', 2022. [Online]. Available: https://www.factmr.com/report/oral-solid-dosage-pharmaceutical-market

[4] S. K. Rada and A. Kumari, 'Fast dissolving tablets: waterless patient compliance dosage forms', *J. Drug Deliv. Ther.*, vol. 9, no. 1, pp. 303–317, Jan. 2019, doi: 10.22270/jddt.v9i1.2292.

[5] F. L. Lopez, T. B. Ernest, C. Tuleu, and M. O. Gul, 'Formulation approaches to pediatric oral drug delivery: benefits and limitations of current platforms', *Expert Opin. Drug Deliv.*, vol. 12, no. 11, pp. 1727–1740, Nov. 2015, doi: 10.1517/17425247.2015.1060218.

[6] K. Kawashima, Y. Motohashi, and I. Fujishima, 'Prevalence of Dysphagia Among Community-Dwelling Elderly Individuals as Estimated Using a Questionnaire for Dysphagia Screening', *Dysphagia*, vol. 19, no. 4, pp. 266–271, Nov. 2004, doi: 10.1007/s00455-004-0013-6.

[7] S. Logrippo *et al.*, 'Oral drug therapy in elderly with dysphagia: between a rock and a hard place!', *Clin. Interv. Aging*, vol. Volume 12, pp. 241–251, Jan. 2017, doi: 10.2147/CIA.S121905.

[8] K. Schapira, H. A. McClelland, N. R. Griffiths, and D. J. Newell, 'Study on the Effects of Tablet Colour in the Treatment of Anxiety States', *BMJ*, vol. 2, no. 5707, pp. 446–449, May 1970, doi: 10.1136/bmj.2.5707.446.

[9] R. M. Amawi and M. J. Murdoch, 'Understanding Color Associations and Their Effects on Expectations of Drugs' Efficacies', *Pharmacy*, vol. 10, no. 4, p. 82, Jul. 2022, doi: 10.3390/pharmacy10040082.

[10] M. Jivraj, L. G. Martini, and C. M. Thomson, 'An overview of the different excipients useful for the direct compression of tablets', *Pharm. Sci. Technol. Today*, vol. 3, no. 2, pp. 58–63, Feb. 2000, doi: 10.1016/S1461-5347(99)00237-0.

[11] S. P. Chaudhari and P. S. Patil, 'Pharmaceutical Excipients: a review', *Int. J. Adv. Pharm. Biol. Chem.*, vol. 1 (1), 2012.

[12] 'Modern Pharmaceutics, 1. Basic Principles and Systems', *DRUGS Pharm. Sci.*, vol. 188.

[13] J. Prescott and R. A. Barnum, ‘On powder flowability’, *Pharm. Technol.*, vol. 24, pp. 60–84, 2000.

[14] C.-Y. Wu, B. Armstrong, and N. Vlachos, ‘Characterization of Powder Flowability for Die Filling’, *Part. Sci. Technol.*, vol. 30, no. 4, pp. 378–389, Jul. 2012, doi: 10.1080/02726351.2011.588302.

[15] D. Geldart, E. C. Abdullah, A. Hassanpour, L. C. Nwoke, and I. Wouters, ‘Characterization of powder flowability using measurement of angle of repose’, *China Particuology*, vol. 4, no. 3–4, pp. 104–107, Jul. 2006, doi: 10.1016/S1672-2515(07)60247-4.

[16] Kevin MG Taylor and Michael E Aulton, ‘Aulton’s Pharmaceutics: The Design and Manufacture of Medicines’, *Elsevier Health Sciences*, 2021.

[17] D. Schulze, *Powders and Bulk Solids: Behavior, Characterization, Storage and Flow*. Cham: Springer International Publishing, 2021. doi: 10.1007/978-3-030-76720-4.

[18] G. Lumay, P. Janssen, and A. Neveu, ‘The flowability of lactose powders to optimise tableting processes’, 2020, [Online]. Available: https://dfepharma.com/media/edbluiyo/2020-odd_granutools-the-flowability-of-lactose-powders-to-optimise-tableting-processes-1.pdf

[19] L. L. Augsburger and S. W. Hoag, Eds., *Pharmaceutical dosage forms. Tablets*, 3rd ed. New York: Informa Healthcare USA, 2008.

[20] C. Shi, H. Zhao, Y. Fang, L. Shen, and L. Zhao, ‘Lactose in tablets: Functionality, critical material attributes, applications, modifications and co-processed excipients’, *Drug Discov. Today*, vol. 28, no. 9, p. 103696, Sep. 2023, doi: 10.1016/j.drudis.2023.103696.

[21] J. T. Fell and J. M. Newton, ‘Determination of Tablet Strength by the Diametral-Compression Test’, *J. Pharm. Sci.*, vol. 59, no. 5, pp. 688–691, May 1970, doi: 10.1002/jps.2600590523.

[22] F. Podczeck, ‘Methods for the practical determination of the mechanical strength of tablets—From empiricism to science’, *Int. J. Pharm.*, vol. 436, no. 1–2, pp. 214–232, Oct. 2012, doi: 10.1016/j.ijpharm.2012.06.059.

[23] B. A. C. Carlin, ‘Direct Compression and the Role of Filler-binders’, in *Pharmaceutical dosage forms - Tablets*, 3rd Edition., Informa Healthcare USA, 2008, p. 44.

[24] K.-S. Seo, R. Bajracharya, S. H. Lee, and H.-K. Han, ‘Pharmaceutical Application of Tablet Film Coating’, *Pharmaceutics*, vol. 12, no. 9, p. 853, Sep. 2020, doi: 10.3390/pharmaceutics12090853.

[25] W. Ketterhagen *et al.*, ‘Modeling tablet film-coating processes’, in *Predictive Modeling of Pharmaceutical Unit Operations*, Elsevier, 2017, pp. 273–316. doi: 10.1016/B978-0-08-100154-7.00010-7.

[26] L. A. Felton and S. C. Porter, ‘An update on pharmaceutical film coating for drug delivery’, *Expert Opin. Drug Deliv.*, vol. 10, no. 4, pp. 421–435, Apr. 2013, doi: 10.1517/17425247.2013.763792.

3. Published Papers

3.1 Sodium Lauryl Sulfate as lubricant in tablets formulations: is it worth?

Beatrice Sabbatini [1], Diego Romano Perinelli [1], Giovanni Filippo Palmieri [1], Marco Cespi [1], Giulia Bonacucina [1].

[1] School of Pharmacy, University of Camerino, Camerino, MC 62032, Italy.

Published on International Journal of Pharmaceutics (2023) 643, 123265

DOI: https://doi.org/10.1016/j.ijpharm.2023.123265

Sodium Lauryl Sulfate as lubricant in tablets formulations: is it worth?

Abstract

Lubricants are excipients used in tablet formulations to reduce the powder sticking within the die or on the punches surface during the manufacturing process. Despite these excipients are always required for the tablets production, their amount must be carefully evaluated since lubricants can negatively impact on mechanical strength, disintegration and dissolution behavior of solid dosage forms. Alternative compounds have been suggested to overcome the issues of conventional lubricants and sodium lauryl sulfate (SDS) is one of the most promising one. Despite SDS has been object of several investigations, a definitive conclusion on its effectiveness cannot still be drawn. Particularly, its efficacy on tablets disaggregation and API dissolution is still unclear. Here, the effect of SDS on all the relevant features of tablets and tableting process has been evaluated on immediate release hydrophobic tablets formulations in comparison with conventional lubricants. The results of this investigation are quite outspoken: SDS has a low lubricant power while it determines only a limited improvement on tablets hardness. It greatly improves the tablets wettability but only on model formulations, the presence of superdisintegrants resets its effectiveness and any possible effect on tablets disaggregation. None of the tested formulations showed improvement on the API dissolution rate.

Keywords

Lubrication, Sodium dodecyl sulfate, Magnesium stearate, Sodium Stearyl Fumarate, Contact angle, drug release.

1.Introduction

Lubricants are essential excipients for tablets manufacturing that operate by reducing the strength of adhesive interactions between particles and metal surfaces, and consequently by favoring the process of tablet ejection from the die and the following scraping of it from the lower punches surface [1,2]. The reduction of the ejection and take off forces makes the overall powder tableting process much smoother, allowing the production of tablets without or with a low occurrence of the typical defects due to powder sticking within the die or on the punches surface. Today, the lubricants used in tablets manufacturing are the so-called "boundary lubricants", constituted by solid materials having specifically features such as a low shear stress, a relatively high melting point, small particle size (consequently, large surface area), a certain amphiphilic activity, and a film-forming ability. These materials spread around drug and excipients powder particles creating a kind of non-continuous film, which reduces the friction forces during the compaction process [1]. Magnesium or calcium stearate, stearic acid, sodium stearyl fumarate and hydrogenated vegetable oils are the most common lubricants used for the formulation of commercial tablets [3]. Despite these excipients are always required in tablets formulations, they can have a negative impact on mechanical strength, disintegration and dissolution behavior. The last two aspects seem to be related to the hydrophobic nature of the lubricants, which can obstacle (hinder) water penetration into tablets, thereby retarding the disintegration and dissolution process [4–8].

To overcome these issues related to the common "boundary lubricants", several others materials have been proposed and evaluated [9–13]. Among these, sodium lauryl sulfate (SDS) is surely the one attracted more interest, probably due to its chemical similarity with magnesium stearate in addition to its known abilities as wetting and dissolution enhancer agent. The literature data indicate that SDS possess a certain lubricant ability even if not comparable to that of classic lubricants, although it seems to positively affect tablets mechanical features [14–17]. Data on lubricant ability and on the effect on tablets mechanical resistance of SDS are generally convergent for all the investigations. The same cannot be said concerning the effect of SDS on tablets disintegration and drug dissolution. The effect of SDS on tablet disintegration is rarely reported and the few data available are not in agreement. Aly reports an improvement effect of SDS [16], while in other investigations it has been observed none or even negative impact [15,17]. Interestingly, de Backere et al. [17] reported an inverse correlation between lubricant hydrophobicity and disintegration time, in agreement with the "competition-for-water"

hypothesis formulated by Ekmekciyan et al. [18]. The dissolution enhancement effect is often considered the main advantage for the use of SDS, and more in general, for the use of a surfactant lubricant in the formulation of solid oral dosage forms [19]. As such the European Medicines Agency (EMA) has identified SDS as a "Dissolution / wetting agent in solid oral dosage forms" [20]. Indeed, SDS, as well as many others water-soluble surfactants, is able to improve the drug dissolution rate through micellar solubilization [21] and, in some cases, also at concentration below the critical micelle concentration (CMC) through others mechanisms [22]. Nevertheless, a negative effect of SDS due to the formation of a less soluble salt or complex has been also reported for some drugs [23–26]. Although the effect of SDS as a solubility enhancer has been largely studied, its efficacy when used without any other lubricants is still debated and unclear. Indeed, the few published results are not in agreement, reporting an improvement of dissolution performance for celecoxib [15] and the opposite effect for ritonavir [24]. Other studies have focused exclusively on the dissolution enhancement ability of SDS in tablets lubricated with MgSt. Again, the results are not convergent, showing both a reduction [27,28] and an improvement [29] of the API dissolution rate.

Literature analysis does not provide a definitive evaluation on the possibility of using SDS as tablets lubricant. Thus, with the aim to elucidate the real possibility of using SDS as lubricant, this surfactant has been employed as an alternative lubricant with the respect to some of the most common "boundary lubricants" as magnesium stearate and sodium stearyl fumarate. The study has been carried out on immediate release hydrophobic tablets formulations, using Acetaminophen or hydrochlorothiazide as model drugs and calcium hydrogen phosphate as filler. Acetaminophen and hydrochlorothiazide are APIs classified according to the European Pharmacopeia as sparingly soluble in water and very slightly soluble in water, representing good drug models to test the possible dissolution improvement due to lubricants. Calcium hydrogen phosphate was chosen as a filler since it is an insoluble compound commonly used in tableting process, known to generate high residual die wall stress and wall friction during tableting [30]. Therefore, it represents a good model material to test the lubrication attitude. The effect of the lubricant type has been evaluated in relation to the tableting process (lubrication ability) and to the features of the produced tablets (mechanical strength, wetting ability, disintegration and API dissolution).

2. Materials and methods

2.1 Materials

Acetaminophen was a gift from from Janssen Pharma. Sodium Stearyl Fumarate (Pruv®, JRS Pharma), croscarmellose sodium (Vivasol® JRS Pharma), sodium Starch Glycolate (Vivastar®, JRS Pharma) and anhydrous calcium hydrogen phosphate (Emcompress, JRS Pharma), was donated by JRS Pharma, while Cross-linked PVP (Kollidon® CL, BASF Pharma) was donated by BASF pharma. Sodium Lauryl Sulfate (purity ≥ 98.5%) was purchased from Sigma-Aldrich, (St. Louis, MO, USA), magnesium stearate benzoic acid and hydrochlorothiazide were purchased from ACEF (Fiorenzuola d'Arda, IT).

Throughout the manuscript the materials are reported with the following abbreviations: acetaminophen (AAP), hydrochlorothiazide (HCT), benzoic acid (BA), magnesium stearate (MgSt), Sodium Stearyl Fumarate (SSF), Sodium Lauryl Sulfate (SDS), croscarmellose sodium (CCS), sodium Starch Glycolate (SSG), Cross-linked PVP (XPVP) and anhydrous calcium hydrogen phosphate (DCP).

2.2 Methods

2.2.1 Blends preparation and characterization

Blends constituted by a tablet filler (DCP, from 62 to 69%), an active pharmaceutical ingredient (AAP or HCT at 30%), a disintegrant (CCS, SSG or XPVP from 0 to 5%) and a lubricant (MgSt, SSF or SDS from 0 to 3%) were prepared using a V-shape mixer (Laboratori Mag Divisione Artha, Italy) operating at 50 rpm for 5 minutes. All the components were added together in the mixer except for the lubricant that was added at the end of the process, with an additional mixing time of 2 minutes. Additional blends were prepared using BA as active compound.

All the blends were characterized in term of real density using a helium pycnometer (AccuPyc 1330, Micromeritics, USA).

2.2.2 Tablets preparation and characterization

500 mg tablets were prepared from the blends using a 10-stations rotary tablet press (RONCHI, RIVA PICCOLA, Cinisello Balsamo, Milano, IT), equipped with flat faced round punches with a diameter of 11.28 mm and operating at 20 rpm. All the tablets were prepared setting the punch penetration to obtain a compression force of 25 kN (250 MPa). For each batch of tablets, the compression and ejection forces were recorded. The tablets were characterized in term of hardness (TBH 30 hardness tester, Erweka, Langen, DE),

thickness (Digital Caliper, Mitutoyo, JP) and weight. Tensile strength (TS) was calculated using the following equation:

$$TS = \frac{2 \cdot Hardness}{\pi \cdot Thickness \cdot \text{Diameter}} \qquad \text{eq. 1}$$

Tablets porosity was calculated as follows:

$$Porosity\ (\%) = (1 - D) * 100 \qquad \text{eq. 2}$$

Where D is the relative density calculated as the ratio of the tablet apparent density to the the powder pycnometer density.

2.2.3 Tablet wettability

The tablet wettability was examined by measuring the contact angle between the tablet surface and a 5 µL drop of deionized water. The wettability experimental set-up was build up in a manner similar to that proposed by Lamour et al. [31]. Specifically, the measurement was performed using a 12-megapixel camera (iPhone 13, Apple, USA) equipped with a 25x macro lens (SelvimTech, EU), positioned at 1 cm from the tablets. A beam of light generated by a fiber optic source (LE5214 and LE5210, Euromex, NL) passing through an opaque glass has been used to light up the tablets to obtain good contrast. The schematic representation of wettability experimental set-up is shown a supplementary figure (**Figure SF1A)**.

For each tablet, a video has been recorded and frames were extracted at predetermined time intervals (an example of extracted frame is reported in **Figure SF1B**). All the extracted frames were analyzed through the ImageJ software [32] using the plugin "contact angle" (also known as Brugnara plugin) [33,34]. An example of the edge detection of such a plugin is shown in **Figure SF1C**. Each formulation was analyzed at least in triplicate.

2.2.4 Disintegration studies

Disintegration time (DT) was measured in deionized water using a disintegration test apparatus (Tecno Galenica, IT) operating at 37°C. Disintegration time was taken at the total disintegration of the tablets, that is when fragments can be no longer detected on the screen of the test tubes.

The disintegration times were determined analyzing 6 tablets of each formulation.

2.2.5 Dissolution studies

Dissolution tests have been carried out through a USP dissolution apparatus type II (AT7 smart, Sotax, CH) using 900 mL of deionized water as dissolution medium, maintained at 37°C and applying a paddle rotation speed of 50 rpm. Additional tests were carried out

changing the paddle rotation speed from 50 to 100 and 200 rpm. Drug release was monitored spectrophotometrically (UV-1800, Shimadzu Corporation, JP) at the maximum wavelength of 242.5, 316 and 272.2 nm for AAP, HCT and BA APIs, respectively, at the following time intervals: 0, 5, 10, 15, 30, 45, 60, 90 and 120 min. Each formulation was analyzed at least in triplicate.

3. Results and discussions

3.1 Effect of lubricants and disintegrants on tableting and tables features

The SDS lubrication power has been evaluated comparing the ejection force measured during the tableting cycle of AAP and HCT blends having all the same composition except for the lubricant type (MgSt, SSF and SDS) and amount (from 0 to 3% w/w). The results (**Figure 1** panels AAP_1 and HCT_1) clearly indicate marked differences between the lubricants. MgSt and SSF performed much better than SDS at all concentrations. Even at the highest concentration used (3% w/w), SDS is not able to fully match the performance of the other tested lubricants at 1% w/w, in agreement with the findings of Dun at al. [15]. According to these authors, the amount of SDS necessary to match the lubricant ability of 1% w/w MgSt could reach values up to around 5% w/w, as a function of the compaction mechanism of the formulation components (brittle component are much less sensitive to the lubricant type compared to deformable ones). The effect of the disintegrant (CCS) amount on the ejection force at fixed concentration of lubricant (3% w/w) has been evaluated as well. In this case, the results (**Figure 1** panel AAP_2 and HCT_2) suggest that the ejection force is not influenced by the CCS amount, at least when it is added at concentrations between 0 and 5% w/w, the normal range of use. According to these results, no interaction between CCS and lubricants on the ejection force can be supposed, in agreement with previous studies performed on stearic acid as lubricant [35,36].

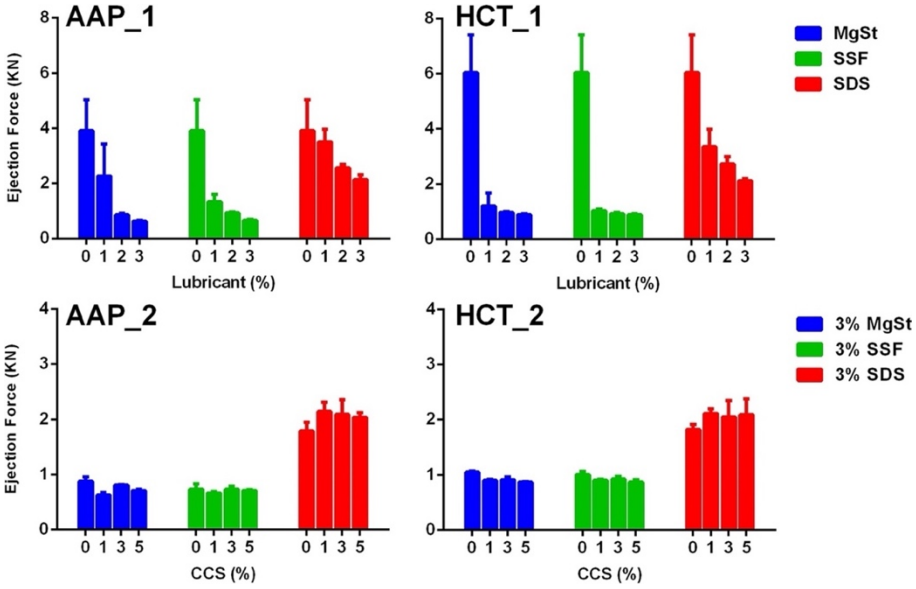

***Fig. 1**. In the upper panels it is shown the effect of the lubricant type and concentration (0–3 %) of formulations containing a constant amount of CCS (1%) and AAP (panel AAP_1) or HCT (panel HCT_1) as API on the ejection force. In the lowers panels it is shown the effect of the lubricant type and CCS*

concentration of formulations containing a constant amount of lubricant (3%) and AAP (panel AAP_2) or HCT (panel HCT_2) as API, on the ejection force.

Lubricants are essential excipients for tablet formulations, however, they usually lower the tabletability of powder blends [37,38], even if this effect appears much more pronounced mainly in the presence of deforming materials [1,15,39,40]. The results in **Figure 2** (panel AAP_1 and HCT_1) confirm the literature data, taking into account that AAP is an almost deformable material [41,42] while HCT is a brittle one [43]. The three lubricants lower the tabletability in AAP formulations, while such effect is almost negligible when HCT was used. In this context, the use of SDS in the formulations containing some deformable materials (such as AAP) provides an improvement compared to MgSt but not versus SSF. The results about the comparison between MgSt and SDS are in agreement with Dun et al [15]. Instead, the performances of SDS and SSF have never been directly compared before, although it is reported that SSF usually has a lower impact on tablets hardness if compared to MgSt [1]. In the lower panels of **Figure 2** (panel AAP_2 and HCT_2), the effect of CCS is shown. CCS seems to influence in a positive manner the tensile strength of tablets containing AAP, independently by the lubricant type.

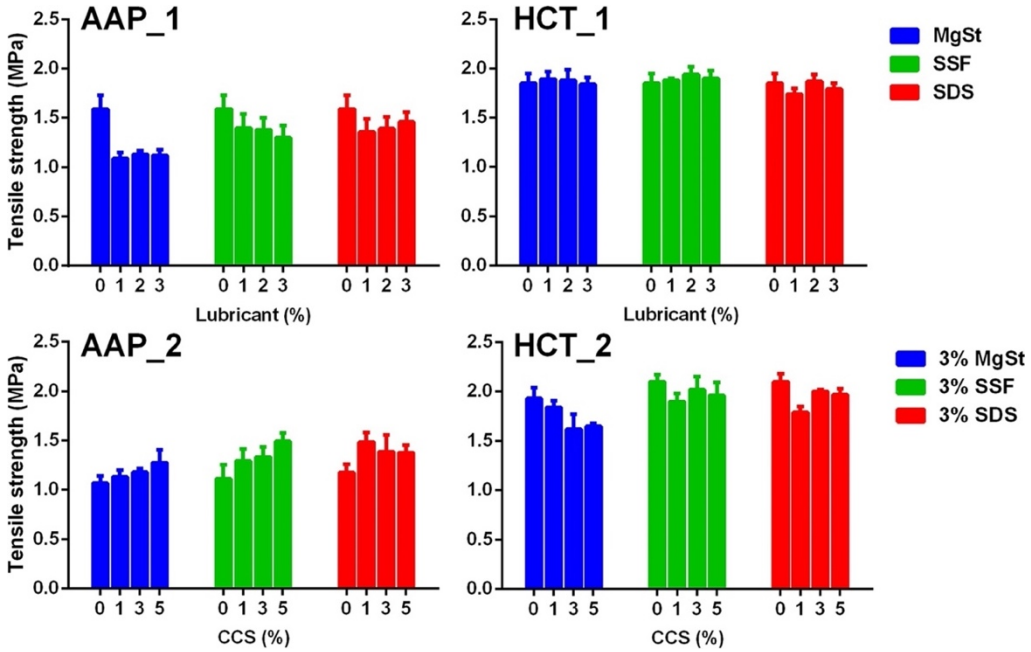

***Fig. 2**. In the upper panels it is shown the effect of the lubricant type and concentration of formulations containing a constant amount of CCS (1%) and AAP (panel AAP_1) or HCT (panel HCT_1), on the tablet tensile strength. In the lowers panels it is shown the effect of the lubricant type and CCS concentration of formulations containing a constant amount of lubricant (3%) and AAP (panel AAP_2) or HCT (panel HCT_2), on the tablets tablet tensile strength.*

3.2 Effect of lubricants and disintegrants on tablet wettability

The effect of the lubricant type and the disintegrant (concentration and type) on wettability was evaluated measuring the contact angle between water and the tablet surface. Preliminary, the three different lubricants were compared each other at a constant concentration (3% w/w) using tablets prepared without the disintegrant. The results (**Figure 3**), demonstrated that SDS has a huge impact on tablet wettability, strongly reducing the interfacial tension with water, in comparison to tablets lubricated with MgSt or SSF.

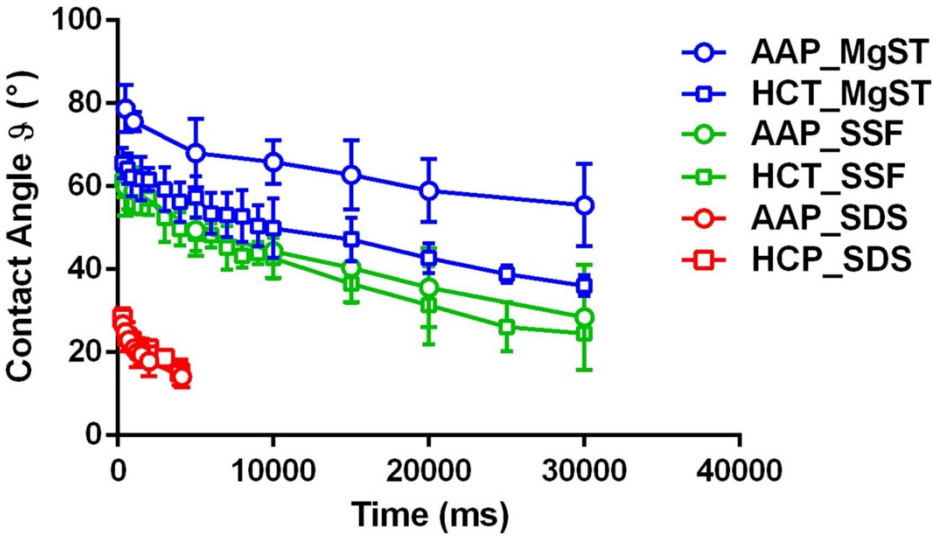

Fig. 3. *Effect of lubricant type (at a concentration of 3%) on the contact angle kinetics in tablets containing AAP or HCT as API. The disintegrant is not present in the tablet formulations.*

The differences were still more evident considering the kinetics of water absorption on tablet surface. In the presence of SDS, the droplet on the tablet surface almost disappeared after 4s, making the contact angle measurements at higher times practically impossible. Instead, in the case of MgSt and SSF, the water droplet slowly spreads on tablets surface and the absorption was slower. In these cases, the contact angle measurements were carried out up to 30 s, which is the maximum time up to which the droplet was analysable, even if it is still visible for longer times (in some cases over 2 minutes). MgSt and SSF showed a similar behavior, with the latter characterized by a lower contact angle and thus a slightly better wettability. The different drugs had only a minimal effect on the contact angle measurements. These results are expected according to the nature of the different lubricants and also according to the previous findings published in the literature [15]. However, when the measurements were performed on more complex formulations, and specifically on those containing disintegrants, the results were surprising. In the presence of disintegrants, the droplets were absorbed much faster leaving at its place a kind of

"solid bubble" constituted by dry swollen powder (**Figure 4**). This effect was described in 2021 by Markl et al [44] while observing sessile drop images in a study focused on the relevance of water absorption and swelling behavior in tablets disintegration. According to the authors, in presence of swellable materials (MCC and CCS), the interaction between tablets surface and water is characterized by in initial fast absorption phase (the duration was max 3-4 s) followed by a swelling process. Interestingly, the authors observed this sequence also in a formulation where the CCS (5% w/w) was the only swellable material, suggesting that the absorption/swelling process happens even in the presence of a small amount of swellable component, as observed in the present study. Here, the absorption/swelling process triggered by CCS has a huge effect on the duration of the water absorption and on the time evolution of the contact angle values.

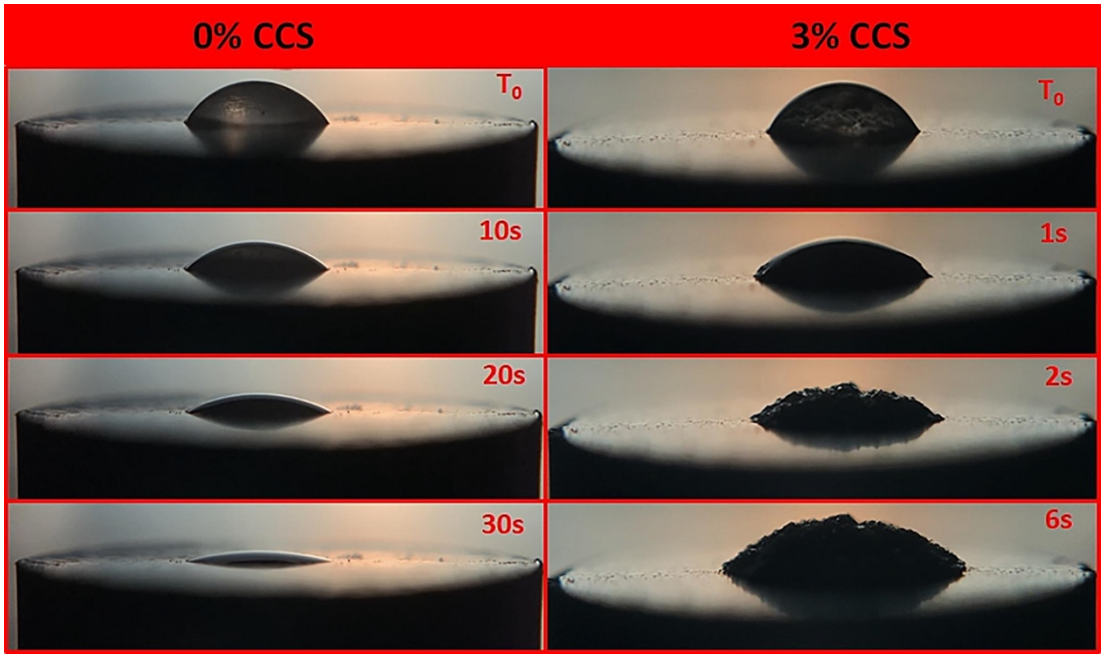

Fig. 4*. Visual comparison of the kinetics of the drop absorption in tablets without (0% CCS) and with disintegrant (3% CCS). The images refer to the formulations containing AAP as API and 3% of SSF as lubricant.*

The absorption time (meant as the last time when the droplet is visible and analysable on the tablet's surface) showed an impressive reduction as the amount of CCS increased (**Figure 5**). For example, in the case of tablets containing AAP as API and MgSt as lubricant the addition of 1% w/w and 3% w/w of CCS determined a reduction of the absorption time of 18 and 46 times respectively.

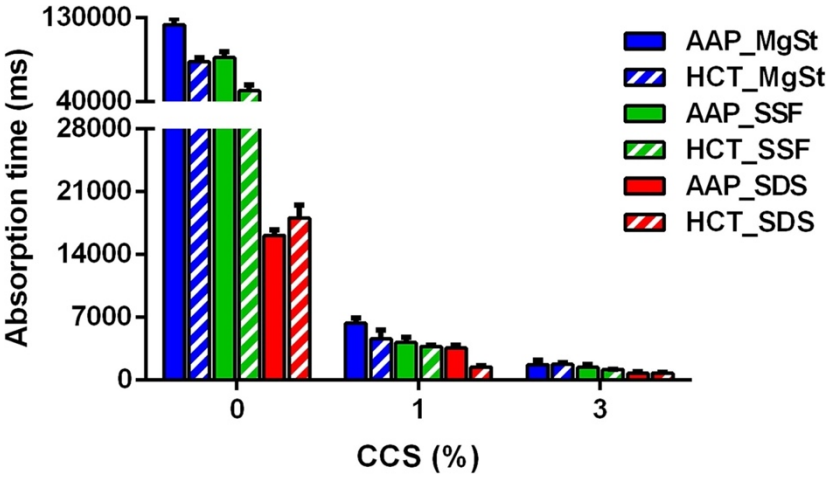

***Fig. 5**. Effect of the CCS amount on the droplet absorption time in presence of different lubricants (3%).*

Again, the contact angle kinetics (**Figure 6**) also changed in a massive way. In this case, despite the initial value (t0) was practically unaffected by the presence of disintegrant, the contact angle values decreased very fast becoming impossible to be measured after few seconds. Both these effects were more pronounced on the formulations showing the worst wettability without CCS, namely those containing MgSt, and in a less extent, those containing SSF. The effect was also evident when SDS was used as lubricant, even if the absolute change of the absorption time and contact angle kinetics due to the CCS addition was much more limited. Therefore, it appears clear that the presence of CCS suppresses or reduces drastically all the differences in terms of wettability due to the different lubricant used.

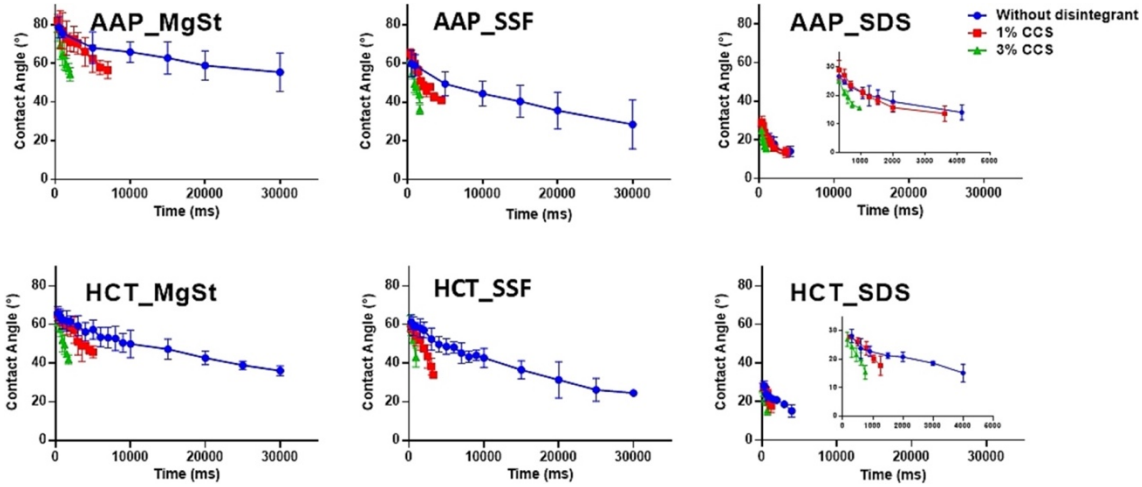

***Fig. 6**. Effect of lubricant type (at a concentration of 3%) and CCS concentration on the contact angle kinetics in tablets containing AAP or HCT as API.*

To verify if this effect was specific of CCS or was a general feature of all the disintegrants, further tests were carried out using also the 1% w/w of SSG and XPVP as disintegrant in tablets lubricated with MgSt. The results (**Figure SF2**) indicated that all the

superdisintegrants drastically improved the tablets wettability, making the water absorption kinetics almost overlapping.

3.3 Effect of lubricants and disintegrants on tablet disintegration

The contact angle measurements suggested that lubricants should not possess any influence on water absorption kinetics in the case that a disintegrant is present in a hydrophobic formulation. From a practical point of view, it means that the disintegration behavior should not be affected by the lubricant in presence of a disintegrant. The results of disaggregation tests (**Figure 7** upper panels AAP_1 and HCT_1) confirm this hypothesis. The tablets without disintegrant (containing a constant amount of lubricant at 3% w/w) remained intact during the test for more that 15 minutes; however, as the disintegrant was added, the disaggregation time felt at values below 20 s as a function of the CCS concentration. The type of lubricant did not show any influence on the process and the disaggregation time seemed controlled exclusively by the presence of the disintegrant. For a more detailed analysis, tablets containing 1% w/w of CCS were tested at increasing concentration of lubricants (**Figure 7** lower panels AAP_2 and HCT_2). Once again, the type of lubricant did not show any effect, while the concentration affected the process only in a marginal way (the maximum variation of disaggregation time was around 10 s).

These results clearly indicate that for immediately release hydrophobic tablets the use of a wetting agent or the substitution of a standard lubricant with a wetting agent does not improve the disintegration behavior and the reason is related to the effect of the disintegrant on the water absorption kinetic.

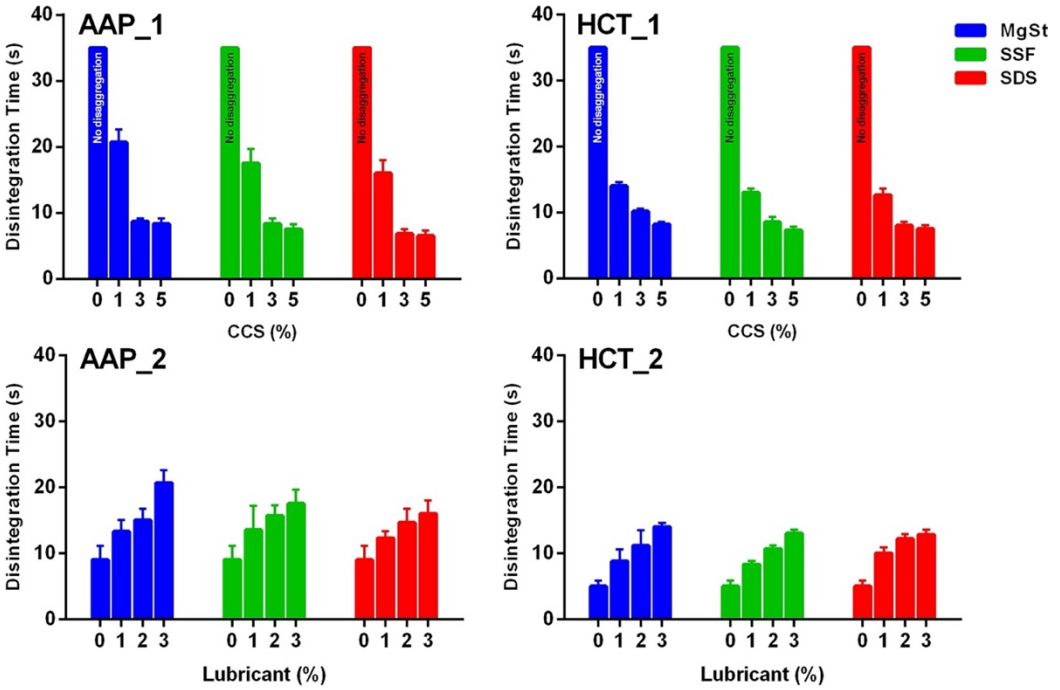

Fig. *7. Effect of the CCS amount on the disintegration time of tablets prepared with the three different lubricants (3%) for the two API studied (upper panels). Effect of the lubricant amount on the disintegration time of tablets prepared with the three different lubricants and 1% of CCS for the two API studied (lower panels).*

3.4 Effect of lubricants and disintegrants on API dissolution

Dissolution tests were performed to verify if the use of SDS in place of a hydrophobic lubricant can improve the dissolution behavior. The results (**Figure 8**) clearly showed that SDS has a negative effect on API dissolution for both the drugs tested, AAP and HCT, when compared with traditional lubricants. Interestingly, by increasing the basket rotation speed such differences were reduced up to almost disappear (F**igure 9A**), suggesting an effect related to the API dissolution rate.

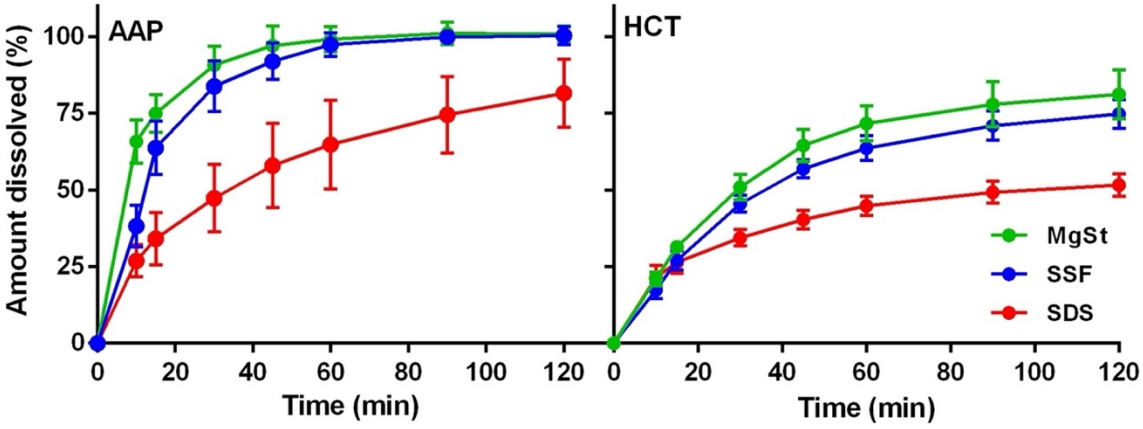

Fig. 8. *Effect of the lubricant type (3%) in AAP or HCT tablets containing 1% of CCS.*

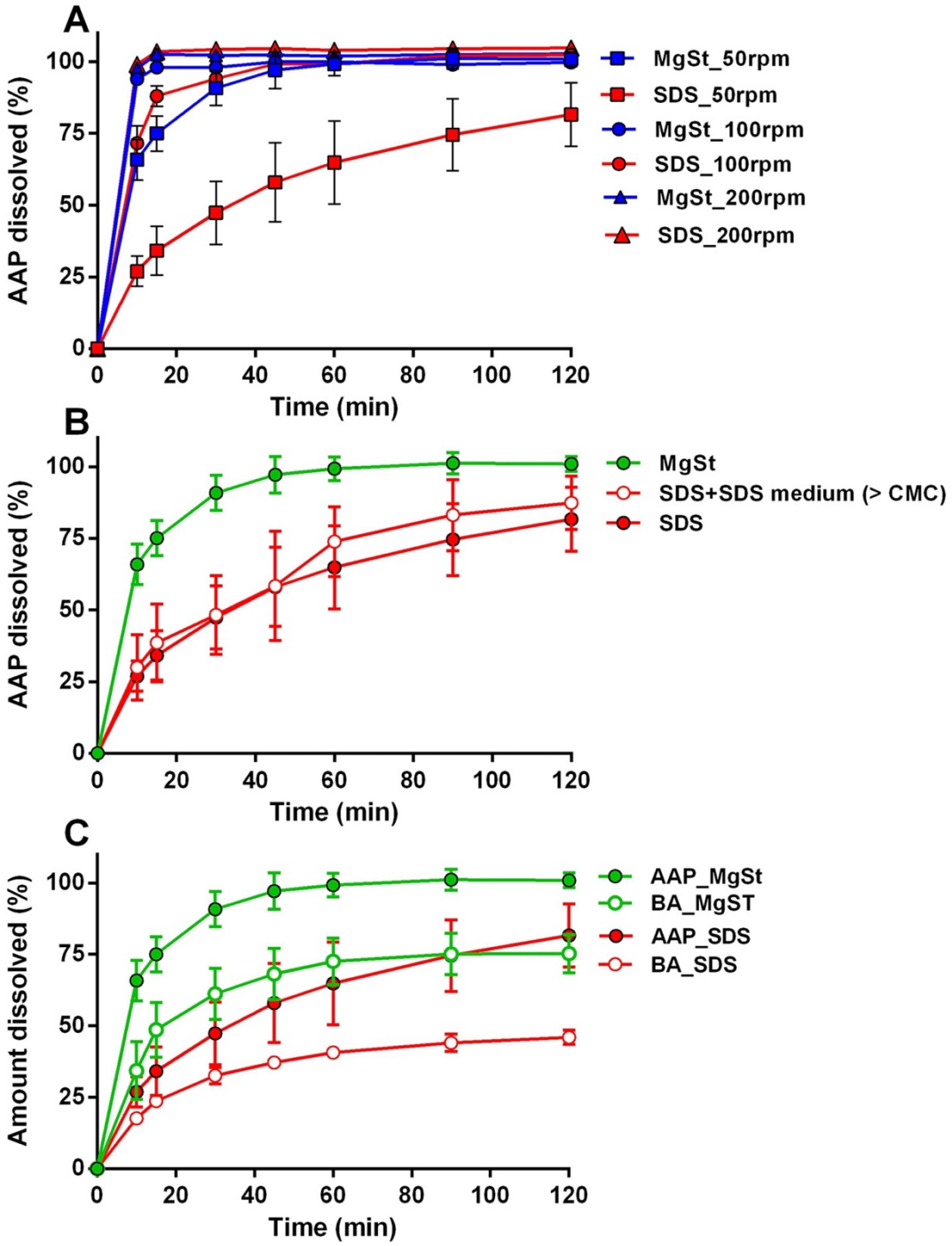

***Fig. 9**. **(A)** Effect of paddle rotation speed on the dissolution behavior of AAP tablets containing 1% w/w of CCS and 3% w/w of lubricant (MgSt or SDS). **(B)** Effect of SDS in the medium (concentration higher than its CMC) on the dissolution behavior of AAP tablets containing 1% w/w of CCS and 3% w/w SDS. The curve of MgSt tablets was added for comparison. **(C)** Effect of lubricant type (3% w/w) on the dissolution behavior of AAP or BA tablets containing 1% w/w of CCS.*

The effect of SDS on API dissolution was initially unexpected; however, from a detailed analysis of literature, similar results were found. Zhao et al reported a negative effect of SDS on the dissolution of AAP and acetylsalicylic tablets [28]. The authors hypothesized that such effect was due to a reduction in tablets porosity because of the SDS addition, although they did not measure the tablets porosity. Differently, in the present work, the

tablets porosity has been measured and it did not change in a relevant manner (**Figure SF3**) when MgSt or SSF are substituted by SDS. Therefore, the hypothesis of Zhao et al. appears to be unlikely at least for the present results. Another possibility to explain the slowing effect of SDS on the API release has been proposed by Guo et al by studying the release of ritonavir tablets [24]. The authors observed a reduction of API release when the SDS concentration was lower than its critical micelle concentration (CMC), due to the formation of a API-SDS salt with a lower solubility respect to the API alone. However, when the SDS concentration was higher than CMC the dissolution rate increased markedly. To verify this hypothesis further dissolution tests were performed by adding SDS in the dissolution media at a concentration above the CMC (CMC 6.5-9.2 mM [45], concentration used 20 mM). The results, (**Figure 9B**), did not show any significant differences on AAP release, even when SDS is present in the medium as micellar aggregates. Finally, it has been verified the hypothesis related to the formation of a lower solubility salt or complex between APIs and SDS. Such possibility has been reported also by Bhattachar et al for trimethoprim and for an unspecified basic compound [25], by Desai et al for metformin [23], and by Huang et al for a not defined cationic drug [26]. In all cases, the drugs involved in the salts formation were weak bases as in the case of AAP and HCT studied in the present work. To prove the hypothesis of the formation of an insoluble salt/complex it has been replicated the test carried out by Guo et al using ritonavir tablets [24]; different amounts of SDS were added to an AAP solution and the presence of turbidity was monitored after each addition. The test has been performed using a concentration of AAP equal to 150mg/900ml (the highest concentration used for the dissolution test). In addition, such tests were repeated also using higher concentration of AAP. In no case turbidity was observed. From the other side, when the same experiments were repeated by changing the AAP with calcium chloride an immediate formation of a turbid dispersion occurred, due to the presence of the insoluble salt calcium lauryl sulfate. The hypothesis of the formation of a low solubility complex is also unlikely from a stoichiometric point of view. In fact, the molar ratio between APP and SDS in the present study is equal to 5.2; so, even if a soluble salt was formed, no more than the 20% of the active compounds should be involved (the most likely stoichiometry ratio for the salt is 1:1). Consequently, salt formation could not explain the differences observed, especially in the first time points of the dissolution profiles; in fact, in the first three time points (t10, t15 and t30) the amount AAP released from MgSt tablets is at least the double of that released from SDS tablets. For a further corroboration of the impossibility of the

salt formation, the dissolution behavior of an acid model drug, the benzoic acid (BA), formulated in tablets lubricated with MgSt or SDS has been studied. This compound should not form any salt with SDS (both are acid compounds); however, also in this case, the BA release rate was still slow down by the presence of SDS (**figure 9C**).

4. Conclusions

SDS has been tested as an alternative lubricant with the respect to MgSt and SSF, by evaluating its impact on the ejection process during tableting and on the tablet's characteristics (mechanical properties, disintegration ability and API's dissolution behavior). SDS assures a modest improvement of the tabletability, despite its poor performance in term of lubricant power. It shows a relevant wetting effect exclusively on model tablet formulations without disintegrant. The presence of a disintegrant resulted to suppress the effect of SDS on tablet wettability, being the only excipient influencing the water absorption kinetics as well as the disintegration phenomenon. None of the tablets lubricated with SDS showed any improvement in term of API's dissolution, even resulting in a lowering of the drug dissolution rate.

The results of this investigation are quite outspoken not supporting the use of this compound in tablet formulation.

Supplementary material

Supplementary data to this article can be found online at https://doi.org/10.1016/j.ijpharm.2023.123265.

References

[1] J. Wang, H. Wen, D. Desai, Lubrication in tablet formulations, Eur. J. Pharm. Biopharm. 75 (2010) 1–15. doi:10.1016/j.ejpb.2010.01.007.

[2] J. Li, Y. Wu, Lubricants in pharmaceutical solid dosage forms, Lubricants. 2 (2014) 21–43. doi:10.3390/lubricants2010021.

[3] U.S. FDA, Inactive Ingredient Search for Approved Drug Products, (n.d.). https://www.accessdata.fda.gov/scripts/cder/iig/index.cfm.

[4] M.E. Johansson, Influence of the granulation technique and starting material properties on the lubricating effect of granular magnesium stearate., J. Pharm. Pharmacol. 37 (1985) 681–685. doi:10.1111/j.2042-7158.1985.tb04942.x.

[5] M.E. Johansson, Investigations of the mixing time dependence of the lubricating properties of granular and powdered magnesium stearate., Acta Pharm. Suec. 22 (1985) 343–350.

[6] J.F. Bavitz, P.K. Shiromani, Granulation Surface Area as Basis for Magnesium Stearate Concentration in Tablet Formulations, Drug Dev. Ind. Pharm. 12 (1986) 2481–2492. doi:10.3109/03639048609063194.

[7] M.E. Johansson, The effect of scaling-up of the mixing process on the lubricating effect of powdered and granular magnesium stearate, Acta Pharm. Technol. 32 (1986).

[8] A. Uzunović, E. Vranić, Effect of magnesium stearate concentration on dissolution properties of ranitidine hydrochloride coated tablets., Bosn. J. Basic Med. Sci. 7 (2007) 279–283. doi:10.17305/bjbms.2007.3060.

[9] H. Aoshima, A. Miyagisnima, Y. Nozawa, Y. Sadzuka, T. Sonobe, Glycerin fatty acid esters as a new lubricant of tablets, Int. J. Pharm. 293 (2005) 25–34. doi:https://doi.org/10.1016/j.ijpharm.2004.12.007.

[10] M. Turkoglu, I. Sahin, T. San, Evaluation of hexagonal boron nitride as a new tablet lubricant, Pharm. Dev. Technol. 10 (2005) 381–388. doi:10.1081/PDT-65684.

[11] D. Shibata, Y. Shimada, Y. Yonezawa, H. Sunada, N. Otomo, K. Kasahara, Application and evaluation of sucrose fatty acid esters as lubricants in the production of pharmaceuticals, J. Pharm. Sci. Technol. 62 (2002) 133–145. https://www.scopus.com/inward/record.uri?eid=2-s2.0-15044343339&partnerID=40&md5=1475bacf44edae6144f52fb379206440.

[12] A. N'Diaye, V. Jannin, V. Bérard, C. Andrès, Y. Pourcelot, Comparative study of the lubricant performance of Compritol® HD5 ATO and Compritol® 888 ATO: effect of polyethylene glycol behenate on lubricant capacity, Int. J. Pharm. 254 (2003) 263–269. doi:https://doi.org/10.1016/S0378-5173(03)00027-9.

[13] W.A.J. STRICKLAND, T. HIGUCHI, L.W. BUSSE, The physics of tablet compression. X. Mechanism of action and evaluation of tablet lubricants., J. Am. Pharm. Assoc. Am. Pharm. Assoc. 49 (1960) 35–40.

[14] M. Perrault, F. Bertrand, J. Chaouki, An experimental investigation of the effect of the amount of lubricant on tablet properties, Drug Dev. Ind. Pharm. 37 (2011) 234–242. doi:10.3109/03639045.2010.505013.

[15] J. Dun, F. Osei-Yeboah, P. Boulas, Y. Lin, C.C. Sun, A systematic evaluation of dual functionality of sodium lauryl sulfate as a tablet lubricant and wetting enhancer, Int. J. Pharm. 552 (2018) 139–147. doi:10.1016/j.ijpharm.2018.09.056.

[16] S.A.S. Aly, The resistance to compression index as a parameter to evaluate the efficacy of lubricants in pharmaceutical tabletting, J. Drug Deliv. Sci. Technol. 16 (2006) 151–155. doi:https://doi.org/10.1016/S1773-2247(06)50023-1.

[17] C. de Backere, J. Quodbach, T. De Beer, C. Vervaet, V. Vanhoorne, Impact of alternative lubricants on process and tablet quality for direct compression, Int. J. Pharm. 624 (2022) 122012. doi:https://doi.org/10.1016/j.ijpharm.2022.122012.

[18] N. Ekmekciyan, T. Tuglu, F. El-Saleh, C. Muehlenfeld, E. Stoyanov, J. Quodbach, Competing for water: A new approach to understand disintegrant performance, Int. J. Pharm. 548 (2018) 491–499. doi:https://doi.org/10.1016/j.ijpharm.2018.07.025.

[19] J. van der Merwe, J. Steenekamp, D. Steyn, J. Hamman, The Role of Functional Excipients in Solid Oral Dosage Forms to Overcome Poor Drug Dissolution and Bioavailability, Pharmaceutics. 12 (2020). doi:10.3390/pharmaceutics12050393.

[20] EMA/CHMP/351898/2014, Background review for sodium laurilsulfate used as an excipient, 2015. https://www.ema.europa.eu/en/documents/report/background-review-sodium-laurilsulfate-used-excipient-context-revision-guideline-excipients-label_en.pdf.

[21] R. Nagarajan, Solubilization by amphiphilar aggregates, Curr. Opin. Colloid Interface Sci. 2 (1997) 282–293. doi:https://doi.org/10.1016/S1359-0294(97)80037-4.

[22] M.N. Alizadeh, A. Shayanfar, A. Jouyban, Solubilization of drugs using sodium lauryl sulfate: Experimental data and modeling, J. Mol. Liq. 268 (2018) 410–414.

doi:https://doi.org/10.1016/j.molliq.2018.07.065.

[23] D. Desai, B. Wong, Y. Huang, Q. Ye, D. Tang, H. Guo, et al., Surfactant-mediated dissolution of metformin hydrochloride tablets: wetting effects versus ion pairs diffusivity., J. Pharm. Sci. 103 (2014) 920–926. doi:10.1002/jps.23852.

[24] Y. Guo, C. Wang, J. Dun, L. Du, M. Hawley, C.C. Sun, Mechanism for the Reduced Dissolution of Ritonavir Tablets by Sodium Lauryl Sulfate., J. Pharm. Sci. 108 (2019) 516–524. doi:10.1016/j.xphs.2018.10.047.

[25] S.N. Bhattachar, D.S. Risley, P. Werawatganone, A. Aburub, Weak bases and formation of a less soluble lauryl sulfate salt/complex in sodium lauryl sulfate (SLS) containing media., Int. J. Pharm. 412 (2011) 95–98. doi:10.1016/j.ijpharm.2011.04.018.

[26] Z. Huang, S. Parikh, W.P. Fish, Interactions between a poorly soluble cationic drug and sodium dodecyl sulfate in dissolution medium and their impact on in vitro dissolution behavior., Int. J. Pharm. 535 (2018) 350–359. doi:10.1016/j.ijpharm.2017.10.063.

[27] P. Knöös, S. Onder, L. Pedersen, L. Piculell, S. Ulvenlund, M. Wahlgren, Surfactants modify the release from tablets made of hydrophobically modified poly (acrylic acid)., Results Pharma Sci. 3 (2013) 7–14. doi:10.1016/j.rinphs.2013.08.001.

[28] J. Zhao, O. Koo, D. Pan, Y. Wu, D. Morkhade, S. Rana, et al., The Impact of Disintegrant Type, Surfactant, and API Properties on the Processability and Performance of Roller Compacted Formulations of Acetaminophen and Aspirin., AAPS J. 19 (2017) 1387–1395. doi:10.1208/s12248-017-0104-6.

[29] E. Kimaro, P. Tibalinda, R. Shedafa, M. Temu, E. Kaale, Formulation development of chewable albendazole tablets with improved dissolution rate, Heliyon. 5 (2019) e02911. doi:https://doi.org/10.1016/j.heliyon.2019.e02911.

[30] B. Uzondu, L.Y. Leung, C. Mao, C.Y. Yang, A mechanistic study on tablet ejection force and its sensitivity to lubrication for pharmaceutical powders, Int. J. Pharm. 543 (2018) 234–244. doi:10.1016/j.ijpharm.2018.03.064.

[31] G. Lamour, A. Hamraoui, A. Buvailo, Y. Xing, S. Keuleyan, V. Prakash, et al., Contact Angle Measurements Using a Simplified Experimental Setup, J. Chem. Educ. 87 (2010) 1403–1407. doi:10.1021/ed100468u.

[32] C.A. Schneider, W.S. Rasband, K.W. Eliceiri, NIH Image to ImageJ: 25 years of image analysis, Nat. Methods. 9 (2012) 671–675. doi:10.1038/nmeth.2089.

[33] M. Brugnara, Contact_Angle.jar, (2004). https://imagej.nih.gov/ij/plugins/contact-angle.html.

[34] D. Williams, A.T. Kuhn, M. Amann, M.B. Hausinger, M.M. Konarik, E.I. Nesselrode, Computerised Measurement of Contact Angles, Galvanotechnik. 101 (2010).

[35] A. Stamm, C. Mathis, The compression of powders. The measurement of ejection force for characterization of "compressibility" , Ann. Pharm. Fr. 33 (1975) 641–650.

[36] C. Ferrero, N. Muñoz, M. V Velasco, A. Muñoz-Ruiz, R. Jiménez-Castellanos, Disintegrating efficiency of croscarmellose sodium in a direct compression formulation, Int. J. Pharm. 147 (1997) 11–21. doi:10.1016/S0378-5173(96)04784-9.

[37] W.A. STRICKLAND, E. NELSON, L.W. BUSSE, T. HIGUCHI, The physics of tablet compression. IX. Fundamental aspects of tablet lubrication., J. Am. Pharm. Assoc. Am. Pharm. Assoc. (Baltim). 45 (1956) 51–55. doi:10.1002/jps.3030450116.

[38] A.F. Asker, K.M. Saied, M.M. Abdel-Khalek, Investigation of some materials as dry binders for direct compression in tablet manufacture. Part 5: Effects of lubricants and flow conditions., Pharmazie. 30 (1975) 378–382.

[39] A.H. De Boer, G.K. Bolhuis, C.F. Lerk, Bonding characteristics by scanning electron microscopy of powders mixed with magnesium stearate, Powder Technol. 20 (1978) 75–82. doi:https://doi.org/10.1016/0032-5910(78)80011-4.

[40] P.J. Jarosz, E.L. Parrott, Effect of Lubricants on Tensile Strengths of Tablets, Drug Dev. Ind. Pharm. 10 (1984) 259–273. doi:10.3109/03639048409064649.

[41] M.-C. Lin, W.C. Duncan-Hewitt, Deformation kinetics of acetaminophen crystals, Int. J. Pharm. 106 (1994) 187–200. doi:https://doi.org/10.1016/0378-5173(94)90002-7.

[42] M. Cespi, D.R. Perinelli, L. Casettari, G. Bonacucina, G. Caporicci, F. Rendina, et al., Use of in-die powder densification parameters in the implementation of process analytical technologies for tablet production on industrial scale, Int. J. Pharm. 477 (2014) 140–147.

[43] A. Mitrevej, D. Faroongsarng, N. Sinchaipanid, Compression behavior of spray dried rice starch, Int. J. Pharm. 140 (1996) 61–68. doi:https://doi.org/10.1016/0378-5173(96)04576-0.

[44] D. Markl, N. Maclean, J. Mann, H. Williams, A. Abbott, H. Mead, et al., Tablet disintegration performance: Effect of compression pressure and storage conditions on surface liquid absorption and swelling kinetics, Int. J. Pharm. 601 (2021) 120382. doi:https://doi.org/10.1016/j.ijpharm.2021.120382.

[45] D.R. Perinelli, M. Cespi, N. Lorusso, G.F. Palmieri, G. Bonacucina, P. Blasi, Surfactant Self-Assembling and Critical Micelle Concentration: One Approach Fits All?, Langmuir. 36 (2020) 5745–5753. doi:10.1021/acs.langmuir.0c00420.

This paper has been published on International Journal of Pharmaceutics as open access (CC-BY license). https://doi.org/10.1016/j.ijpharm.2023.123265

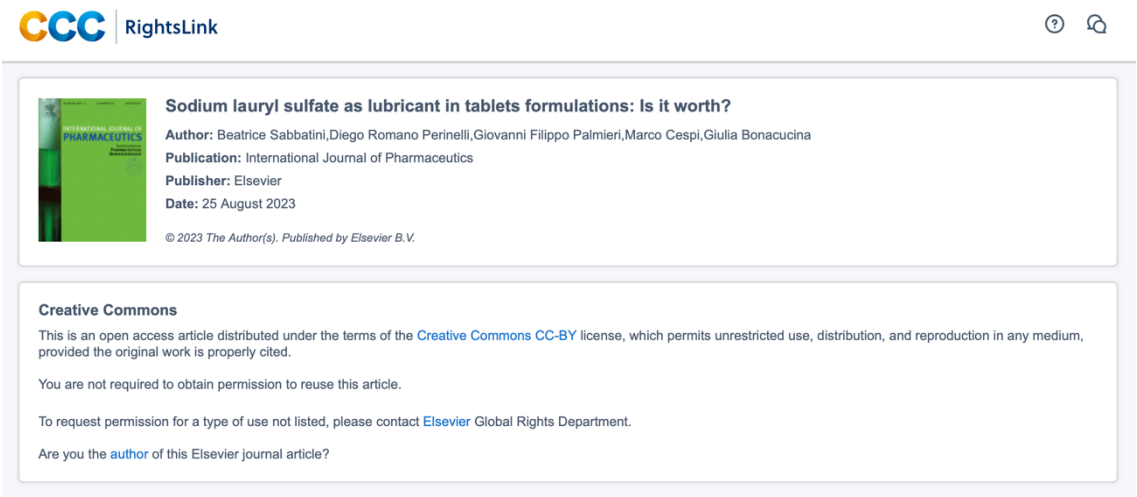

3.2 Exploring Immersion Coating as a Cost-Effective Method for Small-Scale Production of Enteric-Coated Gelatin Capsules

Beatrice Sabbatini [1], Diego Romano Perinelli[1], Giovanni Filippo Palmieri[1], Marco Cespi[1]* and Giulia Bonacucina[1]

[1] School of Pharmacy, University of Camerino, Camerino, MC 62032, Italy.

Published on Pharmaceuticals (2024), 17(4), 433.

DOI: https://doi.org/10.3390/ph17040433

Exploring Immersion Coating as a Cost-Effective Method for Small-Scale Production of Enteric-Coated Gelatin Capsules

Abstract:

The coating process for solid dosage forms is widely used in the pharmaceutical industry but presents challenges for small-scale production, needed in personalized medicine and clinical or galenic settings. This study aimed to evaluate immersion coating, a cost-effective small-scale method, for enteric-coated gelatin capsules using standard equipment. Two enteric coating polymers and different polymer concentrations were tested, along with API solubility. Results were compared with commercially available enteric capsule shells. Successful preparation of enteric coating capsules via immersion necessitates a comprehensive grasp of API and enteric polymer behavior. However, utilizing commercially available enteric capsule shells does not guarantee ease or robustness, as their efficacy hinges on the attributes of the active ingredient and excipients. Notably, coating with Eudragit S100 stands out for its superior process robustness, requiring minimal or no development time, thus representing the best option for small-scale enteric capsule production.

Keywords:

Eudragit; Hypromellose acetate succinate; Paracetamol; Tramadol HCl; Enteric capsules; Enteric coating; DRcaps®; Vcaps® Enteric.

1. Introduction

The coating of a solid dosage form is a widespread process in the pharmaceutical industry because it offers a solution to many challenges encountered by scientists in the past. Indeed, there are various reasons for coating a dosage form [1,2]. Among these, coating can mask bad taste and odor [3,4], and it can protect the drug from oxygen, humidity, or other environmental factors [4,5]. The coating's role can be aesthetic because it can improve the identification of the medicine (it has been proven that a colored film can aid in drug recognition, especially for elderly patients in polytherapy), and it can hide imperfections of the pharmaceutical form, particularly in the presence of APIs and excipients with different colors [6]. The coating can be also used to modify the drug release kinetics to obtain constant and prolonged release or ensure release in specific districts of the GI tract [7,8]. It is also possible, by combining coating with other modified release technologies, to obtain very complex release profiles, such as programmed ones [9]. One of the most common coatings used for modifying release applications is that applied to prevent the dissolution of the drug in the stomach and aim to release it in the intestine. This type of coating is usually called 'gastro-resistant or enteric coating', and it allows the administration of APIs targeted to the intestine or those that must avoid the stomach [10]. The enteric release of the drug is usually obtained by film coating using polymers with pH-dependent water solubility. Methacrylic acid–methyl methacrylate copolymers, cellulose derivatives with weak acid groups (such as cellulose acetate phthalate or hypromellose acetate succinate), or polyvinyl acetate phthalate are examples of polymers commonly used for enteric coating [1,2].

The industrial production of enteric film-coated dosage forms is a well-established process carried out using fluid bed or coating pan equipment. In almost all cases, the process involves the spray application of the coating solution and simultaneous drying, allowing to produce a large number of coated dosage forms in the same batch [1]. While industrial methods are highly effective for large-scale production, they are completely unsuitable for small batches, as required in personalized medicine and clinical production of coated dosage forms (e.g., hospital pharmacy or galenic preparation in a local pharmacy). The alternatives developed for these particular situations include two approaches: the use of capsule shells made of polymers having a pH-dependent dissolution or the design of inexpensive and easy-to-manage equipment that allows the coating of small batches. The first approach requires the use of the so-called Enteric Capsule Drug Delivery Technology (ECDDT). Despite these capsule shells having higher

costs than traditional ones, they do not require additional equipment, and the preparations and formulations are exactly like the traditional ones. Several types of ECDDTs are now available on the market (such as Vcaps® Enteric and DRcaps®) [11]. In addition, the development of new ECDDTs represents an interesting topic for researchers in the pharmaceutical area [12,13]. Despite them potentially being the ideal solutions, the literature results are controversial, and in many cases, failures in obtaining enteric release profiles were reported [14]. The second approach is represented by equipment based on the immersion coating procedure (such as the ProCoater® by Torpac, Fairfield, NJ, USA), which allows the coating of small batches of oblong tablets or capsules by dipping these dosage forms into the coating solution [15]. These instruments enable the coating of a certain number of units simultaneously, and the coating solution can be used for several batches subsequently. However, dip coating presents several challenges for the formulator because the immersion of the dosage form in the coating solution is far more stressful than spraying or atomizing the solution on the pharmaceutical form. In addition, there are several variables to be optimized, such as the choice of the polymer, its percentage in the solution, the type and amount of plasticizer, the choice of solvents, and the formulation of the dosage form to be coated. Moreover, the success of the coating also depends on the process parameters, including the immersion time, the removal of excess liquid, and the type and duration of drying. Very few pieces of data are available for the process carried out through the immersion coating procedure, and most users rely on indications derived from studies performed with traditional spray-based methods. Among the published data, Moghimipour et al. [16] studied the effect of multiple coating layers of Eudragit FS 30D, an aqueous dispersion of methacrylic acid–methyl methacrylate copolymers, while Fülöpová et al. [17] evaluated the application of three types of enteric coating polymers on gelatin capsules or DRcaps®. Interestingly, the last study demonstrated that the coated gelatin capsules never achieved gastro-resistance, regardless of the type of polymer coatings and the concentration of the dispersions. In both cases, the coating process was not described.

The aim of this study was to assess the immersion coating of gelatin capsules using commercially available equipment to achieve standardized results. Two different grades of two enteric coating polymers were chosen, specifically Eudragit® S100, Eudragit® L100 (acrylic-based polymers), HPMC AS-MF, and HPMC AS-HF (cellulose-based polymers). Coating was carried out using organic polymer dispersions at two concentration levels. The capsules were filled with a formulation containing two model

APIs with significantly different water solubility: paracetamol (AAP), defined as sparingly soluble by the European Pharmacopoeia (EP), and tramadol hydrochloride (Tram), reported by the EP as very soluble in water. The solubility of both drugs is pH-independent under the tested conditions (pKa of 9.38 and 9.41 for AAP and Tram, respectively [18,19]). The results were compared with those obtained through the ECDDT approach, using both single and cap-in-cap DRcaps® or Vcaps®.

2. Results and Discussion

2.1. Coating solution rheology

The rheological analyses were performed to assess the rheological behavior of the prepared coating solutions and to explore variations among formulations with different polymers and varying percentages of the added polymer.

All the samples exhibited a power law index within the range of 0.96–1.01, indicating a linear increase in stress with the applied shear rate (Figure 1, left panel). Consequently, the samples displayed Newtonian behavior. The viscosity of the coating solution increased proportionally with the polymer content in the formulation. Specifically, formulations containing 10% polymer exhibited a viscosity approximately 8–10 times higher than those with a concentration of 5%. Samples prepared with cellulose derivatives demonstrated higher viscosity compared to Eudragit counterparts at all concentrations. However, no discernible differences were observed between samples containing Eudragit-type or cellulose-type polymers (Figure 1, right panel). In all cases, the viscosity of the samples consistently fell within the ideal range of 0.15–0.4 Pa*s for coating solutions applied with standard methods [20].

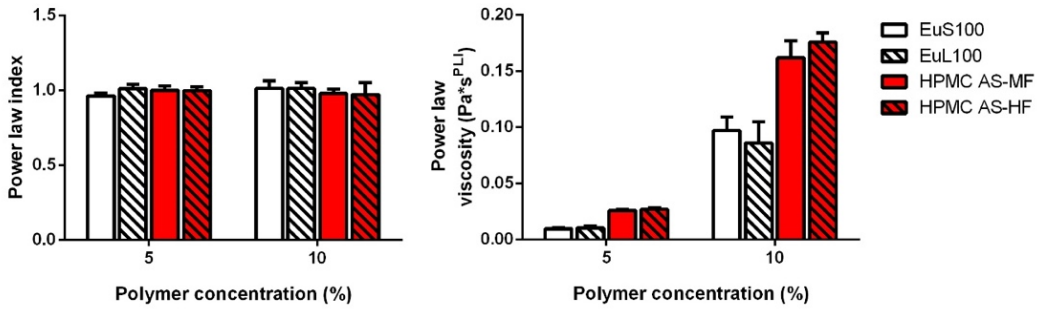

Figure 1. *Effect of polymer type and concentration on the power law index (left panel) and the power law viscosity (right panel) as determined from a power law modelling of the viscometry data.*

2.2 Dissolution studies

The initial preliminary test conducted involved the dissolution of the uncoated capsules filled with the formulations of both drugs, AAP and Tram. The release rate of both APIs exhibited rapid release initially, reaching a semi-steady state around 20 min at pH 1.5 and 30 min at pH 6.8. This discrepancy at the two pH is consistent with the basic nature of the two drugs. Minimal differences were observed between the two APIs, particularly in the minutes before reaching the plateau, where Tram, owing to its higher water solubility, demonstrated a faster release (Figure 2).

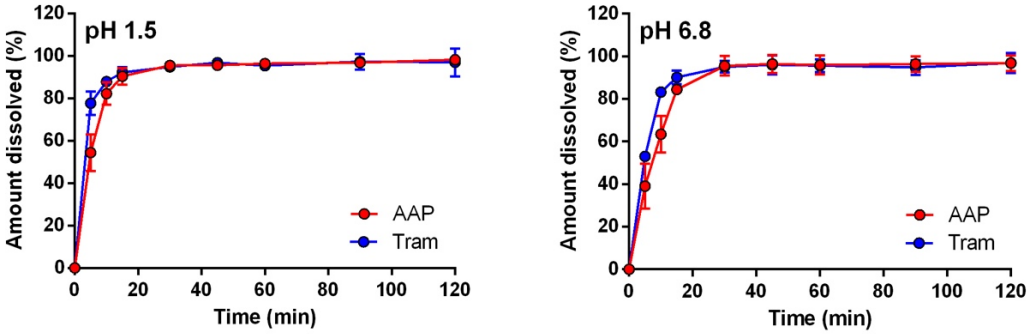

Figure 2. *Release profiles of uncoated capsules containing AAP or Tram at pH 1.5 and 6.8.*

2.2.1 Capsules coated with Eudragit polymers

The results of applying EuS100 at two concentrations for both AAP and Tram capsules are presented in Figure 3A. In all cases, the Eudragit S100 coating ensured an enteric release, with no significant drug release in the acidic medium, meeting the criteria for being considered gastro-resistant. However, differences were observed in the release kinetics in the intestinal-like fluid, dependent on the polymer concentration in the coating dispersion and the type of drug. Specifically, an increase in polymer concentration from 5% to 10% resulted in incomplete drug release after two hours (after two hours, the amount of drug release at pH 6.8 was around 60 and 70% for AAP and Tram, respectively). This aspect was more pronounced for AAP than for Tram, and it can likely be attributed to their different solubilities.

The results exhibited marked differences when EuS100 was replaced with EuL100 (Figure 3B). Specifically, at the lowest polymer concentration, the coating failed to prevent the dissolution of AAP or Tram in the acidic medium. Similarly, tramadol capsules coated with 10% EuL100 dispersion yielded the same outcome. In all the cases, the capsules did not open during the tests and were intact from a macroscopic point of view. On the other hand, when applying the coating from the 10% formulation to AAP

capsules, no significant amount of drug was detected in the first two hours, while a rapid and complete release was observed in the intestinal-like fluid.

The results obtained with both types of Eudragit were surprising. While differences at pH 6.8 were expected due to the distinct features of the polymers, the outcomes at acidic pH were less predictable. In theory, both polymers should guarantee acid resistance. However, these results were always achieved using the highest polymer concentration in the presence of the lower solubility drug (AAP) or using EuS100. Interestingly, Fülöpová et al. [17] presented work on the coating of capsules using an immersion procedure. The authors evaluated EuS100-coated capsules filled with caffeine. Despite the application methods and polymer solution concentration being very similar with those of the present work, their coated capsules systematically failed the release test in the acid environment. Some results were obtained also using a formulated mixture of methacrylate-based polymers (Acryl-EZE). From the other side, the coated hypromellose capsules using a standard drum coating equipment seemed to provide different results. In fact, Fu et al. [21] reported gastro-resistance in capsules coated with different types of polymers, among which also EuSL100, although only disintegration and acid uptake tests were carried out. Apparently, in the work of Fu et al., the capsules were empty so that any influence of the excipients or APIs could not be hypothesized.

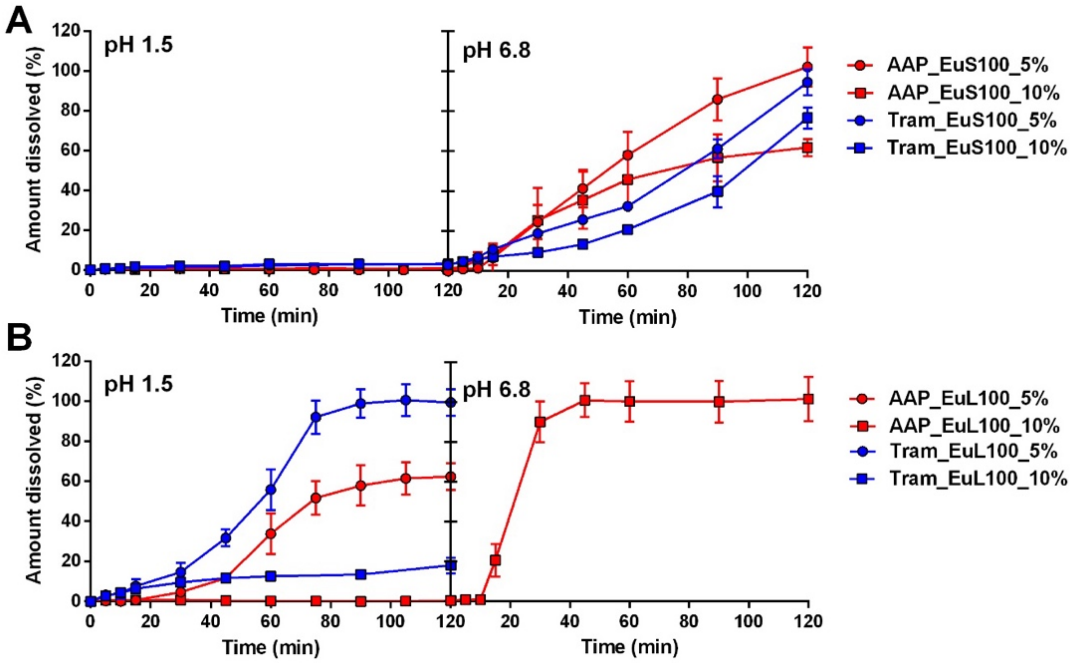

Figure 3. *Release profiles of capsules containing AAP or Tram coated with EuS100 (A) and EuL100 (B).*

2.2.2 Capsules coated with Hypromellose acetate succinate polymers

The same analysis was conducted on AAP and tramadol capsules coated with the two grades of hypromellose acetate succinate, HPMC AS-MF and HPMC AS-HF (Figure 4A and B, respectively). In all cases, regardless of the drug type, polymer amount, or grade, the capsules demonstrated drug release in the acidic medium, indicating the failure of these formulations in ensuring the enteric release of the APIs. Upon comparing the dissolution results of all the coated capsules, the best performance was observed with HPMC AS-HF applied from a 10% polymer dispersion, although it did not meet the EP requirements. Once again, the role of drug solubility is evident; the amount of drug released from capsules with the same coating is consistently higher in the presence of Tram, even if only when the coating provides a certain gastro-resistance (HPMC AS-HF). HPMC AS films are commonly used for the preparation of enteric-protected solid oral dosage forms. Fu et al. [22] reported gastro-resistance also for capsules coated with HPMC AS grades M and H, even if only through disintegration and acid uptake tests. Interestingly, HPMC AS grade H gave the same acid uptake as EuL100, while grade M reported the worst performance although also within the acceptance limits. So, the rank in term of acid resistance suggested by those authors is comparable with the results of our work, also taking into account that gastro-resistance was obtained only with EuL100 at the highest concentration and AAP as API.

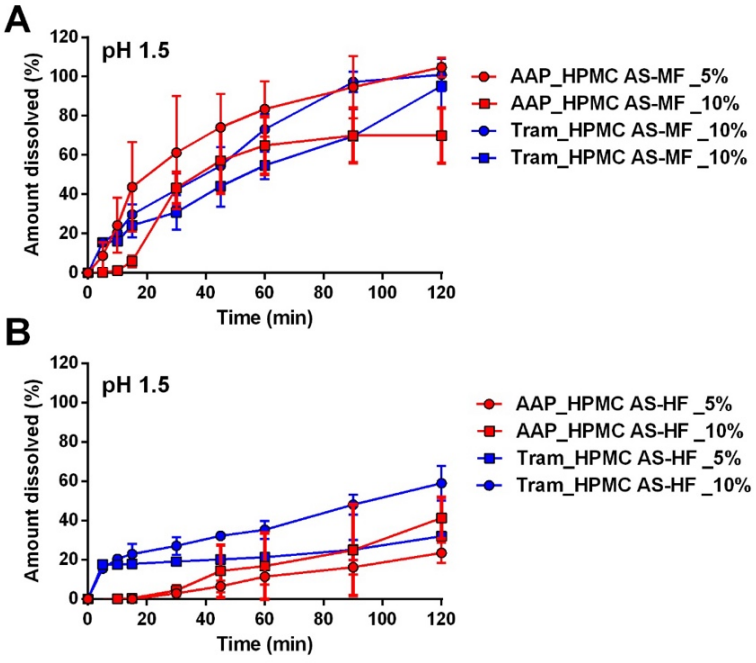

Figure 4. *Release profiles of capsules containing AAP or Tram coated with HPMC AS-MF (A) and HPMC AS-HF (B).*

HPMC AS films are commonly employed in the formulation of enteric-protected solid oral dosage forms, such as tablets or pellets. The existing literature suggests that the successful achievement of enteric formulations is dependent on the thickness of HPMC AS films [22]. To investigate and validate this hypothesis, a double coating (DC) was applied to the capsules. The DC process, involving two coating applications with a 10% polymer solution, was chosen to prevent an excessive increase in the viscosity of the polymer solution. As a result, the DC procedure led to a notable increase in the weight of the capsules, from approximately 2% to 6–8% and, consequently, an augmentation in the coating thickness. However, despite the enhancement in gastric resistance (see Figure S1), it still falls short of achieving the required values (less than 10% drug release in an acidic medium). Therefore, it is likely that an even greater quantity of polymers would need to be added, although such an approach may not be practically viable in immersion coating due to the excessively long time required for coating capsules.

The inadequacy of HPMC AS in capsule coating could also be attributed to other factors, such as the insufficient adherence of the coating to the capsule surface. Typically, coatings are applied to tablets or pellets with a microscopic rough surface, facilitating the adhesion process. In contrast, capsules have a much smoother surface, potentially complicating the adhesion process. Additionally, a high interfacial tension could impede the uniform spreading of the polymer solution on the gelatin surface, resulting in uneven film formation. To validate this hypothesis, it was decided to use hypromellose capsule shells instead of gelatin. The hypromellose capsules were filled with the identical formulation as the gelatin capsules, incorporating the same APIs and excipients. Subsequently, they were coated with film solutions containing HPMC AS-MF at 10% and 10% DC. The drug dissolution profile (Figure 5) seems to confirm the hypothesis, as formulations containing AAP in hypromellose capsules do not release the API in the gastric medium when coated with a film containing 10% and 10% DC of HPMC AS-MF. However, the same phenomenon does not occur with capsules containing Tram, underscoring once again that the drug's solubility directly influences the performance of the film coating.

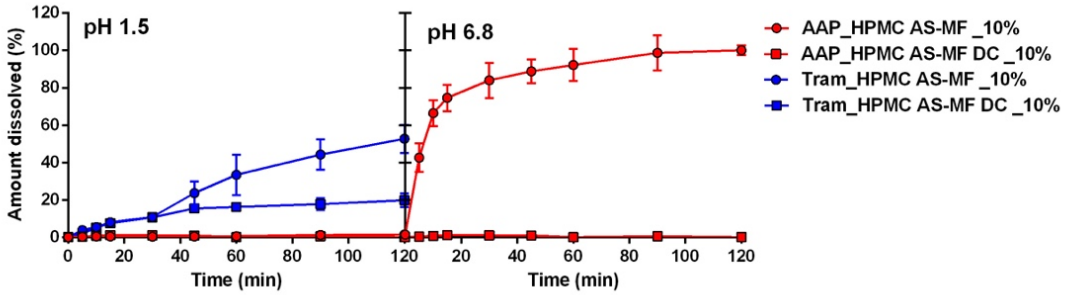

Figure 5. *Release profiles of hypromellose capsules containing AAP or Tram coated with HPMC AS-MF single and double (DC) coating.*

2.2.3 Commercial capsules for enteric/delayed release

An alternative approach to preparing gastro-resistant capsules involves the use of capsule shells made from specific polymers designed to ensure release in the stomach. DRcaps® are delayed release capsules composed of hypromellose and Gellan gum. The manufacturing company guarantees a release retention for about 45 min, and they are evidently not intended for the preparation of gastro-resistant capsules. Nevertheless, they are at times employed for this purpose in galenic preparations. More frequently, in the compounding of medicines within pharmacy laboratories, they are utilized to prepare gastro-resistant capsules using the cap-in-cap approach—where a filled DRcaps® is placed within a larger DRcaps®. In this manuscript, both single and cap-in-cap DRcaps® were evaluated using the same formulations employed for the coated capsules. As expected, the single DRcaps® did not prevent any drug release in the gastric environment for the required time (Figure 6A). When using a highly soluble API like Tram, the DRcaps® was also unable to ensure delayed release; instead, it exhibited a sustained release pattern following an almost zero-order kinetic. On the other hand, when using AAP, the release results were in line with the indications provided by the DRcaps® manufacturer. The cap-in-cap approach yielded completely different results (Figure 6B). The dissolution of AAP in the acid medium and in the phosphate buffer was almost negligible, indicating that using one DRcaps® inside another completely prevented AAP release for at least 4 h. Conversely, when employing a highly soluble drug like Tram, the cap-in-cap approach provided gastro-protection without preventing release in the basic environment. However, at pH 6.8, the dissolution rate of tramadol was very slow, and after 2 h, the amount of dissolved drug was below 30%. Additional attempts to achieve enteric release of the drug was carried out by placing a standard gelatin capsule inside a DRcaps® (Figure 6B). Once again, no proper gastro-resistant capsules were obtained. In

those cases, the dissolution kinetics resembled that of delayed release dosage forms, with a lag time of approximately 45 min, independent of the drug solubility. The latest result indicates that if the capsule shell is not in direct contact with the powder, the release rate is almost entirely controlled by the external capsule, in this case, a DRcaps®.

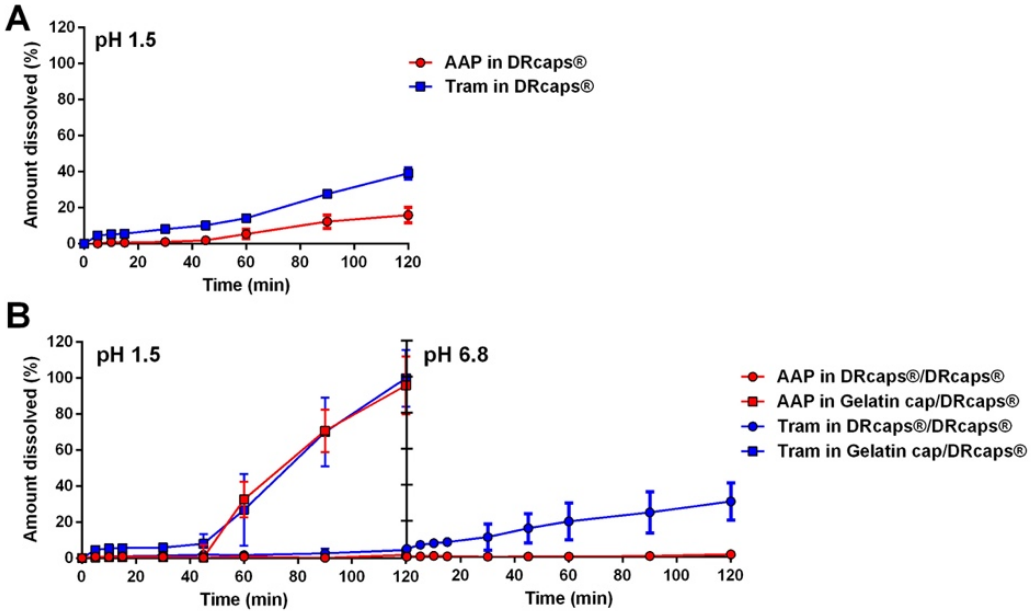

Figure 6. *Release profiles of DRcaps® capsules containing AAP or Tram (A) and of different combinations of DRcaps® in the cap-in-cap method (B).*

The other type of commercial capsules evaluated were the Vcaps Enteric®. These capsule shells are composed of a mixture of HPMC and HPMC AS, aiming to ensure a pH-dependent release of the API due to the presence of a polymer with pH-dependent solubility (HPMC AS). The dissolution tests were initially carried out on Vcaps filled with the same formulations used for all the previous evaluations, mixtures of silicified MCC with AAP or Tram. The results were surprising (figure 7), with the API beginning to be released in the first 45 min, in accordance with the drug solubility. However, the behavior of these capsules differed from that observed in the previous tests, as they were characterized by an unusual and unexpected event: after a short period of time in the acid medium, a gradual separation of the capsule's cap from the body occurred, reaching the point where the two parts of the capsule shell appeared completely separated in most of the capsules tested. The failure of Vcaps with several APIs was reported by Moghrabi and Fadda [14]. The authors attributed these results to different deformation rates of the cap and body, leading to a certain opening at the junction of these two pieces. On the other hand, successful enteric release with Vcaps was reported for Octreotide acetate [23]

and ketoconazole [24], although using very particular formulations such as spray-dried microparticles and amorphous solid dispersions (prepared with other enteric polymers). From our analysis as well as from those reported in the literature, it cannot be conclusively determined whether the cap and body separation is intrinsically due to the design of Vcaps or if it is related to some defect in the batch used; however, it is likely that the presence of swelling materials inside the capsule may contribute to their opening. The formulation used for capsule filling was composed of 86.5% SMCC, an excipient consisting of microcrystalline cellulose and colloidal silicon dioxide. This material is insoluble in water, but when in contact with an aqueous phase, it absorbs water and swells. Any capsule shell cannot completely prevent the diffusion of water, and in the presence of swellable materials, an increase in internal pressure is expected. To prove this hypothesis, it has been decided to test different formulations where the SMCC was substituted with anhydrous lactose (LAC) or anhydrous dibasic calcium phosphate (DCP). LAC is a compound soluble in water but is unable to swell when in contact with it, while DCP is practically insoluble in water and does not exhibit swelling when in contact with water. The dissolution data (figure 7) showed a slight improvement in the presence of LAC, with a lower amount of dissolved API compared to that released with the formulation containing SMCC. However, it was still possible to observe the separation of the capsule's cap from its body. No macroscopic differences were observed in the separation process, and the lower release rate of the two drugs is very likely due to the solubility of the excipient. In fact, the presence of a highly soluble compound slows down the API dissolution process as both compete for water. In the presence of DCP, the dissolution profile exhibited a drastic improvement, although an enteric release was possible only for the less soluble drug, namely AAP (figure 7). These results do not allow for an exact definition of the relevance of swelling; however, they certainly highlight the role of compound solubility in capsules designed for enteric release. The presence of materials capable of interacting with water represents a significant factor in the possible failure of the formulation. The pivotal influence of certain physicochemical properties of APIs and excipients was previously reported by Moghrabi and Fadda [14]. The results reported here complement their analysis, contributing to providing a much more defined picture of the real applicability of Vcaps.

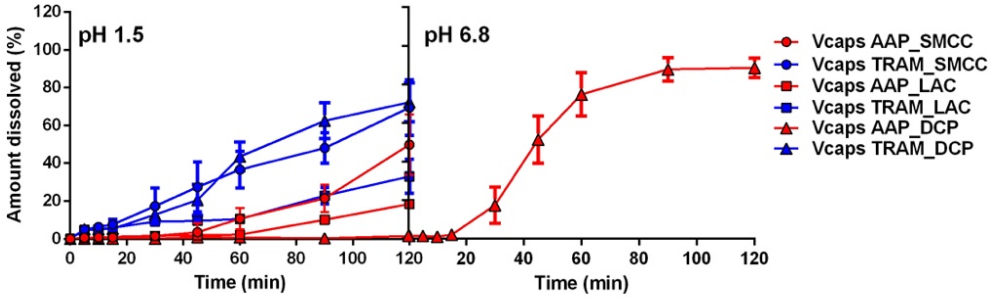

Figure 7. *Release profiles of Vcaps capsules containing AAP or Tram as API and silicified microcrystalline cellulose (SMCC), anhydrous lactose (LAC) and anhydrous Dibasic Calcium Phosphate (DCP) as filler.*

Finally, we need to report that very recently Evonik industries launched a new platform of ready-to-fill capsules: EUDRACAP™ [25]. The platform is constituted by hypromellose capsules coated with Eudragit polymers, and according to the results of the present manuscript, they could represent ideal solutions for preparation of enteric-coated capsules. At the moment, there are no published independent results to support (or discourage) the use of EUDRACAP.

3. Materials and Methods

3.1. Materials

Paracetamol and tramadol HCl (both supplied by Janssen Pharma) were chosen as model drugs. Methacrylic acid–methyl methacrylate copolymers (Eudragit S100 and L100) were from Evonik Industries (, Essen, Germany). Hypromellose acetate succinate (MF and HF grades) were obtained from Shin-Etsu Chemical (, Tokyo, Japan). Silicified microcrystalline cellulose (Prosolv sMCC90, JRS Pharma, , Rosenberg, Germany), anhydrous lactose (SuperTab 24AN, DFE Pharma, , Goch, Germany) anhydrous dibasic calcium phosphate (DI-CAFOS A 60, Budenheim, , Budenheim, Germany), and Triethyl Citrate (RoFarma Italia, , Gaggiano, Italy) were used as received. Isopropanol (Carlo Erba, , Cornaredo, Italy) and Yellow Eosin (Carlo Erba, IT) were of standard chemical grades. Gelatin capsules were purchased from ACEF (Fiorenzuola D'Arda, Italy), while HPMC cps (size 0), DRcaps® (size 2 and size 0), and Vcaps® Enteric capsules (size 0) were obtained from Lonza (Lonza Capsules & Health Ingredients, Basel, Switzerland).

Throughout the text, the following abbreviations are used: paracetamol (AAP), tramadol HCl (Tram), Eudragit S100 (EuS100), Eudragit L100 (EuL100), hypromellose acetate succinate MF (HPMC AS-MF), hypromellose acetate succinate HF (HPMC AS-HF),

Triethyl Citrate (TEC), Prosolv sMCC90 (SMCC), SuperTab 24AN (LAC), DI-CAFOS A 60 (DCP), and isopropanol (Iso).

3.2. Blends preparation and capsule filling

Powder blends were prepared with a composition of 13.5% active pharmaceutical ingredient (API), either AAP or TRA, and 86.5% excipients (SMCC, LAC, or DCP), using a V-shaped mixer (Laboratori Mag divisione Artha, Garbagnate Milanese, Italy) operating at 50 rpm for 5 min. After preparing the blends, capsules were filled using a semi-automatic machine (FLY 120 NEW, AD Pharm, San Vendemiano, Italy) capable of filling up to 120 capsules. Each capsule contained 0.035 g of API and 0.225 g of excipients. All prepared capsules underwent evaluation for weight uniformity, and any capsules with a variation exceeding 10% (according to EP standards) of the theoretical weight were excluded from the study. A summary of capsules content is reported in Supplementary Table S1.

3.3. Coating solution formulation

A preliminary analysis was carried out by immersing capsule shells in 50 mL mixtures composed of various iso–water ratios for 30 s to assess their resistance. The immersion duration was chosen in accordance with the recommendations of the coating equipment manufacturer. The maximum allowable water content was 8% (higher values determined capsule deformation), leading to the utilization of the iso–water ratio of 92:8 in formulating the coating solutions. The final formulations were prepared in a mixture of iso–water 92:8, employing four different polymers—EuS100, EuL100, HPMC AS-MF, and HPMC AS-HF—at concentrations of 5% and 10%. TEC was utilized as a plasticizer at a concentration of 10% with respect to the weight of the polymers. Yellow Eosin at 0.05% was added for coloration of the coating. The composition of all formulations is detailed in Table 1.

Table 1. Coating solution compositions.

Component	5% Polymer Formulation	10% Polymer Formulation
	Amount (%) *	Amount (%) *
Polymer **	5	10
TEC	0.5	1
Yellow Eosin	0.05	0.05
Iso–water (92:8) mixture	94.45	88.95

* Percentage respect to the total solution weight. ** EuS100, EuL100, HPMC AS-MF, and HPMC AS-HF.

3.4. Film solution rheology

The viscosity of the coating solutions, as outlined in Table 1, was assessed (n = 3) using a rotational rheometer (Kinexus Lab+, Malvern, UK) equipped with a C40/4 geometry. The analysis involved incrementally increasing the shear rate from 1 to 150 s^{-1} and measuring the shear stress at 25 °C. The gathered data were graphically represented as a plot of shear rate versus stress and subsequently analyzed using a power law model:

$$\sigma = PLV\ \gamma^{\wedge PLI} \quad (1)$$

where g is the shear rate, s is the yield stress, PLV is the power law viscosity (or consistency index), and PLI is the power law index (or flow index). The power law model is able to describe the flow behavior of Newtonian, pseudoplastic, or shear-thickening samples.

3.5. Capsule coating

The capsules were coated using ProCoater® (Torpac, NL) equipment. This instrument employed a dip-based method for coating capsules or oblong tablets. The coating process was carried out according to the manufacturer's instructions. In brief, the capsules were positioned in the holder and subsequently immersed in the coating solution for 30 s. Following immersion, excess liquid was removed by scrolling, and the holder with the capsules was then placed in an oven at 40 °C for 20 min. At the end of this step, only one half of each capsule was coated. The same procedure was repeated by overturning the holder to coat the other half of the capsules, ensuring complete coverage of the entire shell. This process was repeated for all the coating solutions in Table 1, resulting in the preparation of 40 coated capsules for each formulation. Images of the initial capsules as well as of capsules after the two coating steps are reported in supplementary figure S2.

3.6. Dissolution studies

Dissolution tests was carried out using a USP dissolution apparatus type I at 50 rpm (AT7 Smart, Sotax, Nordring, Switzerland), according to the EP [26]. The dissolution procedure for the capsules involved two consecutive steps:

- The dosage forms were positioned in the basket within the vessel, where a liquid simulating stomach conditions (pH 1.5) was previously introduced and heated to 37 °C. In this medium, the capsules were expected to remain stable without releasing the API; the maximum allowable drug release was set at 10% or less [26] over a 2 h period.

- Immediately following the first step, the basket containing the capsules was transferred to a vessel filled with a liquid simulating intestinal fluids (pH 6.8) and left for an additional two hours.

Samples (1 mL) of the dissolution medium were collected using a syringe with 0.45 μm filters (Minisart syringe filter, sartorius, DE) at specific intervals during the dissolution tests:

- Gastric-like medium (minutes): 5-10-15-30-45-60-75-90-105-120;
- Intestinal-like medium (minutes): 5-10-15-30-45-60-90-120.

The drug content in these samples was determined using UV spectroscopy (UV-1800 Shimadzu, Kyoto, Japan) at wavelengths of 242.5 nm for AAP and 271 nm for Tram. Preliminarily, a calibration curve at the two wavelengths was built for both the API in the concentration range of 0.005–0.042 mg/mL (the coefficients of determination r^2 were 0.998 and 0.999 for AAP and Tram, respectively).

Each formulation underwent assessment in triplicate at a minimum.

4. Conclusions

This work provides insight into the current options for personalized administration using capsules of APIs requiring enteric release. The formulation of successful enteric coating capsules using immersion methods requires a deep understanding of the properties of APIs and particularly of the enteric polymers. The success of the formulations is strongly related to the solubility of the drug, and the type and amount of polymer included are crucial elements as well. From this perspective, the use of Eudragit S100 is strongly suggested since it assures high robustness of the process, allowing the obtaining of an enteric preparation without a complex development phase.

On the other hand, the use of commercially available capsules does not appear to be an easier or feasible option. The cap-in-cap technique with DRcaps® proved inadequate to guarantee an enteric release of the drugs, and the use of a single DRcaps® was insufficient to prevent the release of the API in the gastric-like medium. Vcaps Enteric were able to produce enteric release dosage forms, but their performance appears strongly related to the characteristics of the active ingredient and excipients used.

References

1. Salawi, A. Pharmaceutical Coating and Its Different Approaches, a Review. *Polymers (Basel).* **2022**, *14*, doi:10.3390/polym14163318.

2. Seo, K.-S.; Bajracharya, R.; Lee, S. H.; Han, H.-K. Pharmaceutical Application of Tablet Film Coating. *Pharmaceutics* **2020**, *12*, doi:10.3390/pharmaceutics12090853.

3. Faisal, W.; Farag, F.; Abdellatif, A. A. H.; Abbas, A. Taste Masking Approaches for Medicines. *Curr. Drug Deliv.* **2018**, *15*, 167–185, doi:10.2174/1567201814666171013145958.

4. Joshi, S.; Petereit, H.-U. Film coatings for taste masking and moisture protection. *Int. J. Pharm.* **2013**, *457*, 395–406, doi:10.1016/j.ijpharm.2013.10.021.

5. Odani, N.; Mohan, S.; Kato, E.; Feng, H.; Li, Y.; Hossain, M. N.; Drennen, J. K.; Anderson, C. A. Determining the effect of photodegradation on film coated nifedipine tablets with terahertz based coating thickness measurements. *Eur. J. Pharm. Biopharm.* **2019**, *145*, 35–41, doi:https://doi.org/10.1016/j.ejpb.2019.09.024.

6. Felton, L. A.; Porter, S. C. An update on pharmaceutical film coating for drug delivery. *Expert Opin. Drug Deliv.* **2013**, *10*, 421–435, doi:10.1517/17425247.2013.763792.

7. Siepmann, F.; Siepmann, J.; Walther, M.; MacRae, R. J.; Bodmeier, R. Polymer blends for controlled release coatings. *J. Control. release Off. J. Control. Release Soc.* **2008**, *125*, 1–15, doi:10.1016/j.jconrel.2007.09.012.

8. Rhodes, C. T.; Porter, S. C. Coatings for controlled-release drug delivery systems. *Drug Dev. Ind. Pharm.* **1998**, *24*, 1139–1154, doi:10.3109/03639049809108573.

9. Stubbe, B. G.; De Smedt, S. C.; Demeester, J. "Programmed Polymeric Devices" for Pulsed Drug Delivery. *Pharm. Res.* **2004**, *21*, 1732–1740, doi:10.1023/B:PHAM.0000045223.45400.01.

10. Maderuelo, C.; Lanao, J. M.; Zarzuelo, A. Enteric coating of oral solid dosage forms as a tool to improve drug bioavailability. *Eur. J. Pharm. Sci.* **2019**, *138*, 105019, doi:https://doi.org/10.1016/j.ejps.2019.105019.

11. Franc, A.; Vetchý, D.; Fülöpová, N. Commercially Available Enteric Empty Hard Capsules, Production Technology and Application. *Pharmaceuticals* 2022, *15*.

12. Barbosa, J. A. C.; Al-Kauraishi, M. M.; Smith, A. M.; Conway, B. R.; Merchant, H. A. Achieving gastroresistance without coating: Formulation of capsule shells from

enteric polymers. *Eur. J. Pharm. Biopharm. Off. J. Arbeitsgemeinschaft fur Pharm. Verfahrenstechnik e.V* **2019**, *144*, 174–179, doi:10.1016/j.ejpb.2019.09.015.

13. Zema, L.; Loreti, G.; Melocchi, A.; Maroni, A.; Palugan, L.; Gazzaniga, A. Gastroresistant capsular device prepared by injection molding. *Int. J. Pharm.* **2013**, *440*, 264–272, doi:10.1016/j.ijpharm.2012.05.071.

14. Moghrabi, F. S.; Fadda, H. M. Drug Physicochemical Properties and Capsule Fill Determine Extent of Premature Gastric Release from Enteric Capsules. *Pharmaceutics* **2022**, *14*, doi:10.3390/pharmaceutics14112505.

15. Torpac Inc PRO COATER Enteric / Film Coat Capsules & Caplets Available online: https://torpac.com/procoater/coater-main.htm (accessed on Feb 5, 2024).

16. Moghimipour, E.; Rezaei, M.; Kouchak, M.; Fatahiasl, J.; Angali, K. A.; Ramezani, Z.; Amini, M.; Dorkoosh, F. A.; Handali, S. Effects of coating layer and release medium on release profile from coated capsules with Eudragit FS 30D: an in vitro and in vivo study. *Drug Dev. Ind. Pharm.* **2018**, *44*, 861–867, doi:10.1080/03639045.2017.1415927.

17. Fülöpová, N.; Pavloková, S.; DeBono, I.; Vetchý, D.; Franc, A. Development and Comparison of Various Coated Hard Capsules Suitable for Enteric Administration to Small Patient Cohorts. *Pharmaceutics* **2022**, *14*, doi:10.3390/pharmaceutics14081577.

18. National Center for Biotechnology Information PubChem Compound Summary for CID 1983, Acetaminophen Available online: https://pubchem.ncbi.nlm.nih.gov/compound/Acetaminophen. (accessed on Nov 4, 2023).

19. Smyj, R.; Wang, X.-P.; Han, F. Chapter Eleven - Tramadol Hydrochloride. In *Profiles of Drug Substances, Excipients, and Related Methodology*; Brittain Excipients and Related Methodology, H. G. B. T.-P. of D. S., Ed.; Academic Press, 2013; Vol. 38, pp. 463–494 ISBN 1871-5125.

20. DOW Methocel Cellulose Ethers in Aqueous Systems for Tablet Coating 2002.

21. Fu, M.; Blechar, J. A.; Sauer, A.; Al-Gousous, J.; Langguth, P. In Vitro Evaluation of Enteric-Coated HPMC Capsules—Effect of Formulation Factors on Product Performance. *Pharmaceutics* **2020**, *12*, doi:10.3390/pharmaceutics12080696.

22. Obara, S.; Kokubo, H. Application of HPMC and HPMCAS to Aqueous Film Coating of Pharmaceutical Dosage Forms. In *Aqueous Polymeric Coatings for Pharmaceutical Dosage Forms*; McGinity, J. W., Felton, L., Eds.; Informa Healthcare USA, Inc.: New york, 2008.

23. Li, T.; Wan, B.; Jog, R.; Costa, A.; Burgess, D. J. Pectin microparticles for peptide delivery: Optimization of spray drying processing. *Int. J. Pharm.* **2022**, *613*, 121384, doi:10.1016/j.ijpharm.2021.121384.

24. Monschke, M.; Kayser, K.; Wagner, K. G. Influence of Particle Size and Drug Load on Amorphous Solid Dispersions Containing pH-Dependent Soluble Polymers and the Weak Base Ketoconazole. *AAPS PharmSciTech* **2021**, *22*, 44, doi:10.1208/s12249-020-01914-7.

25. Evonik Industries AG READY-TO-FILL COATED CAPSULES FOR FAST DRUG DEVELOPMENT Available online: https://healthcare.evonik.com/en/drugdelivery/oral-drug-delivery/oral-excipients/eudracap-portfolio (accessed on Mar 17, 2024).

26. Chapter 2.9.3, Dissolution Test for Solid Dosage Form. In *European Pharmacopoeia 10.0*; Strasbourg.

This paper has been published on Pharmaceuticals as open access (CC-BY license).

DOI: https://doi.org/10.3390/ph17040433

Supplementary materials

"Exploring Immersion Coating as a Cost-Effective Method for Small-Scale Production of Enteric-Coated Gelatin Capsules"

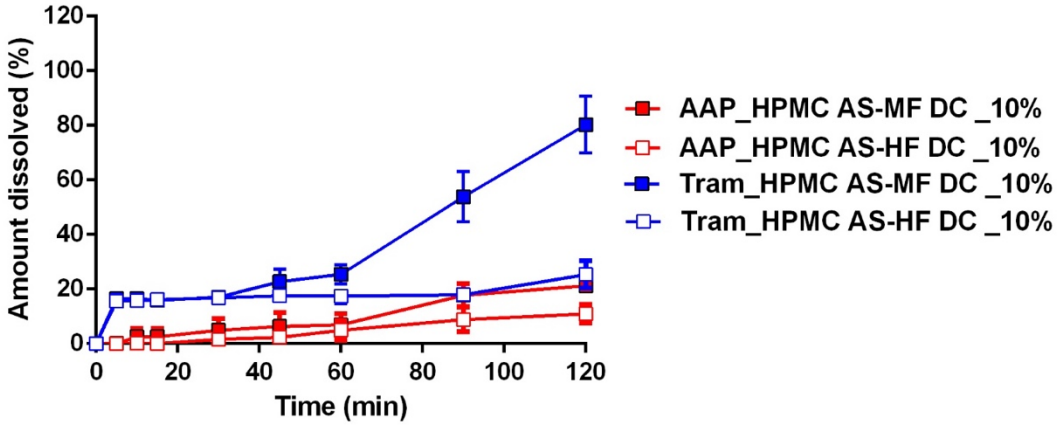

Figure S1. Release profiles of capsules containing AAP or Tram double coated (DC) with HPMC AS-MF and HPMC AS-HF.

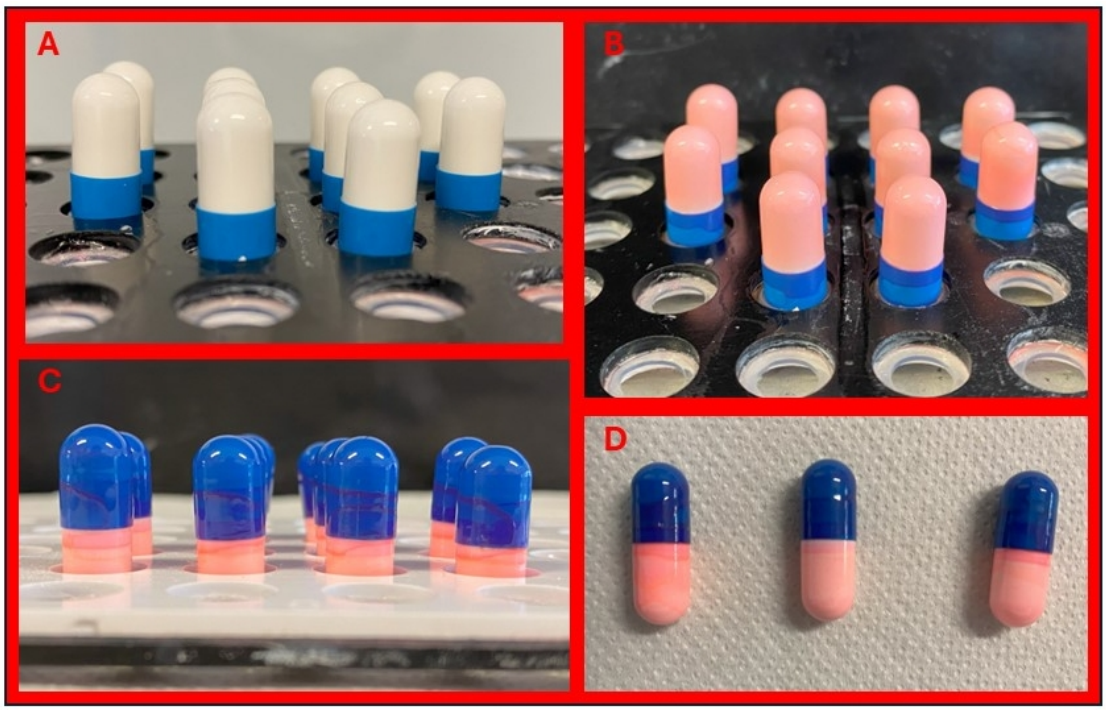

Figure S2. Images of capsule before, during and after the coating process. A) un-coated capsules; B) Capsules after the first step of coating and drying (coating of the lower half, that is the body and part of the cap); C) Capsules after the second step of coating and drying (coating of the higher half, that is the cap and part of the body); D) Coated capsules removed from the holder.

Table S1. Capsule content for each type of type of enteric capsule system tested.

Tested capsules	Capsules content	
	API (35 mg)	Excipients (225 mg)
Un-coated capsules	AAP	SMCC
Un-coated capsules	Tram	SMCC
AAP_EuS100	AAP	SMCC
Tram_EuS100	Tram	SMCC
AAP_EuL100	AAP	SMCC
Tram_EuL100	Tram	SMCC
AAP_HPMC AS-MF	AAP	SMCC
Tram_HPMC AS-MF	Tram	SMCC
AAP_HPMC AS-HF	AAP	SMCC
Tram_HPMC AS-HF	Tram	SMCC
AAP in DRcaps®	AAP	SMCC
Tram in DRcaps®	Tram	SMCC
AAP in DRcaps®/ DRcaps®	AAP	SMCC
Tram in DRcaps®/ DRcaps®	Tram	SMCC
AAP in gelatin caps/ DRcaps®	AAP	SMCC
Tram in gelatin caps/ DRcaps®	Tram	SMCC
Vcaps AAP_Lac	AAP	LAC
Vcaps Tram_Lac	Tram	LAC
Vcaps AAP_SMCC	AAP	SMCC
Vcaps Tram_SMCC	Tram	SMCC
Vcaps AAP_DCP	AAP	DCP
Vcaps Tram_DCP	Tram	DCP

4. A Comprehensive Study of Flowability Indexes for Pharmaceutical Applications and their modelling

Abstract:

The evaluation of bulk solids flowability is crucial in several industrial processes, including those used for the preparation of pharmaceutical OSD. Despite this, achieving a comprehensive understanding of this property is still challenging. This study investigates compendial flow indexes (FIs) of samples with different physical- chemical characteristics in terms of precision, Intra-day precision, alongside statistical evaluation of their relationship and their modelling. Our findings revealed that only HR and ffc assure high precision in the entire range of measured values.

The three FIs did not uniformly correlate across the entire range of flowability, suggesting potential influences from diverse properties or variations in their relative influence. Moreover, the modelling of the FIs resulted in better predictions for HR, followed by ffc; both modelling procedures, including regressions and neural networks, provided almost comparable results. The results of this research provide an advanced understanding of bulk solids flowability assessment, offering insights into flow indexes' relationships and predictive modelling for pharmaceutical applications.

Keywords:

Lactose; microcrystalline cellulose; dicalcium phosphate; Schulze shear cell; Flow Function (ffc); powder flow-meter.

Paper submitted to Powder Technology

1. Introduction

Solid dosage forms such as tablets and capsules are the most common pharmaceutical dosage forms due to several advantages they possess. Among these, the high compliance for most patient groups, ease and rapidity of production, suitability for most Active Pharmaceutical Ingredients (APIs), and lower cost compared to many other dosage forms. From an industrial perspective, significant progress has been observed in manufacturing processes for their preparation over the last decades. The industrial equipment has been constantly upgraded to enable the use of unprocessed powder materials, particularly through the direct compression process (DC) or continuous manufacturing approaches, operating at high velocity to reduce manufacturing time and costs [1]. To produce tablets through the DC process at high speed, the materials must possess specific features, among which flowability is one of the critical ones [2,3]. Flowability represents the ability of a material to flow under gravity or external forces through an orifice or along an inclined surface. Powders with poor flowability tend to remain blocked in the hopper of the tableting machine or capsule filler machine or are unable to fill the die or capsules in a homogeneous manner. As a result, tablets or capsules lack consistency in term of weight and are not suitable for commercialization [4].

Understanding and optimizing the flow behaviour of bulk solids is crucial for the pharmaceutical industry, as well as in other manufacturing fields. Flowability, a derived property, is influenced by a combination of intrinsic (fundamental) and physical-chemical properties like particle size distribution, shape, density, surface properties, moisture content, and cohesive forces. This understanding is essential for designing equipment, storage systems, and producing additives that enhance flow efficiency. Quantifying material flowability is also significant, indeed various flowability indexes (FI's) are described in the literature, ranging from specific applications to broader usage [5–10]. In the pharmaceutical field, common FIs include those outlined in the European Pharmacopoeia (EP) chapter on "Powder Flow" [11], such as angle of repose (AOR), compressibility index (CI), Hausner ratio (HR), flow rate through an orifice (FRO), and shear cell methods (SC). These methods are categorized as static flow (AOR, CI and HR) or dynamic flow (FRO and SC). Static methods focus on equilibrium properties influenced by interparticle cohesion and friction, while dynamic methods involve external forces like gravity and shear, affected by wall friction, cohesion, and equipment shape [12]. Different FIs are typically tailored for specific applications and used to quantify powder flowability based on various material properties. At the same time, different FIs

are affected in a different extent by the material properties and this results in discrepancies in the flowability classification [13,14]. This diversity in FIs results is due to the complex nature of powder flow and the necessity to take multiple factors into account when characterizing flowability. The relationship between different FI's is a further crucial aspect to be considered. In fact, while some investigations have explored correlations between certain FIs [14–18], a comprehensive understanding is still lacking. This is partly because most of these studies are based on limited number of samples or materials with restricted variability in terms of properties and flow behaviour.

The objective of this study is to deepen the understanding of commonly used flowability indexes in the pharmaceutical field, specifically focusing on a static method like the Hausner ratio and two dynamic methods such as the flow rate through an orifice and the shear cell methods. This research aims to investigate the quality of these indexes in terms of variability and precision, as well as the relationship between the indexes. To achieve this goal, a wide selection of pharmaceutical materials was utilized, including blends or fractions of materials, for a total of 24 different samples. This comprehensive approach ensures coverage of a wide range of material properties and flow behaviours. The selected materials primarily consist of those used in tablet manufacturing or capsule filling (diluents, binders, disintegrants and co-processed) with the inclusion of excipients suitable for wet granulation or dry powder inhalers. Additionally, efforts were made to establish models capable of correlating the properties of the measured samples with the results obtained from the FIs. Therefore, the research is intended to offer insights into how material characteristics impact flowability indexes, thus enhancing our ability to predict and optimize powder flow behaviour in pharmaceutical processes.

2. Materials and methods

2.1 Materials

Different grades of α-monohydrate Lactose (SuperTab®30GR, Pharmatose® 200M, Pharmatose® 100M, Pharmatose® 80M, Lactochem® Microfine and Respitose® SV003), two grades of spray dried lactose (SuperTab® 11SD, SuperTab® 50ODT), two grades of anhydrous lactose (SuperTab® 24AN, SuperTab® 21AN), two grades of Microcrystalline cellulose (Pharmacel® 102 and Pharmacel® 112), silicified microcrystalline cellulose (Pharmacel® sMCC90), Croscarmellose Sodium (Primellose®), Sodium Starch Glycolate (Primojel®) were all obtained from DFE

Pharma GmbH & Co. (Goch, DE). Anhydrous Dibasic Calcium Phosphate (Di-Cafos® A150) was purchased from Budenheim KG (Budenheim, DE).

2.2 Methods

2.2.1 Samples preparation

The 16 different materials of section 2.1 were tested as received. In addition, 4 different binary blends (the composition is reported in table 1) were prepared by loading 500g of the two materials at 1:1 ratio with a 3D mixer (Turbula T2C, Willy A. Bachofen AG, Basel, CH) operating at 67 rpm. All the blends included possessed a monomodal particle size distribution, as those of pure materials. Finally, two fine fractions (FF) were prepared from Pharmatose® 80M and SuperTab® 21AN (by collecting the undersize material recovered from a 200 and 53 μm sieve, respectively), and two coarse fractions (CF) from SuperTab® 21AN and Pharmatose® 100M, prepared by collecting the oversize materials recovered from a 53 μm sieve.

Details of all the samples and their abbreviations are reported in table1.

Table 1 *Samples abbreviations and median size*

Material	Abbreviation	Commercial name	Median size (µm)[A]	Other informations [A]
Dicalcium phosphate	DCP_A150	DI-CAFOS A150	150	Anhydrous form
Lactose	L_Mic	Lactochem Microfine	3	Micronized
	L_80M	Pharmatose 80M	250	
	L_100M	Pharmatose 100M	150	
	L_200M	Pharmatose 200M	40	
	L_Resp	Respitose SV003	61	
	L_11SD	SuperTab 11SD	120	Spray dried
	L_21AN	SuperTab 21AN	170	Anhydrous form
	L_24AN	SuperTab 24AN	140	Anhydrous form
	L_30GR	SuperTab 30GR	140	Granulated
	L_50ODT	SuperTab 50 ODT	130	Spray dried
Microcrystalline cellulose	MCC_102	Pharmacel 102	90	LOD 3.8%[b]
	MCC_112	Pharmacel 112	90	LOD 1.3% [d]
Silicified microcrystalline cellulose	SMCC_90	Pharmacel SMCC 90	110	LOD 4.4% [d]
Crosscarmellose sodium	CCS	Primellose	50	
Sodium starch glycolate	SSG	Primojel	40	
Fractions	L_80M_FF	Pharmatose 80M		undersize 200 µm
	L_21AN_FF	SuperTab 21AN		undersize 53 µm
	L_21AN_CF	SuperTab 21AN		oversize 53 µm
	L_100M_CF	Pharmatose 100M		oversize 53 µm
Blends[c]	B1	SuperTab 30GR and Pharmatose 200M		
	B2	SuperTab 24AN and Pharmacel 102		
	B3	SuperTab 24AN and SuperTab 30GR		
	B4	Pharmacel 102 and Primellose		

[A]provided by the manufacturer or distributor (https://faravelli.it/docs/LISTINOPHARMAITALIAWEB.pdf for DCP_A150 and https://dfepharma.com/excipients/ for all the other products) or relative to the sample preparation as for the fractions.
[b] The LOD is the loss of drying and and represents the amount water within the sample.
[c] The blends are prepared in a ratio 1:1 w/w

2.2.2 Samples images

Particle images were acquired using a Phenom ProX scanning electron microscope (Thermo Fischer Scientific, Waltham, MA, USA) operating at 5 or 10kV.

2.2.3 Particle Size Distribution (PSD)

The measurement of PSD has been carried out using a Laser diffraction analyser (Helos/KR, Sympatec, Clausthal-Zellerfeld, DE) operating in the dry configuration. Each material has been measured in triplicates.

The cumulative undersize of volumetric distribution was reported using the percentile notation, specifically D_{10}, D_{50} and D_{90}. The width of the particle size distribution was reported in term of SPAN:

$$SPAN = \frac{(D_{90} - D_{10})}{D_{50}}$$

2.2.4 Flowability

The flowability was assessed in term of Hausner Ratio (HR), Flow Function Coefficient (ffc) and Mass Flow (MF) through an orifice.

The HR has been calculated using the following equation:

$$HR = \frac{TD}{\mathrm{BD}}$$

Where TD and BD are the tapped density and bulk density, respectively. TD and BD were determined according to the EP [19]: 100 g of powder were poured into a 250 mL graduated cylinder and put on an automatic tester (Erweka Apparatebau GmbH, Germany). Each sample was measured in triplicate.

The ffc was measured with the Schulze shear cell (RST-XS, Dietmar Schulze, Wolfenbüttel, Germany). The ffc represent the ratio of the consolidation stress (σ_1) over the unconfined yield strength (σ_c):

$$\mathrm{ffc} = \frac{\sigma 1}{\sigma \mathrm{c}}$$

The measurements have been carried out at 4kPa pre-consolidation pressure and this parameter was kept the same for all the materials involved, representing a necessary condition to compare the data from different samples. Each sample was measured in triplicate.

The MF through orifices of different diameters (4, 8, 12, 18, 22 and 28mm) was measured using a granular material flow-meter (GranuFlow, GranuTools, BE). For each orifice size the MF was recorded using a balance connected to a computer and, at the end of the measurement, a curve of the mass flow over time was obtained. The reported values of MF were those determined analysing the data using the Beverloo theoretical model, as reported by the manufacturer.

2.2.5 Flowability indexes modelling

The effect of the PSD, density (excluded for HR modelling), and sample types on the three indexes, as well as the possibility of obtaining a predictive model, was evaluated

using two different approaches: multilinear regression (MLR) and artificial neural network (ANN) multilayer perceptron (MLP).

Prior to any modelling procedure, potential relationships among all the numerical predictors (D_{10}, D_{50}, D_{90}, SPAN, BD and TD) were tested using Pearson correlation analysis. Highly correlated predictors (strong correlation statistically significant at a confidence level of 95%) were not included in the analysis.

MLR has been carried out using the software Minitab® V 18.1 (Minitab LLC, USA), selecting as starting point a full quadratic model:

$$y = \beta_0 + \sum_{i=1}^{n} \beta_i \cdot x_i + \sum_{i=1}^{n} \beta_{ii} \cdot x_i^2 + \sum_{i<j}^{n} \beta_{ij} \cdot x_i x_j$$

Where y is the response, β_0 is the model constant, β_i is the coefficient corresponding to the variables x_i, β_{ii} are the coefficients associated with the variables x_i^2 and β_{ij} are the coefficients associated with the variables x_{ij}.

The coefficients of the models were then gradually reduced by removing the least significant terms using the stepwise backward elimination procedure. The regression was conducted on both the untransformed responses (the three FI's) and the transformed responses (using the Box-Cox transformation with λ values of 0, 0.5, -0.5, -1, 2, and -2 [20]). The entire set of generated models was compared in terms of adjusted and predicted coefficients of determination (r^2_{adj} and r^2_{pred}) and Mallows' Cp. The best models were then thoroughly evaluated in terms of regression significance, multicollinearity of the coefficients (Variance Inflation Factor, VIF), and residuals analysis.

MLP was performed with the software SPSS® V 28.0 (IBM Co., USA) varying the partition ratio between randomly assigned training and testing samples (60/40, 70/30, 80/20) and the training type (batch or online). The structure of the network was determined by selecting the automatic procedure, which utilizes a single hidden layer and chooses the optimal number of units.

The MLR and MLP models were compared in terms of coefficients of determination (r^2_{adj}) between the measured and predicted values and in terms of percentage residues (%R) versus the measured values.

2.2.6 Statistics

All data are reported in term of average and standard deviation unless otherwise specified. The precision analysis has been carried out comparing the coefficient of variation (CV), also known as relative standard deviation, of repeated measure.

Pearson and Spearman correlation analysis were carried out with the software GraphPad Prism V6.01 (GraphPad software Inc. USA) setting the significance level at 5%. When correlation coefficients were found to be statistically significant, the interpretation of their absolute magnitude was reported according to the following cut off: $0.9 < r < 0.1$ very strong correlation; $0.7 < r < 0.89$ strong correlation; $0.4 < r < 0.69$ moderate correlation; $0.1 < r < 0.39$ weak correlation and $0.09 > r$ negligible correlation [21,22].

3. Results and discussion

3.1 Samples properties

Materials were selected based on their characteristics reported by manufacturers or in the literature, aiming to represent the broadest variability among the commonly used excipients in OSD formulations. Scanning Electron Microscopy (SEM) analysis was employed to observe the morphology of the samples. The SEM images revealed that the chosen materials consisted of various types of particles, including regular crystals (e.g., L_200M or L_100M), granules or agglomerates (e.g., L_30GR or DCP_A150), and fibrous structures (e.g., MCC_102 or CCS). An example of SEM images displaying different types of samples is presented in Figure 1.

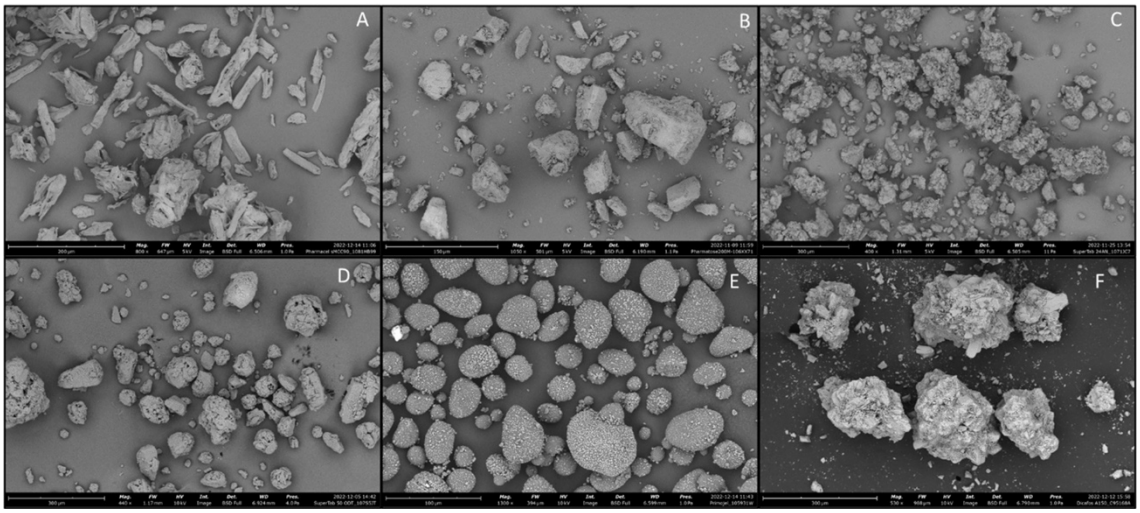

Figure 1 *SEM images of some of the samples in analysis: A) SMCC_90, B) L_200M, C) L_24AN, D) L_50ODT, E) SSG and F) DCP_A150.*

All selected samples exhibited significant differences in terms of bulk and tapped density, as well as of particle size distribution, as depicted in Figure 2. Specifically, bulk density ranged from 0.2 g/cm^3 (e.g., L_MIC) to 0.8 g/cm^3 (e.g., L_80M), while tapped density varied between 0.42 g/cm^3 (e.g., L_MIC) and 0.95 g/cm^3 (e.g., L_80MFF). Furthermore, all samples displayed a monomodal PSD, with D_{50} values ranging from 3 μm (e.g.,

L_MIC) to 236 μm (e.g., L_80M) and SPAN ranging from 1.04 (e.g., SSG) to 2.62 (e.g., B2). It can be observed that certain samples exhibited comparable density values but substantially different PSDs, or vice versa, indicating that these are independent properties.

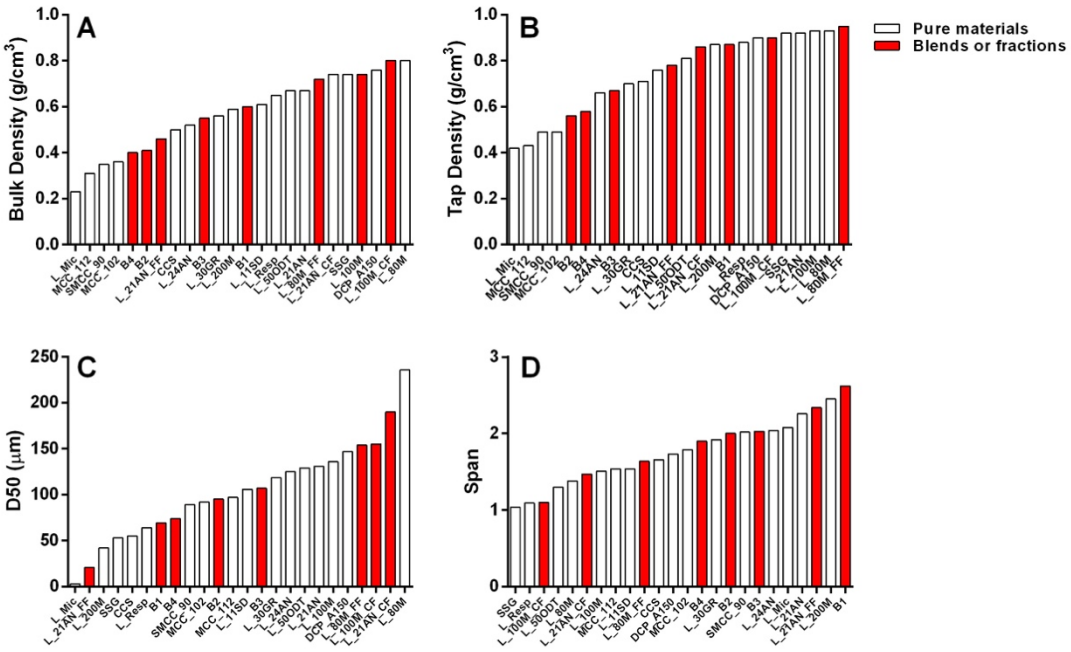

Figure 2 *Representative data for the analysed samples: A) Bulk density, B) Tapped density, C) D50 (median particle size), and D) SPAN of particle size distribution.*

3.2 Precision of flowability indexes

The reliability of an index employed to quantify the flowability of a powder has a direct impact on the quality of the results it produces. In this study, the quality of measurements was assessed in terms of Precision and Intra-day precision. Additionally, the relationship between the variability of flow indexes (ffc, HR, and MF) as a function of their absolute values was evaluated using Spearman correlation analysis. Precision and Intra-day Precision were tested using the coefficient of variation (CV) calculated from three independent measurements.

The precision analysis results, depicted in Figure 3, clearly indicate that HR and ffc are the most reliable indexes, exhibiting low variability with CV values consistently below 10%. Only one sample out of the 24 tested for ffc showed an exception to this trend. Notably, HR demonstrated the highest precision. Moreover, there was no correlation observed between CV and index values for both HR and ffc, suggesting that the precision remains consistent regardless of sample's flowability. Conversely, mass flow

measurements exhibited some remarkably high CV values, exceeding 50%, all of them recorded for mass flow rates lower than around 10g/sec. Furthermore, a negative correlation was observed between variability and mass flow values, particularly the less precise data were associated with samples of medium to low flowability. Lastly, no discernible clustering was observed between pure materials, blends or fractions, indicating that the type of sample does not significantly affect overall precision.

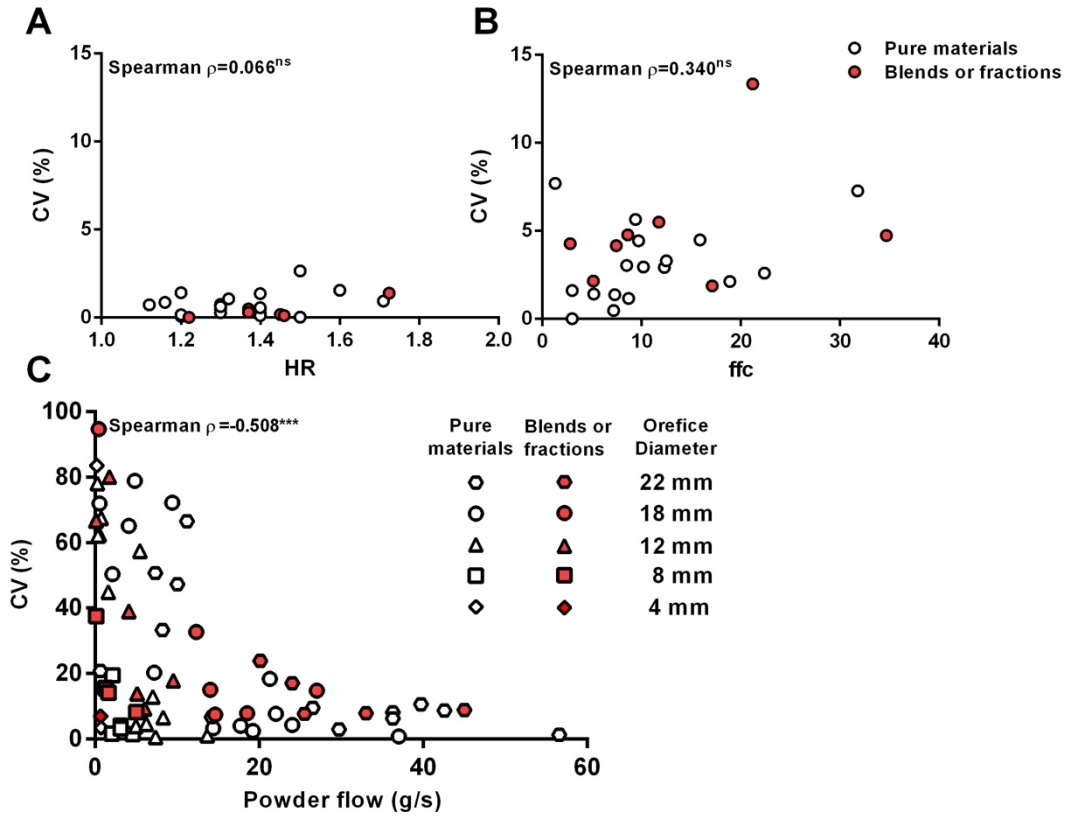

Figure 3 *Effect of the value of A) HR, B) ffc and C) powder flow on the coefficient of variation calculated from three independent measurements for all the samples.*

Intra-day precision was assessed using a limited number of samples (n=3) selected for their markedly different flowability characteristics, specifically L_200M, B2, and L_30GR. These samples were subjected to repeated measurements of the three indexes on multiple days by the same operator. Notably, all samples demonstrated excellent intra-day precision, with minimal variations observed in the results across different days (figure 4). It's worth noting that the data for sample L_200M were not reported in terms of mass flow, as the precision analysis indicated yet the low measurement quality for low flowability samples. These outcomes underscore the robustness and consistency of the measurement methods, as evidenced by the stable values obtained over multiple testing sessions. They also highlight the importance of considering the limitations of

measurement techniques, especially when dealing with samples exhibiting extreme characteristics such as very poor flowability.

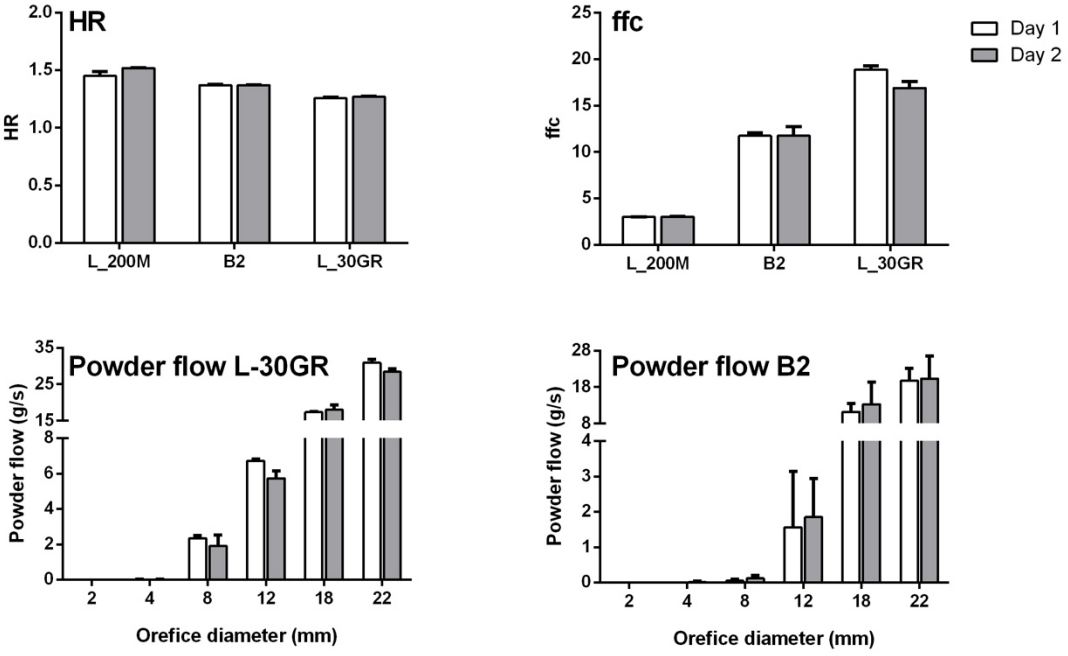

Figure 4 *Intra-day precision of samples HR, ffc and powder flow for the samples L_200M, B2, and L30GR.*

3.3 Relationship between flowability indexes

The three Flow indexes have been compared in pairs, in order to gain a deeper understanding of their potential correlation.

The relationship between HR and ffc is depicted in Figure 5. The general trend observed is not novel; in fact, Leturia et al. [18] reported a similar trend when analysing five different materials and two mixtures. However, the data obtained here, which refers to 24 different materials, allow a much more accurate definition of the relationship between these two indexes. Specifically, it appears that HR and ffc are characterized by a strong correlation (Pearson r around -0.8, statistically significant) only for materials with ffc values lower than 10-11, indicating samples with low or medium flowability. For higher ffc values, the correlation is completely lost. Interestingly, ffc values higher than 10 typically refer to materials defined as free-flowing according to Jenike classification [23,24] and commonly used by most authors [25,26]. However, their HR range measured in this study was from 1.12 to 1.29, indicating materials that are defined as having good or acceptable flow [11,27]. Thus, it seems that these two indexes depend mainly on certain properties for low to medium flowing materials, while their values would be influenced by different properties for materials with good or excellent flow.

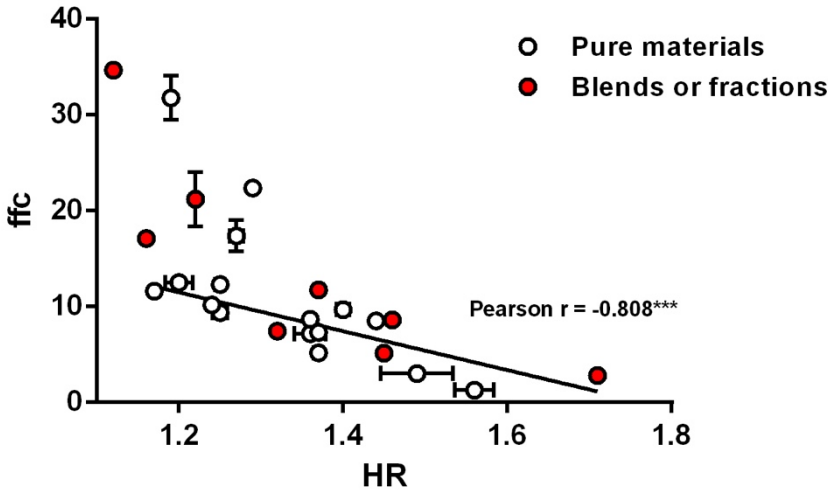

Figure 5 *Relationship and Pearson correlation analysis between the flow function coefficient (ffc) and the Hausner Ratio (HR).*

The evaluation of correlations involving the mass flow of materials was more complex due to the fact that this parameter changes as a function of the orifice diameter. For this reason, the correlations were studied considering the mass flow for each individual orifice. The mass flow values measured with the 4mm orifice were not considered since only 3 out of 24 materials were able to flow through this diameter, enabling the recording of mass flow values. HR and mass flow showed a specific trend (Figure 6). Basically, for each orifice there are HR values above which the materials do not flow through, approximately around 1.3, 1.4, and 1.45 of HR for 8mm, 12mm, and 18-22 mm diameters of the holes, respectively. Above these HR limits, the materials possess too low flowability to flow through the tester's hole and consequently they cannot be measured. Above these thresholds, a statistically significant strong correlation (Pearson r between 0.689 and 0.826) was identified between HR and mass flow, with the exception of data obtained with the 8 mm diameter (only 9 out of 25 samples were able to pass through this orifice). This result suggests that for flowing materials, the two indexes provide the same indications, and consequently, both indexes are affected in a similar manner by the material properties.

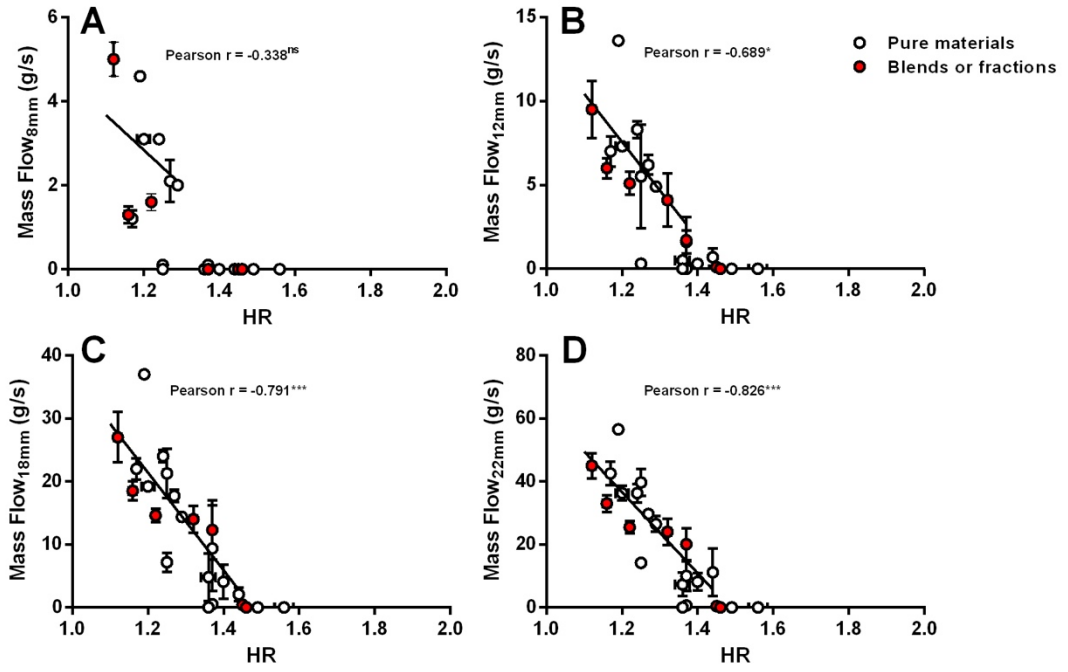

Figure 6 *Relationship and Pearson correlation analysis between HR and the mass flow measured using orifices with different diameters: A) 8mm, B) 12 mm, C) 18 mm and D) 22mm.*

Lastly, the relationship between ffc and mass flow was evaluated. In this case, the relationship appears to be more complex. A certain trend can be observed (Figure 7), specifically, it seems that the data follow a sigmoidal trend, where below ffc around 8.5, the mass flow is consistently zero (no flow through the orifice), while for ffc values higher than 11-12, the mass flow seems to oscillate around an average value without any discernible trend. In the middle, there is a narrow range of ffc where apparently the mass flow increases with the ffc, even if the measured correlation (both Pearson r and Spearman r from 0.5 to 0.7) is not statistically significant, probably due to the low sample size within this range. This result was partially expected considering the previously reported correlation analyses, specifically HR vs ffc and HR vs mass flow. In fact, poorly flowing materials were described similarly by HR and FFC, while free flowing materials showed correlated results in terms of HR and mass flow. Again, it can be stated that ffc values above 11 mainly depend on certain material properties that have minimal or negligible effects on HR or mass flow values. Since it appears that high ffc values are not related to the flow through an orifice, this FI (ffc) cannot be used to discriminate among free-flowing powders in certain specific processes. As a consequence, it is not suitable to predict the die filling in pharmaceutical processes such as tableting or capsule filling

(where mass flow measurements simulate the die or capsule filling process), also in line with the findings of Hildebrandt et al. [28].

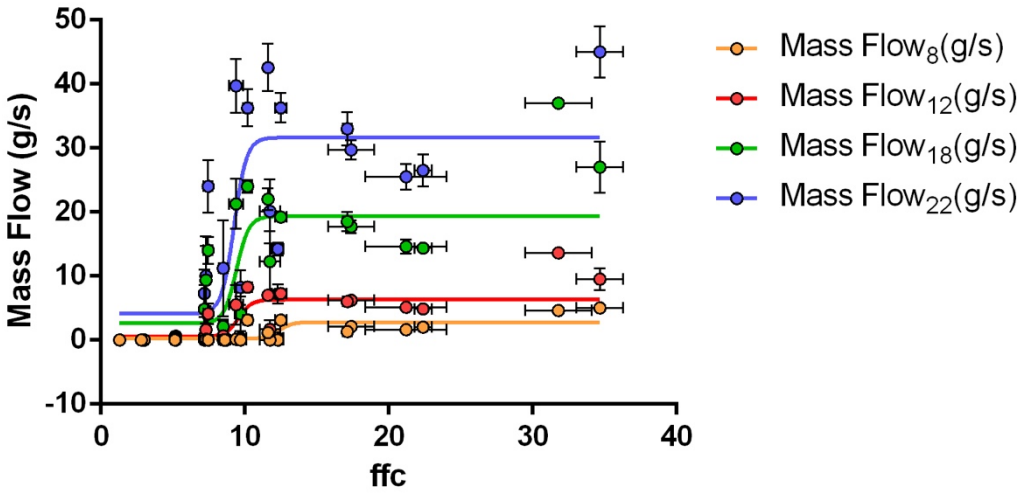

Figure 7 *Relationship between ffc and mass flow measured using orifices with different diameters.*

3.4 Modelling of flowability indexes

FI's were modelled using simple and readily available data, such as those referring to the PSD, density measurements (excluding HR since it is directly calculated from these parameters), and qualitative information such as the type of materials, derived from the particles' images (crystals, granules, agglomerates, fibers, or blends). The latter data can also be easily obtained from materials manufacturers. Prior to the analysis, the correlations among all quantitative predictors were calculated (table ST1), and the predictors with strong correlations (Pearson r greater than 0.7, statistically significant) were not included in the models. Specifically, the only usable predictors were TD, D50, and SPAN, in addition to particle type.

All the FI's were analysed using both the MLR and ANN procedures. The HR was described very well by the MLR procedure, which produced several models with values of r^2_{adj} and r^2_{pred} higher than 0.85 and 0.80, respectively. However, upon deep analysis of the regression results, it was found that in all of these models some coefficients were characterized by severe multicollinearity (VIF values higher or much higher than 5). Multicollinearity strongly and negatively impacts the regression results, making the coefficient interpretation difficult and the model prediction unreliable [29]. The multicollinearity issue was due to the presence of quadratic and interaction terms containing the same predictors as the linear ones. After removing the quadratic and interaction terms, the best model (r^2_{adj} and r^2_{pred} equal to 0.831 and 0.757, respectively)

was found using the untransformed dependent variables and D50, SPAN and type as predictors. According to this model, D_{50} and SPAN have the larger effect on HR, albeit in opposite directions; specifically, an increase in D50 decreases HR, while SPAN has the opposite effect (details of the model are reported in Supplementary materials section SMS1). The ANN procedure is a machine learning technology based on multilayer nonlinear processing, which is capable of learning directly from the data being modelled during a training phase and applying this knowledge to classify or model the analysed data [30,31]. Unlike MLR, ANN is often referred to as a 'black box,' meaning that it can understand the data pattern and provide predictions without providing insights into the data structure. For HR modelling, the best results were obtained using MLP with online training type and 70% of training samples, using a network consisting of one hidden layer with 3 units (details of the MLP analysis are reported in Supplementary materials section SMS2). Sensitivity analysis identified D_{50} as the most important predictor of the ANN (100% of normalized importance), followed by SPAN and type with 59% and 22% of normalized importance, respectively. The comparison of MLR and ANN for HR is reported in Figure 8 in terms of r^2 between the measured and predicted values and in terms of percentage residues (%R). Both approaches modelled HR in a very similar manner, providing good predictions with most residues lower than 5% and none higher than 10%. This result clearly indicates that HR can be estimated a priori in a fairly reliable manner simply by knowing PSD data and the particle type, although the latter information has much lower importance. Interestingly, despite the HR is one of the most studied FI's, there aren't any work devoted to its prediction as a function on the basic chemical-physical features of the particles. Although, HR has been used as predictors in models to estimate several other properties such as tablets tensile strength [32] or ribbons quality during a roller compaction process [33].

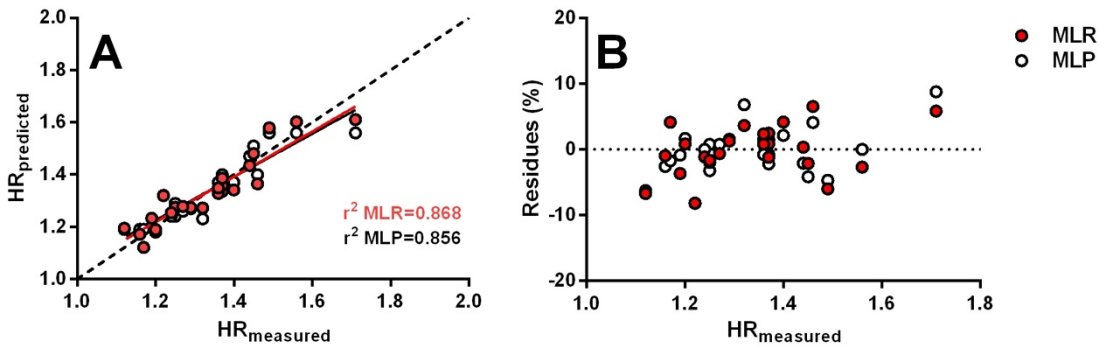

Figure 8 *Comparison of multilinear regression (MLR) and multilayer perceptron (MLP) modelling of HR in term of A) predicted versus measured HR values and B) HR residues from the predicted values versus measured HR values.*

The modelling of ffc was carried out following the same procedures used for HR. The MLR approach provided fair results in the initial screening phase, with r^2_{adj} and r^2_{pred} up to 0.927 and 0.806, respectively. The best results were consistently obtained when the ffc was transformed using λ=-1. However, as also reported for HR, all these models suffered from severe multicollinearity, which obliged to the elimination of quadratic and interaction terms. Using only linear terms, the best model found was characterized by r^2_{adj} and r^2_{pred} of 0.701 and 0.554, respectively, and used the same predictors as the MLR for HR. Thus, the TD predictor was removed from the model, indicating that it does not affect the ffc results. According to the MLR, D_{50} possesses the highest relevance, followed by SPAN and type, which appear to have comparable importance. As shown before for HR, even for the ffc models an increase in D_{50} results in an improvement of flowability (higher ffc), while SPAN has the opposite effect. Ffc was also analysed using the MLP procedure and the best description was obtained with online training type, 70% of training samples, and a network consisting of a hidden layer with 2 units. The relative errors of training and test samples were higher for the ffc MLP analysis than that for HR. The relative importance analysis of the MLP highlighted that D_{50} is the most relevant parameter (100% of normalized importance), followed by SPAN, type, and by far TD. These results are in line with those of the MLR analysis. However, when the modelling results were compared using measured and predicted values and %R (Supplementary Figure SF1), the outcomes appeared very poor. The untransformed predicted values of the MLR model showed very low prediction ability (r^2 of 0.238 against 0.772 for the untransformed and transformed ffc, respectively). On the other hand, the MLP appeared much better in terms of r^2 (0.716), although the evaluation of %R indicated huge deviation from the measured values, making the MLP model unreliable for practical applications.

Considering that ffc showed high correlation with HR exclusively for samples classified as below free-flowing (ffc lower than 10-12), an attempt has been made to model the ffc using only samples in the range of 0-12 (16 samples). This approach could be useful if the model's description is good up to ffc 10, and the prediction for samples having higher ffc always provides results higher than 10, regardless of their real values. The rationale for this approach is based on Jenike classification of the ffc [23,24]: ffc < 2 indicates not flowing or very cohesive material; 2 < ffc < 4 suggests cohesive material; 4 < ffc < 10

indicates easy-flowing material; and ffc > 10 indicates free-flowing material. Moreover, this approach is further supported by the findings of Zettler et al. [34] and Hildebrandt et al. [28]. In the first work, it was reported that the weight uniformity of tablets prepared with a rotary tableting press correlated with ffc values in the tested range of 4-13. On the other hand, Hildebrandt et al. showed no correlation between die filling metrics and ffc in the range above 10. The modelling of the 16 samples using both MLR and MLP provided a good description of the data in terms of goodness-of-fit statistics for regression (r^2_{adj} and r^2_{pred} of 0.817 and 0.691 for the untransformed ffc) and relative errors for the ANN (0.182 and 2.4E-^{5} for training and test, respectively). The detail of MLR and MLP results are reported in the supplementary sections SMS3 and SM4, respectively. The relevance of each descriptor had the same rank as previously reported for the MLP, while according to the MLR, the most relevant parameter was represented by the SPAN followed by D_{50} and type. The comparison between the predicted ffc and measured values is reported in Figure 9. Both approaches ensured an r^2 between the predicted and measured values higher than 0.85, while the residues percentage fell within the range of ±25%, which can be considered acceptable for ffc prediction in the range of 1-11. For example, the %R of sample L_200M is around 24%, which corresponds to a predicted value of 2.3 instead of 3. The only exception is represented by the sample with the lowest ffc, L_Mic, where the %R are higher than 100% for both model predictions. Despite the apparently unacceptable high %R, it has to be considered that they correspond to an ffc estimation of 2.8 and 2.9 for MLR and MLP, respectively, instead of the measured value of 1.3, and consequently such differences do not have any practical relevance.

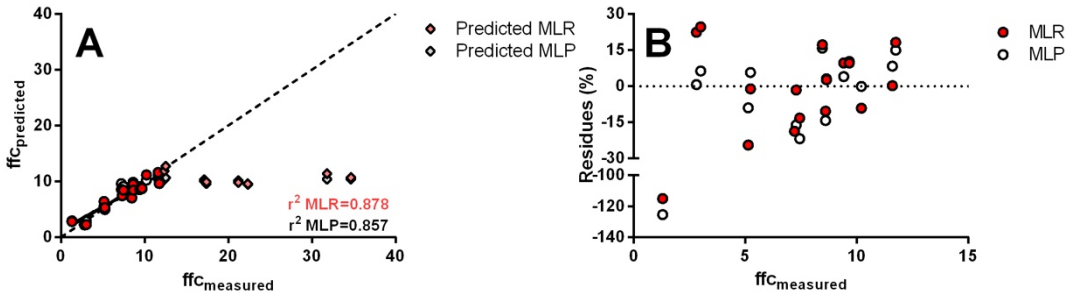

Figure 9 *Comparison of multilinear regression (MLR) and multilayer perceptron (MLP) modelling of ffc up to values of ffc 12, in term of A) predicted versus measured ffc values and B) ffc residues from the predicted values versus measured ffc values. The diamonds in the panel A) represent the models prediction for samples having a measured ffc higher than 12.*

Additionally, this model was used to predict the ffc of the samples that were not included during the building of the model, namely those with a measured ffc higher than 12. In this case, both models predicted almost constant values, between 9.5 and 12.7, which correspond to free-flowing materials according to the classification of Jenike. Thus, building the ffc model only with samples having an ffc lower than 12 allows the prediction of ffc values for all samples except for the free-flowing ones. The latter will be predicted with an ffc higher than 9, independently of their real values. Therefore, these models can be considered quantitative for non-flowing up to easy-flowing samples and qualitative for free-flowing materials.

ffc has been the object of several investigations aimed to develop predictive models starting from the material properties. The first attempt dealing with a dataset of not ideal materials date back to the 2010, when Yu et al. developed a model using the partial least squares (PLS) approach, a method able to deal with the multicollinearity issue in presence of large set of predictors [35]. The prediction ability of this model was comparable with that of the present one, although requiring a more complex approach and the determination of a larger set of predictors. Hildebrandt et al modelled the ffc using the PLS approach operating with a lower number of predictors, which were also easier to be measured (comparable to those used in the present work) [28]. Once again, the results were comparable with that of the present work, also considering that they used the whole range of ffc (for this reason their r^2 between measured and predicted ffc was much lower than ours). So, it appears that the ordinary least squares regression (that used for MLR) for uncorrelated predictors provides similar results that the PLS one for potential correlated predictors. Worst results were reported by Diaz et al. using different regression approaches [36]. In addition to regression procedures, other attempts were carried out using different ANN approaches [36,37]. In all cases, these works provided results not dissimilar from those of this work using shape predictors in addition to the PSD one. It has to be underlined that the use of a more complex ANN architecture, such as the so-called integrated framework approach (two phase models) assured a higher prediction ability [37]. Overall, the results of the present work are mostly comparable with those reported in the literature although obtained using simpler and more readily available predictors such as PSD data and particle type. In this context, it appears that a qualitative predictor (such as the particle type determined by a simple microscopy observation) can replace the much more complex and time-consuming numerical shape descriptors used in most of the literature investigations.

Lastly, an attempt was made to model the mass flow results. In this case, the orifice diameter was included as a further predictor. The mass flow data exhibited an unusual pattern, with many values equal to zero (indicating no flow) as a function of the different materials and orifice diameters used. Additionally, among the three FI's studied, mass flow was by far the least precise method, exhibiting significant variability for the lowest mass flow values. For this index, both MLR and MLP failed to provide a reasonable description (data not shown). Although the two approaches were able to model the data up to an r^2 of 0.841 (MLP) between measured and predicted values, the %R were very high (100% or more) for many mass flow values below 15g/s (approximately 80% of the measurements for the different orifice diameters were in this range). Furthermore, the model was unable to predict the behavior of most samples with no flow through the orifice. Attempts to model the flow through an orifice of not ideal powders have never been reported in the literature.

4. Conclusions

The compendial flowability indexes Hausner ratio, flow rate through an orifice and the flow function coefficient (shear cell method) were characterized by different quality in term of precision. Namely, ffc and particularly HR showed high reproducibility and were independent from the sample's flowability. Conversely, the mass flow had a lower precision which was dependent on the sample's flow (the higher the flow, the higher the precision). The three indexes showed a certain correlation even if not in the whole range of material flowability. For low to medium flowing materials, HR and ffc were strongly correlated, while HR and mass flow correlated only in the case of samples with high flowability. HR could be modelled in a fairly reliable manner using only PSD data and particle type, which thus represent the main parameters determining the value of this index. Ffc could not be satisfactorily modelled in the whole range of measured values, but only in the domain below the free-flowing materials (in which it correlates with HR), indicating that ffc values higher than 10 (free-flowing samples) were mainly dependent on other chemical-physical features than median diameter, SPAN, density, and particles type. Although the developed models for ffc were not able to predict the exact values for free-flowing samples, they always provided a qualitative evaluation, assigning ffc in the range 9.5-13, which is within the range of free-flowing materials. In conclusion, mass flow proved to be the most complex index. It could not be modelled at all in term of PSD data, density and particle type, likely due to its specific pattern, having very low and highly variable values for most materials with medium to low flowability, depending also on the analysis conditions (orifice diameters).

In essence, the results of this work suggest the use of HR and/or ffc as reliable and predictable indexes for the powder flow characterization, until strongly experimental evidence will be available for using others FI's in specific application.

Supplementary information
of
A Comprehensive Study of Flowability Indexes for Pharmaceutical Applications and their modelling

Beatrice Sabbatini[a], Lisa B. Buijvoets[b], Pauline H.M. Janssen[b,c], Diego Romano Perinelli[a], Giulia Bonacucina[a] and Marco Cespi[a*].

Table ST1: Pearson r and statistical significance concerning the correlation analysis between all numerical the predictors. The p-value are reported as superscript using the following notation: ns = p > 0.05; * 0.05 < p < 0.01; ** 0.01 < p < 0.001; *** p < 0.001

	BD	TD	D10	D50	D90	Span
BD	/	0.941***	0.446*	0.636***	0.516**	-0.459*
TD	0.941***	/	0.194^{ns}	0.421*	0.322^{ns}	-0.263^{ns}
D10	0.446*	0.194^{ns}	/	0.683***	0.541***	-0.723***
D50	0.636***	0.421*	0.683***	/	0.948***	-0.395^{ns}
D90	0.516**	0.322^{ns}	0.541**	0.948***	/	-0.150^{ns}
Span	-0.459*	-0.263^{ns}	0.723***	-0.395^{ns}	-0.150^{ns}	/

Section SMS1: Details of multiple regression analysis of HR

Analysis of Variance

Source	DF	Adj SS	Adj MS	F-Value	P-Value
Regression	5	0,38679	0,077358	21,76	0,000
D50	1	0,15131	0,151307	42,56	0,000
Span	1	0,05861	0,058613	16,49	0,001
Type	3	0,03807	0,012692	3,57	0,035
Error	18	0,06400	0,003555		
Total	23	0,45078			

Coefficients

Term	Coef	SE Coef	T-Value	P-Value	VIF
Constant	1,2200	0,0761	16,03	0,000	
D50	-0,001706	0,000262	-6,52	0,000	1,25
Span	0,1389	0,0342	4,06	0,001	1,40
Type					
B	0,0053	0,0403	0,13	0,897	1,53
F	0,0778	0,0418	1,86	0,079	1,29
RC	0,0836	0,0295	2,83	0,011	1,43

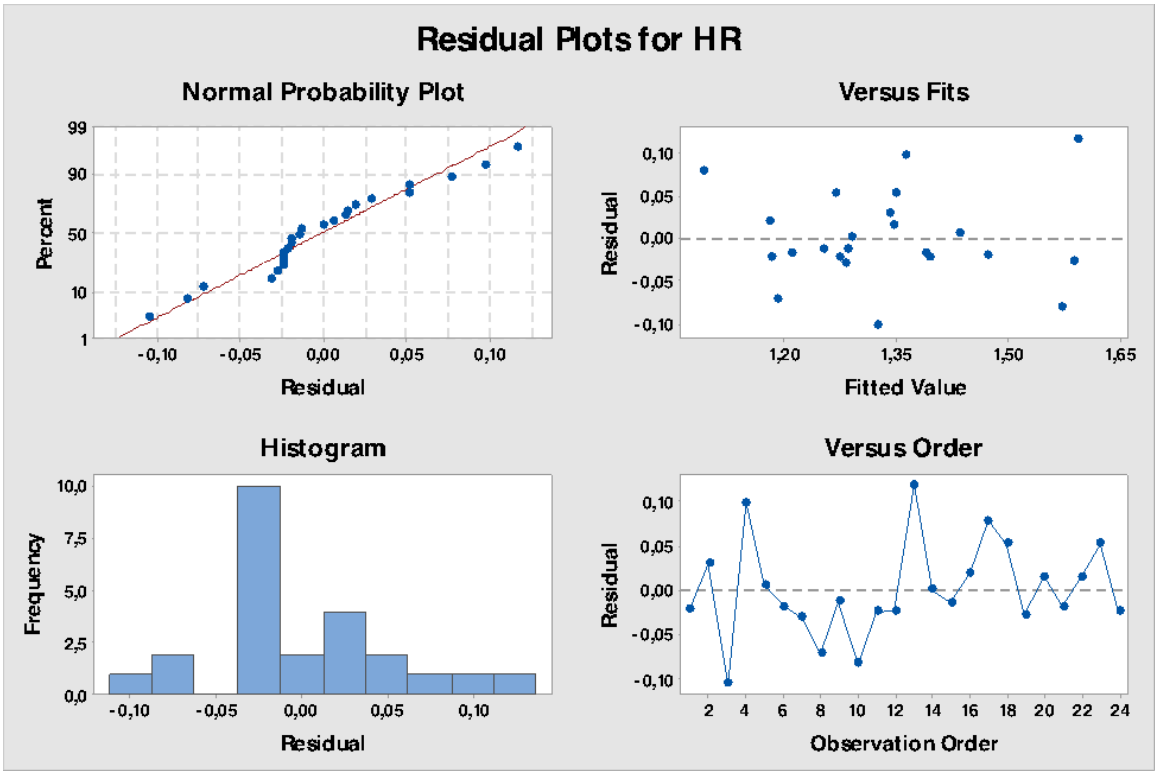

Section SMS2: Details of multilayer perceptron analysis of HR

Network Information

Input Layer	Factors	1	Type
	Covariates	1	D50
		2	Span
	Number of Units[a]		6
	Rescaling Method for Covariates		Standardized
Hidden Layer(s)	Number of Hidden Layers		1
	Number of Units in Hidden Layer 1[a]		3
	Activation Function		Hyperbolic tangent
Output Layer	Dependent Variables	1	HR
	Number of Units		1
	Rescaling Method for Scale Dependents		Standardized
	Activation Function		Identity
	Error Function		Sum of Squares

a. Excluding the bias unit

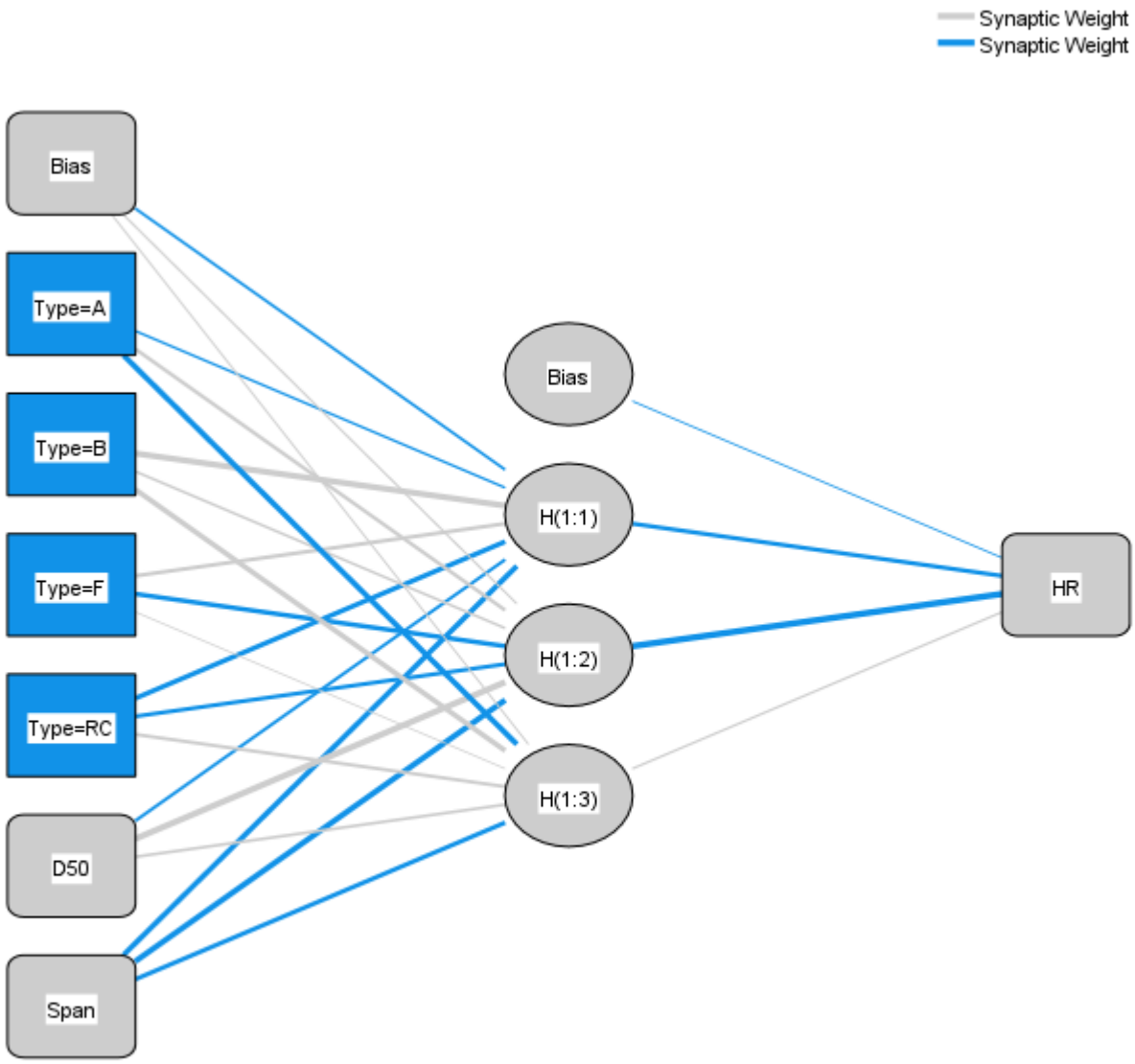

Hidden layer activation function: Hyperbolic tangent

Output layer activation function: Identity

Model Summary

Training	Sum of Squares Error	1,289
	Relative Error	,143
	Stopping Rule Used	1 consecutive step(s) with no decrease in error[a]
	Training Time	0:00:00,00
Testing	Sum of Squares Error	,251
	Relative Error	,293

Dependent Variable: HR

a. Error computations are based on the testing sample.

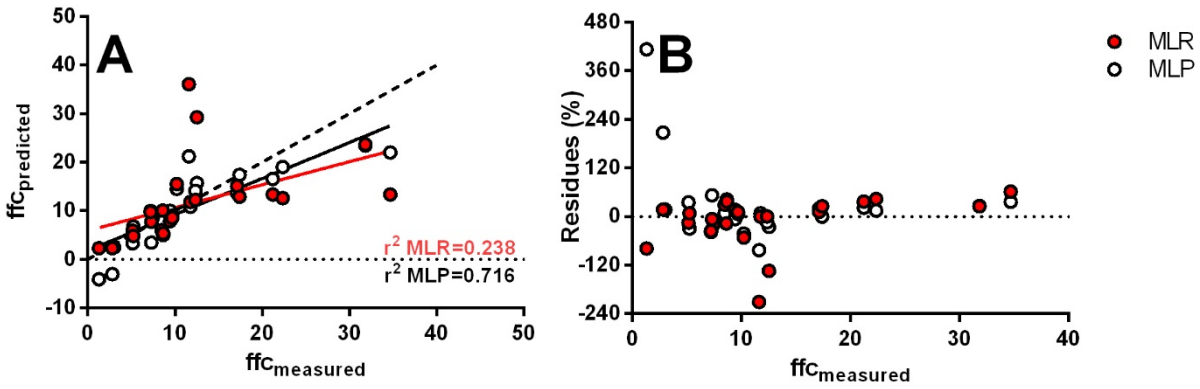

Figure SF1: Modelling of ffc using MLR and MLP

Section SMS3: Details of multiple regression analysis of ffc (modelling using only sample with ffc lower than 12).

Coefficients

Term	Coef	SE Coef	T-Value	P-Value	VIF
Constant	14,80	2,42	6,12	0,000	
D50	0,02531	0,00712	3,56	0,005	1,34
Span	-4,12	1,02	-4,05	0,002	1,55
Type					
B	0,64	1,27	0,50	0,626	2,21
F	-2,36	1,23	-1,92	0,084	2,09
RC	-3,52	1,05	-3,34	0,008	2,51

Analysis of Variance

Source	DF	Adj SS	Adj MS	F-Value	P-Value
Regression	5	127,57	25,514	14,43	0,000
D50	1	22,38	22,385	12,66	0,005
Span	1	29,01	29,005	16,40	0,002
Type	3	45,02	15,007	8,48	0,004
Error	10	17,69	1,769		
Total	15	145,26			

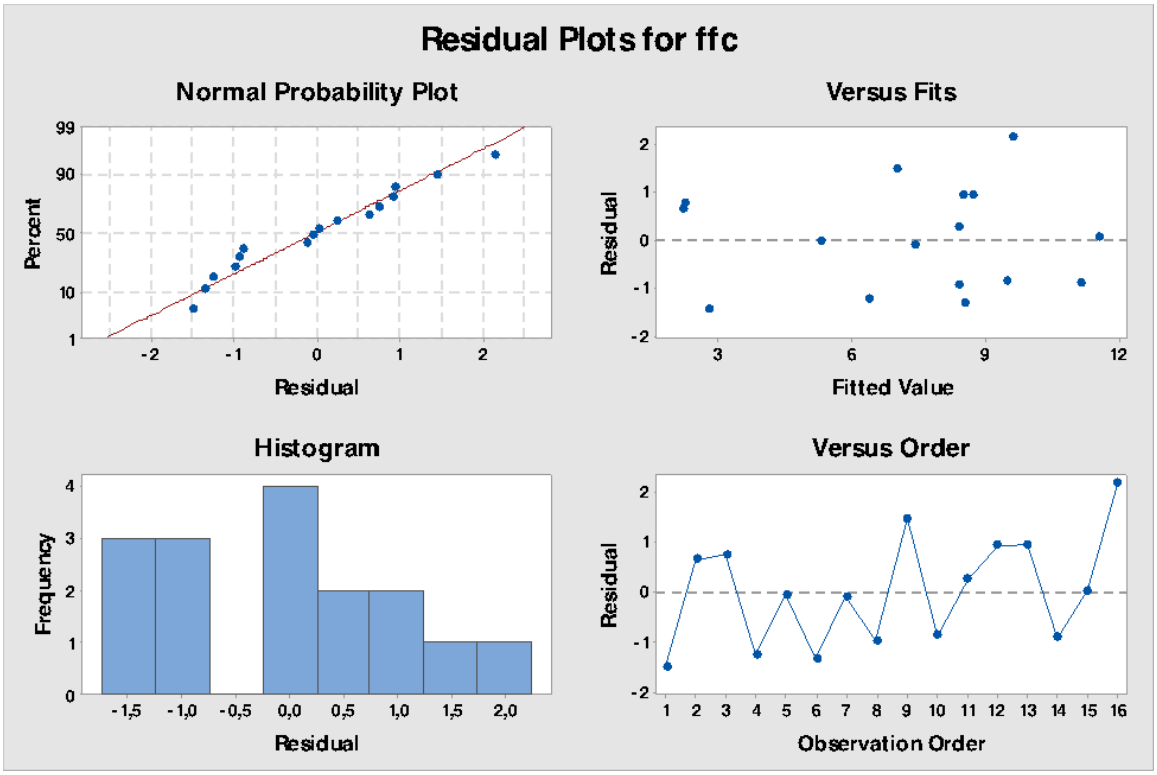

Section SMS4: Details of multilayer perceptron analysis of ffc (modelling using only sample with ffc lower than 12).

Network Information

Input Layer	Factors	1	Type
	Covariates	1	D50
		2	Span
		3	TD
	Number of Units[a]		7
	Rescaling Method for Covariates		Standardized
Hidden Layer(s)	Number of Hidden Layers		1
	Number of Units in Hidden Layer 1[a]		2
	Activation Function		Hyperbolic tangent
Output Layer	Dependent Variables	1	ffc
	Number of Units		1
	Rescaling Method for Scale Dependents		Standardized
	Activation Function		Identity
	Error Function		Sum of Squares

a. Excluding the bias unit

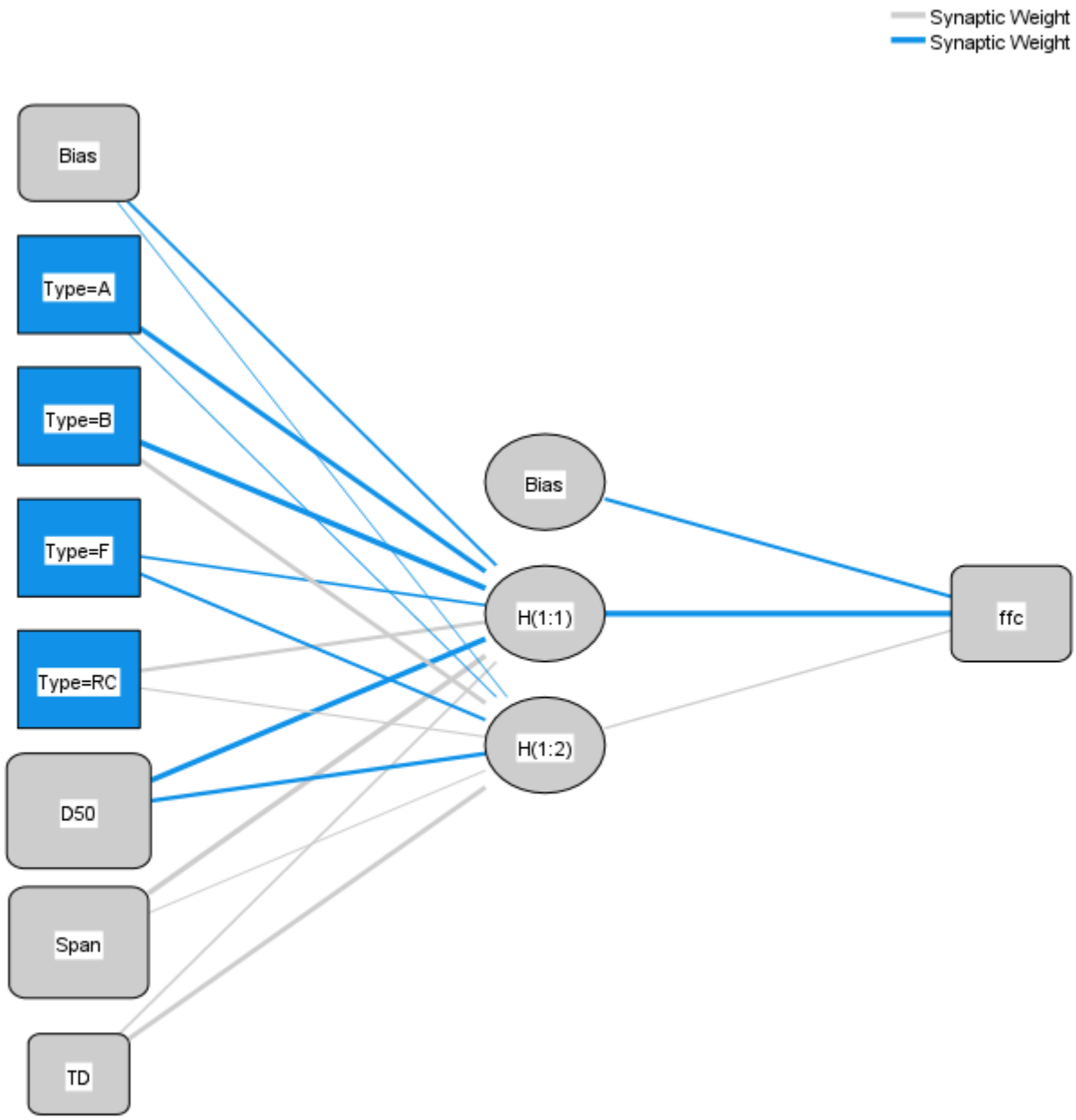

Hidden layer activation function: Hyperbolic tangent

Output layer activation function: Identity

Model Summary

Training	Sum of Squares Error	1,182
	Relative Error	,182
	Stopping Rule Used	1 consecutive step(s) with no decrease in error[a]
	Training Time	0:00:00,00
Testing	Sum of Squares Error	3,761E-5
	Relative Error	2,456E-5

Dependent Variable: ffc

a. Error computations are based on the testing sample.

References:

[1] S. Byrn, M. Futran, H. Thomas, E. Jayjock, N. Maron, R.F. Meyer, et al., Achieving continuous manufacturing for final dosage formation: challenges and how to meet them. May 20-21, 2014 Continuous Manufacturing Symposium., J. Pharm. Sci. 104 (2015) 792–802. doi:10.1002/jps.24247.

[2] C.A. Blackshields, A.M. Crean, Continuous powder feeding for pharmaceutical solid dosage form manufacture: a short review, Pharm. Dev. Technol. 23 (2018) 554–560. doi:10.1080/10837450.2017.1339197.

[3] S. Mangal, F. Meiser, D. Morton, I. Larson, Particle Engineering of Excipients for Direct Compression: Understanding the Role of Material Properties., Curr. Pharm. Des. 21 (2015) 5877–5889. doi:10.2174/1381612821666151008125117.

[4] A. Mehrotra, B. Chaudhuri, A. Faqih, M.S. Tomassone, F.J. Muzzio, A modeling approach for understanding effects of powder flow properties on tablet weight variability, Powder Technol. 188 (2009) 295–300. doi:https://doi.org/10.1016/j.powtec.2008.05.016.

[5] G. Tan, D.A. V Morton, I. Larson, On the Methods to Measure Powder Flow., Curr. Pharm. Des. 21 (2015) 5751–5765. doi:10.2174/1381612821666151008125852.

[6] P.A. Kulkarni, R.J. Berry, M.S.A. Bradley, Review of the flowability measuring techniques for powder metallurgy industry, Proc. Inst. Mech. Eng. Part E J. Process Mech. Eng. 224 (2010) 159–168. doi:10.1243/09544089JPME299.

[7] P. Juliano, G. V Barbosa-Cánovas, Food powders flowability characterization: theory, methods, and applications., Annu. Rev. Food Sci. Technol. 1 (2010) 211–239. doi:10.1146/annurev.food.102308.124155.

[8] R.P.K. Ambrose, S. Jan, K. Siliveru, A review on flow characterization methods for cereal grain-based powders., J. Sci. Food Agric. 96 (2016) 359–364. doi:10.1002/jsfa.7305.

[9] J.Y.S. Tay, C.V. Liew, P.W.S. Heng, Powder Flow Testing: Judicious Choice of Test Methods, AAPS PharmSciTech. 18 (2017) 1843–1854. doi:10.1208/s12249-016-0655-3.

[10] G. Lumay, F. Boschini, K. Traina, S. Bontempi, J.-C. Remy, R. Cloots, et al., Measuring the flowing properties of powders and grains, Powder Technol. 224 (2012) 19–27. doi:https://doi.org/10.1016/j.powtec.2012.02.015.

[11] EDQM, 2.9.36. POWDER FLOW, in: Eur. Pharmacopoeia 10.0, Strasbourg, 2019.

[12] D. Barletta, M. Poletto, A.C. Santomaso, Bulk Powder Flow Characterisation Techniques, in: Powder Flow Theory, Characterisation Appl., The Royal Society of Chemistry, 2019. doi:10.1039/9781788016100-00064.

[13] K. Thalberg, D. Lindholm, A. Axelsson, Comparison of different flowability tests for powders for inhalation, Powder Technol. 146 (2004) 206–213. doi:https://doi.org/10.1016/j.powtec.2004.08.003.

[14] H.P. Goh, P.W.S. Heng, C.V. Liew, Comparative evaluation of powder flow parameters with reference to particle size and shape, Int. J. Pharm. 547 (2018) 133–141. doi:https://doi.org/10.1016/j.ijpharm.2018.05.059.

[15] V.R. Nalluri, M. Kuentz, Flowability characterisation of drug–excipient blends using a novel powder avalanching method, Eur. J. Pharm. Biopharm. 74 (2010) 388–396. doi:https://doi.org/10.1016/j.ejpb.2009.09.010.

[16] M. Krantz, H. Zhang, J. Zhu, Characterization of powder flow: Static and dynamic testing, Powder Technol. 194 (2009) 239–245. doi:https://doi.org/10.1016/j.powtec.2009.05.001.

[17] B.C. Hancock, K.E. Vukovinsky, B. Brolley, I. Grimsey, D. Hedden, A. Olsofsky, et al., Development of a robust procedure for assessing powder flow using a commercial avalanche testing instrument, J. Pharm. Biomed. Anal. 35 (2004) 979–990. doi:https://doi.org/10.1016/j.jpba.2004.02.035.

[18] M. Leturia, M. Benali, S. Lagarde, I. Ronga, K. Saleh, Characterization of flow properties of cohesive powders: A comparative study of traditional and new testing methods, Powder Technol. 253 (2014) 406–423. doi:10.1016/j.powtec.2013.11.045.

[19] EDQM, 2.9.34. BULK DENSITY AND TAPPED DENSITY OF POWDERS, Eur. Pharmacopoeia 10.0. (2019).

[20] J. Osborne, Improving your data transformations: Applying the Box-Cox transformation, Pract. Assessment, Res. Eval. 15 (2019). doi:doi.org/10.7275/qbpc-gk17.

[21] P. Schober, C. Boer, L.A. Schwarte, Correlation Coefficients: Appropriate Use and Interpretation., Anesth. Analg. 126 (2018) 1763–1768. doi:10.1213/ANE.0000000000002864.

[22] M.M. Mukaka, Statistics corner: A guide to appropriate use of correlation coefficient in medical research., Malawi Med. J. 24 (2012) 69–71.

[23] A.W. Jenike, Gravity flow of bulk solids. Bulletin N°108 of the Utah engineering experiment station, Univ. Utah. 52 (1961).

[24] A.W. Jenike, Storage and flow of solids. Bulletin N° 123 of the Utah engineering experiment station, Univ. Utah. 53 (1970).

[25] D. Schulze, Flow properties of bulk solids, in: Powders Bulk Solids Behav. Charact. Storage Flow, Springer Berlin Heidelberg, Berlin, Heidelberg, 2008: pp. 35–74. doi:10.1007/978-3-540-73768-1_3.

[26] J. Schwedes, Review on testers for measuring flow properties of bulk solids, Granul. Matter. 5 (2003) 1–43. doi:10.1007/s10035-002-0124-4.

[27] R.L. Carr, EVALUATING FLOW PROPERTIES OF SOLIDS, Chem. Eng. 72 (1965) 163–168.

[28] C. Hildebrandt, S.R. Gopireddy, A.K. Fritsch, T. Profitlich, R. Scherließ, N.A. Urbanetz, Evaluation and prediction of powder flowability in pharmaceutical tableting., Pharm. Dev. Technol. 24 (2019) 35–47. doi:10.1080/10837450.2017.1412462.

[29] N. Shrestha, Detecting Multicollinearity in Regression Analysis, Am. J. Appl. Math. Stat. 8 (2020) 39–42. doi:DOI:10.12691/ajams-8-2-1.

[30] S. Wang, J. Di, D. Wang, X. Dai, Y. Hua, X. Gao, et al., State-of-the-Art Review of Artificial Neural Networks to Predict, Characterize and Optimize Pharmaceutical Formulation, Pharmaceutics. 14 (2022). doi:10.3390/pharmaceutics14010183.

[31] M. Wesolowski, B. Suchacz, Artificial neural networks: theoretical background and pharmaceutical applications: a review., J. AOAC Int. 95 (2012) 652–668. doi:10.5740/jaoacint.sge_wesolowski_ann.

[32] Y. Hayashi, T. Oishi, K. Shirotori, Y. Marumo, A. Kosugi, S. Kumada, et al., Modeling of quantitative relationships between physicochemical properties of active pharmaceutical ingredients and tensile strength of tablets using a boosted tree., Drug Dev. Ind. Pharm. 44 (2018) 1090–1098. doi:10.1080/03639045.2018.1434195.

[33] R.F. Mansa, R.H. Bridson, R.W. Greenwood, H. Barker, J.P.K. Seville, Using intelligent software to predict the effects of formulation and processing

parameters on roller compaction, Powder Technol. 181 (2008) 217–225. doi:https://doi.org/10.1016/j.powtec.2007.02.011.

[34] A. Zettler, J. Hilden, M. Koenig, C. Breslin, A. Aburub, M. Allgeier, et al., Evaluation of Small-Scale Powder Flow Characterization Tests in the Prediction of Large-Scale Process Failures, J. Pharm. Innov. 11 (2016) 189–199. doi:10.1007/s12247-016-9258-5.

[35] W. Yu, K. Muteki, L. Zhang, G. Kim, Prediction of bulk powder flow performance using comprehensive particle size and particle shape distributions., J. Pharm. Sci. 100 (2011) 284–293. doi:10.1002/jps.22254.

[36] L. Pereira Diaz, C.J. Brown, E. Ojo, C. Mustoe, A.J. Florence, Machine learning approaches to the prediction of powder flow behaviour of pharmaceutical materials from physical properties, Digit. Discov. 2 (2023) 692–701. doi:10.1039/D2DD00106C.

[37] M. Alshafiee, W.H. AlAlaween, D. Markl, M. Soundaranathan, A. Almajaan, K. Walton, et al., A predictive integrated framework based on the radial basis function for the modelling of the flow of pharmaceutical powders., Int. J. Pharm. 568 (2019) 118542. doi:10.1016/j.ijpharm.2019.118542.

5. Other projects: B.I.O.CER.T.O.

The B.I.O.C.E.R.T.O. project has been partly used to fund the PhD scholarship awarded to the PhD candidate Beatrice Sabbatini.

B.I.O.CER.T.O.: BlockchainIsotopicOrigin: CER.tificazione e Tracciabilità sull'Origine biologica dei prodotti.

1. The BIOCERTO project

BIOCERTO is a project funded by the Marche Region which aims to develop a cutting-edge technology to safeguard the rich biodiversity and premium quality production of the Region itself. Through the innovative fusion of the Blockchain technology with Advanced Mass Spectrometry (AMS) isotopic analysis, it is possible to forge a digital identity card for both the territory and its products, thereby improving food safety and quality assurance.

Since every product is strongly intertwined with the original territory and its characteristics, this database will be useful to enhance transparency in the production process but also as a barrier against fraudulent activities.

The project was conducted in collaboration with other research groups at the University of Camerino. This report will primarily focus on characterizing the final product, specifically red and white wines produced in the Marche Region. Through advanced analytical techniques, we aimed to detect the unique qualities that define and deeply characterize these products.

Wine is a complex mixture composed by constituent derived from the original grape and others which are generated during the manufacturing of the final product. The wine general composition is the following: about 84% of water, ~15% of ethanol and other secondary components (~1%) [1]. Analysing properties such as viscosity and density enables the evaluation of the qualitative and quantitative determination of ethanol, sugar, and glycerol. In addition, the correlation between these results and the data obtained with the isotopic analyses develops a fingerprint of the product itself.

Viscosity can therefore be considered an important criterion for wine classification, because it is strongly affected by the wine parameters, including grape variety, year of production and temperature. Moreover, the use of Ultrasonic techniques offers another significant measurement for the aim of this project because they essentially measure two

parameters: the Sound Speed and the Attenuation [2]. The ultrasonic techniques are non-destructive and reliable technique applicable even to the wine, which is an opaque and coloured liquid.

2. Materials and methods

2.1 Materials

Four wines were included in the project, as reported in the following table:

Table 3 List of the wines included in this project, together with the year of production analysed and the production site.

Wine Producer	Year of production	Production site
Passacantando	2021-2022	Tolentino (MC), IT
Brocani	2019-2022	Staffolo (AN), IT
Belisario	2021-2022	Matelica (MC), IT
Maceratino	2021	Macerata (MC), IT

2.2 Wines Rheology

Viscosity analyses were performed using the rotational rheometer Kinexus Lab+ (Malvern, UK) using a C40/4 geometry (Fig.1). The analysis (n=3) was conducted increasing the shear rate from 1 to 100 sec^{-1} and measuring the shear stress at 25°C. The data obtained were graphically represented using the power law model (eq. 1).

(eq.1) $$\sigma = \mathrm{PLV}\,\gamma^{PLI}$$

where γ is the shear rate, σ is the yield stress, PLV is the power law viscosity (or consistency index) and PLI is the power law index (or flow index).

Figure 7 Kinexus Rheometer

2.3 DT 1200

The DT-1200 (Fig. 2) (Dispersion Technology, Inc) features both acoustic and electroacoustic sensors, enabling it to conduct acoustic and electroacoustic measurements autonomously and distinctly.

All the samples have been analysed (n=3) using frequencies ranging from 1 to 100 MHz, in order to obtain Attenuation data of the samples as a function of the frequencies.

Figure 8 DT1200 Electroacoustic spectrometer.

2.4 High-resolution ultrasound (HR-US)

The High-resolution Ultrasound (Ultrasonic Scientific, Ireland) has been used to analyse the wines and obtain Sound Speed and Attenuation data at 25°C for the samples involved in the project. Temperature control was achieved with a HAAKE C25P water bath. The apparatus is equipped with two cells: one containing 1 mL of the sample and the other holding 1 mL of water for reference. Ultrasonic parameters were measured at a frequency of 5.2 MHz, which was previously determined through a broad amplitude frequency scan. The absolute values of Sound Speed and Attenuation were measured over a period of 300 seconds in triplicates.

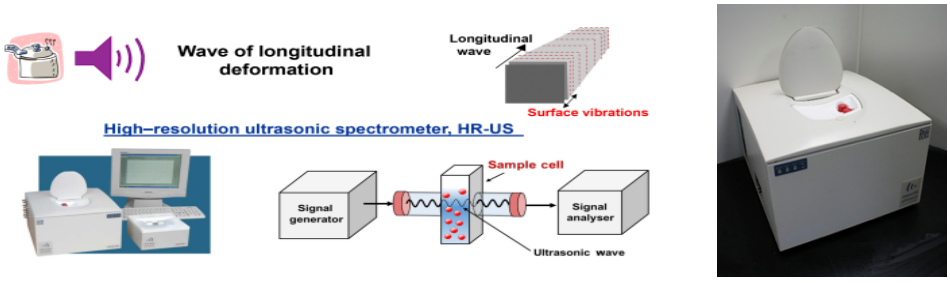

Figure 9 HR-US Spectrometer

3. Preliminary analyses

Preliminary analyses were carried out to evaluate the sensitivity of the selected techniques, such as rheological analysis and acoustic spectroscopy. For this purpose,

commercially available red and white wine (Tavernello bianco and Ronco rosso) were tested using the aforementioned rheological analysis and acoustic spectroscopy to evaluate the differences between various wines and also between wines and water.

The preliminary rheological tests demonstrated that all the samples exhibited a Newtonian behaviour, even though the viscosity of the wines was higher than that of the water, probably due to the composition of the wine (ethanol and other components). Among the wines, the red one had the higher viscosity (fig. 4).

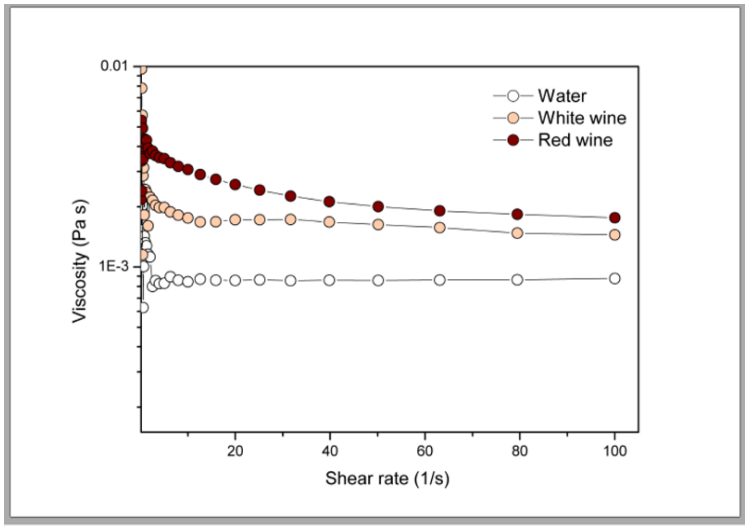

Figure 10 Viscosity measurements for commercial wines and deionized water.

The preliminary analysis carried out using the DT1200 showed differences between the red and white wines and the deionized water (fig. 5), confirming the results obtained during the rheological measurements.

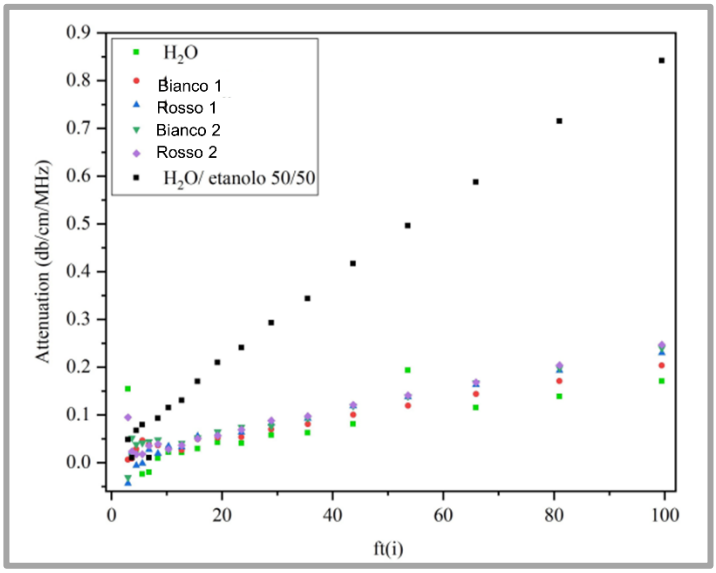

Figure 11 Acoustic spectroscopy analysis for the commercial wines and the deionized water.

The preliminary analyses have confirmed that the chosen techniques have proven useful in characterizing the wines involved in the project. In particular, the rheological analysis has been shown to be the most effective in distinguishing the characteristics of different samples analysed.

4. Results and discussion

The viscosity trend of the analysed wines demonstrates consistency in the results for Maceratino (2021), Passacantando (2021), Belisario (2022), and Brocani (2022). The only data exhibiting a different trend is Passacantando (2022), which shows the tendency to assume pseudoplastic behavior at low shear rate and a higher viscosity compared to the other wines that displayed the typical Newtonian behavior of low-viscosity liquids (Fig. 6).

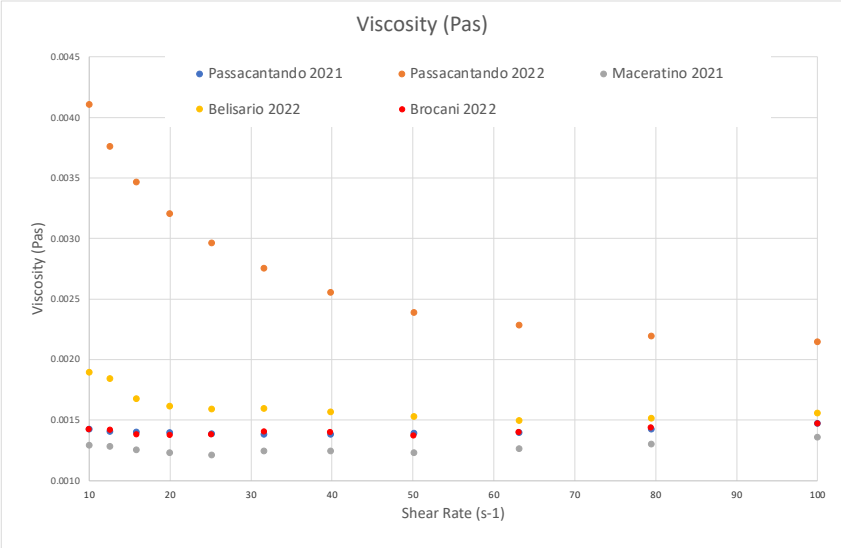

Figure 12 Rheological behaviour of all the wines the analysed.

In addition, a comparison between wines produced in different year has been carried out to highlight potential differences in the rheological behaviour. The results demonstrated that the only difference among wines is still represented by the Passacantando, with significative differences between the 2021's and the 2022's wine (Fig. 7).

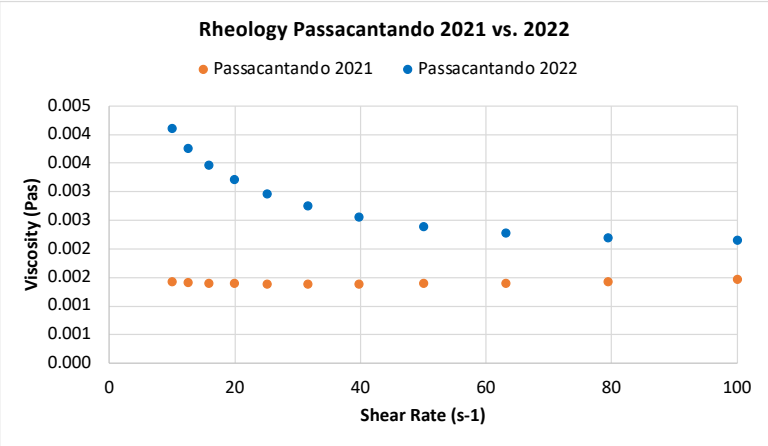

Figure 14 Comparison of the rheological behaviour of Passacantando from year 2021 vs. year 2022.

The chemical composition of different wines influences the quality and the characteristics of the final product and this was also observed by comparing the viscosity of the same wine produced in different years. Aside the Passacantando wine, all the other wines didn't show significant differences (Fig. 8).

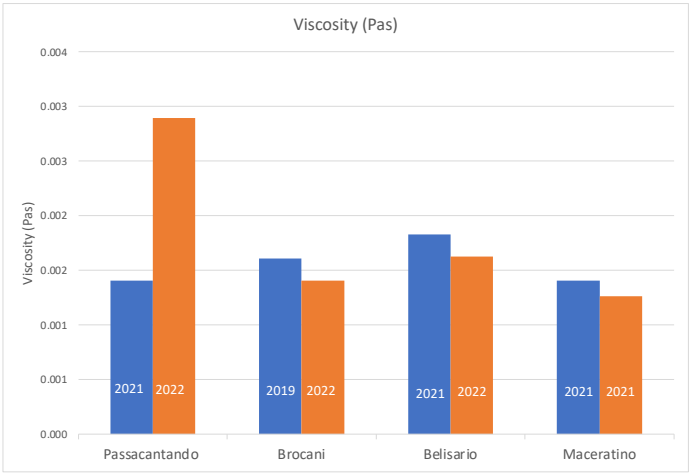

Figure 13 Comparison of the rheological behaviour of wines produced in different years.

The DT1200 measurements were carried out for all the samples involved in the project and the results once again confirmed the rheological analyses. Indeed, the Passacantando 2022 red wine displayed a higher value of attenuation. Although, no relevant differences between the tested wines were found. Actually, all the wines displayed almost all overlapping curves in the attenuation over frequency plot (Fig. 9). As a result, this method proved to be inaccurate in identifying the differences between the different wines included in this project.

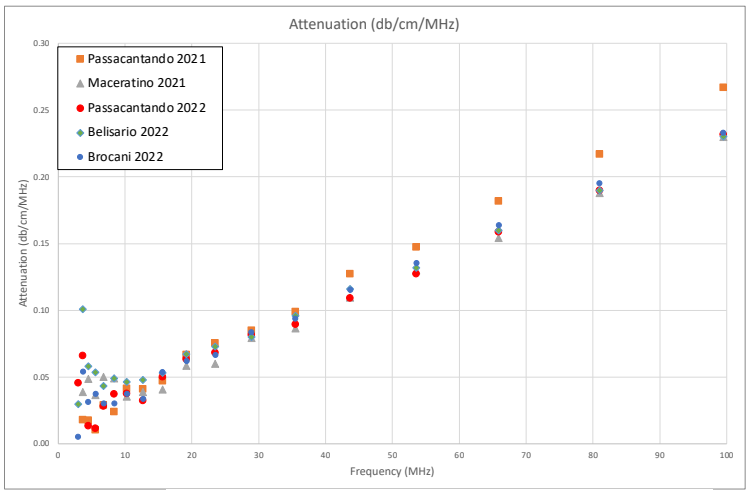

Figure 15 DT1200 analysis for the tested wines.

The results obtained with the HR-US corroborated the rheological characterization. In particular, both the measurements of Sound Speed and Attenuation were higher for the Passacantando red wine (2022) than the Passacantando (2021). Moreover, these values for Passacantando 2022 were also higher than all the other measured wines from year 2022 (Fig. 10).

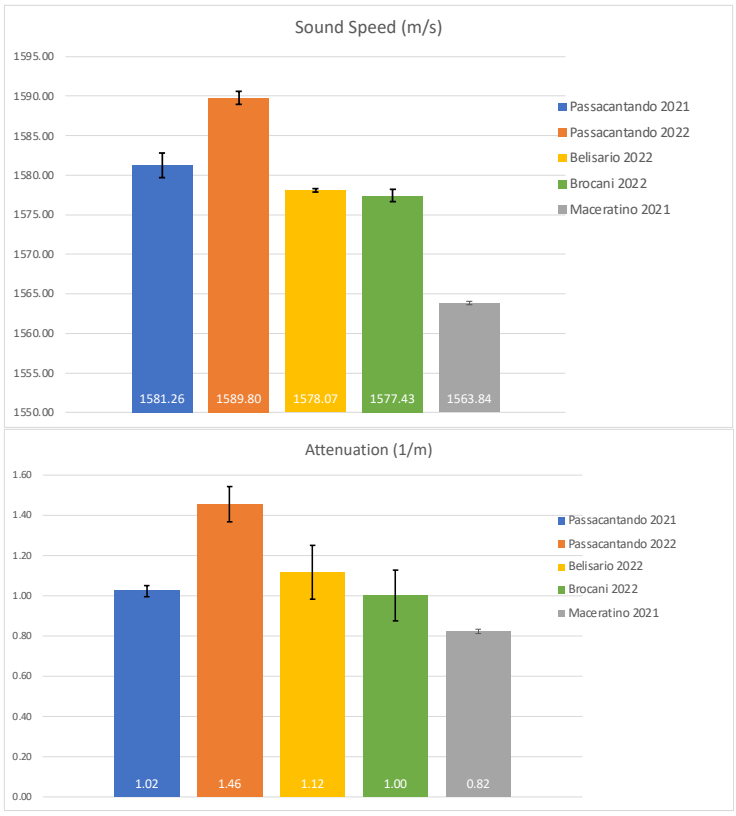

Figure 16 HR-US measurements for all the wines, represented as Sound Speed and Attenuation

The results of the other samples (Brocani, Belisario) did not show any particular differences in the measured parameters, confirming also in this case what it was previously observed for the viscosity values. The only value that differs from the others

is the lower Sound Speed of Maceratino, which is probably due to the higher body of the wine.

Table 2 shows the summary of the collected data, namely the average values obtained for each wine, measured in triplicate.

Table 4 Summary of the wines characterization in terms of Viscosity, Sound Speed and Attenuation for the wines included in the BIOCERTO project.

Wine	Year of production	Viscosity (Pa s)	Sound Speed (m/s)	Attenuation (1/m)
Passacantando	2021	0.0014	1582.26	1.57
	2022	0.0029	1589.80	1.46
Brocani	2019	0.0016	1586.10	1.60
	2022	0.0014	1577.43	1.00
Belisario	2021	0.0018	1586.10	1.60
	2022	0.0016	1577.43	1.00
Maceratino	2019	0.0013	1563.84	0.82

5. Conclusions

The rheological and ultrasound characterization of locally produced wine was carried out to create a fingerprint of the products and, once integrated with the Blockchain technology and the isotopic analysis data, will be able to serve as database to improve food safety and quality assurance. The rheological behaviour proved to be influenced by the year of production and the body of the wine. In particular, the first parameter affected in a significant way the rheological behaviour of the final product. While the DT 1200 was not able to characterize the samples, the analyses carried out with the HR-US confirmed the data obtained by the rheological tests and showed little differences in the same samples.

References

[1] Neto FS, de Castilhos MB, Telis VR, Telis-Romero J. Effect of ethanol, dry extract and reducing sugars on density and viscosity of Brazilian red wines. J Sci Food Agric. 2015 May;95(7):1421-7. doi: 10.1002/jsfa.6835. Epub 2014 Aug 12. PMID: 25046846.

[2] Bonacucina, Giulia et al. "Acoustic spectroscopy: A powerful analytical method for the pharmaceutical field?" International journal of pharmaceutics 503 1-2 (2016): 174-95. https://doi.org/10.1016/j.ijpharm.2016.03.009

6. Published Review

"An overview on natural polymers as reinforcing agents for 3D-Printing"

Beatrice Sabbatini [1], Alessandra Cambriani [1], Marco Cespi [1], Giovanni Filippo Palmieri [1], Diego Romano Perinelli [1] and Giulia Bonacucina [1].

[1] School of Pharmacy, University of Camerino, Via Gentile III da Varano, 62032 Camerino, Italy.

Published on ChemEngineering (2021) 5, 78

DOI: https://doi.org/10.3390/chemengineering5040078

An overview on natural polymers as reinforcing agents for 3D-printing

Abstract

3D printing, or additive manufacturing, is a group of innovative technologies that are increasingly employed for the production of 3D objects in different fields, including pharmaceutics, engineering, agri-food and medicines. The most processed materials by 3D printing techniques (e.g. fused deposition modelling, FDM; selective laser sintering, SLS; stereolithography; SLA) are polymeric materials since they offer chemical resistance, low cost and easy processability. However, one main drawback of using these materials alone (e.g. polylactic Acid, PLA) in the manufacturing process is related to the poor mechanical and tensile properties of the final product. To overcome these limitations, fillers can be added to the polymeric matrix during the manufacturing to act as reinforcing agents. These includes inorganic or organic materials such as glass, carbon fibers, silicon, ceramic or metals. One emerging approach is the employment of natural polymers (polysaccharides and proteins) as reinforcing agents, which are extracted from plants or obtained from biomasses or agricultural/industrial wastes. The advantages of using these natural materials as fillers for 3D printing are related to their availability together with the possibility of producing printed specimens with a lower environmental impact and a higher biodegradability. Therefore, they represent a "green option" for 3D printing processing, and many studies have been published in the last year to evaluate their ability to improve the mechanical properties of 3D printed objects. The present review provides an overview on the recent literature regarding natural polymers as reinforcing agents for 3D printing.

Keywords

cellulose; lignin; chitosan; wood; keratin; hemp; soybean; coffee waste; flax; bamboo

1. Introduction

3D Printing, or additive manufacturing, is an innovative method to produce a three-dimensional object using different processes and raw materials, such as resins and powder grains, generally building a product layer by layer [1].

The invention of 3D printers in 1986 has marked a turning point in different fields including pharmaceutics [2], engineering [3], agri-food [4] [5] and medicines [6] [7]. The rapid manufacturing times and the easy process with the computer assisted design (CAD) are the key of the 3D-printing increasing success [8]. There are three methods mainly used by a 3D printer to produce the objects: Fused Deposition Modelling (FDM), Selective Laser Sintering (SLS) and Stereolithography (SLA) (Figure 1).

Selective Laser Sintering (SLS) is a production method in which the radiation of a laser heats a powder just above the softening temperature of the material. Then, particles are fused together mechanically and solid is deposited layer-by-layer, thereby producing the object [9].

The Stereolithography (SLA) method consists of the solidification of a liquid resin thanks to the photopolymerization. The manufacturing proceeds by curing layer-by-layer the liquid resins until the three-dimensional object it is obtained [10].

The starting material for FDM is usually a thermoplastic filament that is fed into the printer. The following phase consists of an extrusion process of melted materials that is subsequently layer by layer deposited on a surface up to build a specific 3D object (Figure 1). Among the different 3D printing techniques, FDM is the most common and widespread and its success depends on the availability of materials that can be processed with it. Specifically, these materials are represented by thermoplastic polymers characterized by a glass transition temperature in the range of 50 °C up to around 230 °C. Two other very important features are represented by the rheological melting behavior and the mechanical properties of the selected polymers [11].

Up to date, the most common polymeric materials used are represented by polyolefins (i.e. polyethylene PE and polypropylene PP), acrylonitrile-butadiene-Styrene (ABS), polycarbonate (PC), polysulfone (PSU) and biodegradable materials like polylactic Acid (PLA) [12] [13].

The use of polymers as matrices for 3D printing is strongly recommended because they offer good chemical resistance, low cost and easy processability, but one of their main limitations in the manufacturing process is the low functionality and low mechanical and

tensile properties, namely modulus, strength and impact resistance of the final product [14].

Among the different strategies suggested to overcome these issues, the use of reinforcing materials is one of the most promising. The reinforcement is obtained by mixing the polymeric matrix with fillers, characterized by an extraordinary mechanical performance and an excellent functionality [15]. In this way, composite materials, commonly used to perform 3D printing, are obtained. The different reinforcing agents are usually classified according to their morphology (e.g. fibers, particles, flakes and laminates) or length and dimension (micro- or nanomaterials). In addition, the kind of reinforcement defines the composite characteristics according to the concentration, the shape, the size, the distribution and the orientation of the fillers [14].

The most common fillers used as reinforcement are glass and carbon fibers, silicon, ceramic or metals [15]. However, the use of natural materials as reinforcement agents for 3D printing, including biopolymers, is an emerging approach [16]. The aim of this review is to provide a general overview about natural polymers (polysaccharides and proteins) recently employed for 3D printing processes.

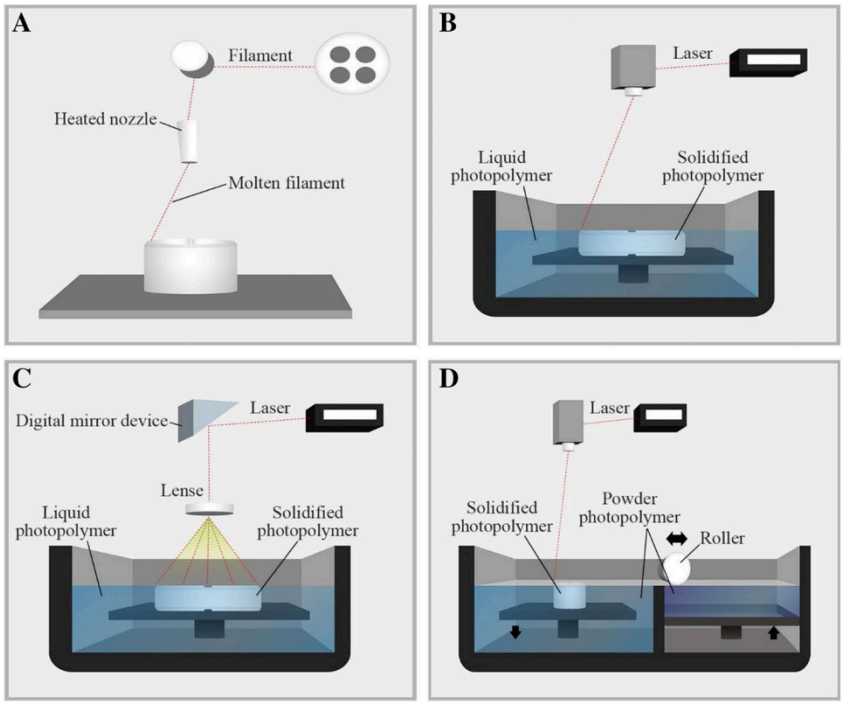

Figure 1 *Graphical schemes of 3D printing techniques.* ***A****. fused deposition method (FDM)* ***B****. stereolithography (SLA)* ***C****. digital light processing (DLP)* ***D****. selective Laser Sintering (SLS). Reproduced from [2].*

2. Natural fillers as reinforcement for 3D printing

The continuous research for a greener economy is leading to the substitution of synthetic or pollutants fillers with natural materials. Indeed, many of these materials could be recovered from industrial wastes, thereby achieving the desirable goals of improving the functionality of the 3D printed specimens and cutting costs at the same time.

The advantages in the use of natural fillers can be sought in their wide availability, in their relatively low cost and biodegradability [17].

The use of these natural polymers includes different kind of chemical species derived from plants, animals and minerals. For instance, many plant-based natural fillers are extracted from agricultural by-products made up by a mixture of different biopolymers like cellulose, lignin, hemicellulose, which are components of parts of the plant (e.g. leaves, seed, fruit, grass) [16].

Among all plants and animal derived biopolymers, the most represented groups are polysaccharides and proteins.

Polysaccharides are macromolecules that are constituted by repeated units of sugars interconnected through glycosidic linkages to form a crystalline and amorphous material. They are abundant in nature and many of them has a complex structure made up by numerous intramolecular and intermolecular hydrogen bonds. The most representative components of this class are cellulose, lignin, chitosan, starch and alginate [18]. Polysaccharides as reinforcement agents were employed as pure fibers (e.g. cellulose, lignin or hemicellulose) or as a mixture extracted from plants (e.g. flax, bamboo, hemp) in which they are the main constituents. Another source of polysaccharide is represented by processes wastes of vegetal matrices such as those from coffee.

Proteins [19] are complex macromolecules built by amino acids joined together via peptide bonds.

They are abundant in nature and have favourable properties as biodegradability and biocompatibility. However, they are mainly employed in 3D process for the construction of soft materials as hydrogels or scaffolds for tissue engineering. The protein used for 3D printing are gelatin, keratin, collagen, silk and soy proteins [20]. The natural polymers (polysaccharides and proteins) discussed in this review for 3D printing applications are summarized in Figure 2.

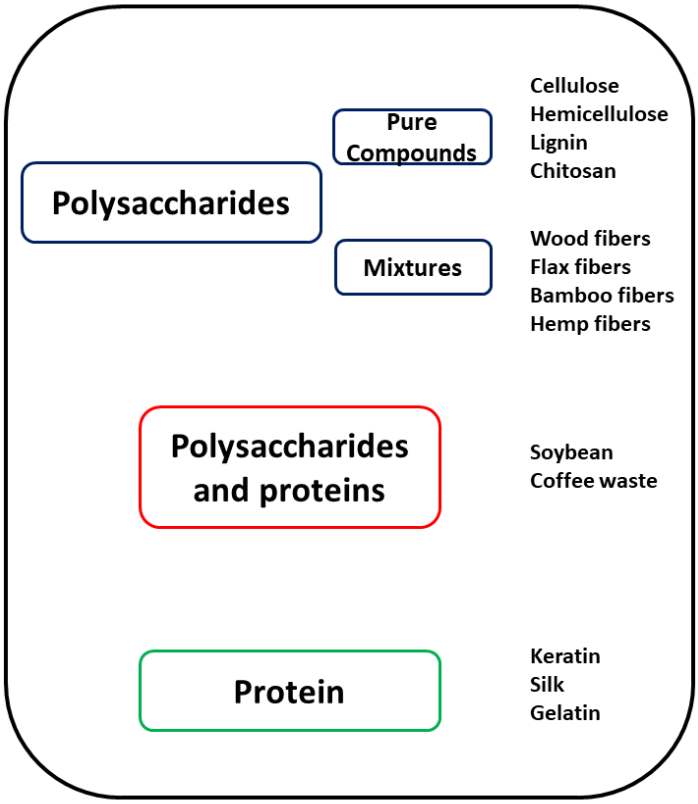

Figure 2 *Scheme reporting the classification of the natural polymers discussed in the review as reinforcing agents for 3D printing.*

3. Natural Materials used as Fillers in 3-D printing

3.1 Cellulose

Cellulose is the most abundant natural biopolymer that can be found mainly in plants but also in animals, fungi, bacteria and algae. From a chemical point of view, cellulose is a natural homopolymer made up by repeated units of glucose bonded with β-1,4 glycosidic bonds. Furthermore, it is a semi-crystalline polymer with a high molecular weight that is assembled thanks to the intra- and intermolecular Van der Waals forces [21] .

The importance of cellulose is well known from at least 150 years, since it has been used in many fields for daily life applications, but only in the last two decades it has been used as biopolymer for biocomposites.

The morphology of the cellulose represents one of the main criteria for classification; in 3D printing different shape of cellulose materials were used as reinforcement for polymers: Cellulose Nanocrystals (CNCs), Cellulose Nanowhiskers (CNWs), Microcrystalline Cellulose (MCC), Cellulose Nanofibers (CNFs).

The first is represented by cellulose nanocrystals (CNCs) [22] [23], that is the final product obtained after the acid hydrolysis of cellulose fibers. CNCs are defect-free fibers with a rod-shape. Different studies support the thesis that the addition of only 0.5% w/w CNCs improves the mechanical properties and the thermal stability of the biocomposites and this is also proved by the analysis conducted by Wang et al. [24].

An element of novelty is brought by the work conducted by Shariatnia et al. [25] where a solution of water and CNCs was sprayed between polymer layers during 3D-printing with the FDM method. This is a real innovation since with the FDM technique problems related to the aggregation of the composite during the extrusion, that causes a clogging of the nozzle are often present due to the water evaporation and the deposition of CNCs. This novel method results in an increased interlayer shear strength (44%) and an improvement in tensile modulus and tensile strength, 20% and 33% respectively, when the CNCs amount in the water dispersion is between 0.5% and 1% w/w.

Another application of cellulose as reinforcement in biocomposites is represented by the use of cellulose nanowhiskers (CNWs). They bring a good enhancement of the dynamic mechanical and thermal properties of the polymers, the tensile strength, the toughness and the elongation at break of the composite [26], despite they also have some drawback: their incorporation in polymer matrix is difficult and not homogeneous and their aggregation makes them less handling (to solve this issue the freeze-drying is performed in order to dry CNWs) [27]. Furthermore, the presence of strong hydrogen bonds and the hydrophilic surface allow to use them only with water-based systems [28]. Many efforts were conducted to chemically modify the structure of CNWs by silylation [29], acetylation [30], use of surfactants [31] and polyethylene glycol (PEG) grafting [32], with the aim to make them compatible with other solvent. However, despite these modifications are possible, the reinforcing ability of the chemically modified CNW is less efficient than that of the untreated CNWs, resulting in lower mechanical properties of the produced composites. About that, the work of Petersson et al. [28] compared the untreated CNWs with the whiskers treated with tert-butanol (B-CNWs) and the wiskers treated with a polyalkoxylated alkylphenol phosphate ester surfactant (Beycostat(E) A B09, also known as BNA), which is the same used in the study by Heux et al. [31]. The structural observation showed that the treatment with the surfactant resulted in a better distribution of the CNWs in the polymer matrix, followed by the B-CNWs composites and the worst distributed in the PLA matrix was the PLA-CNWs. All the samples were stable at a temperature between 25°C and 200°C and they also were able to enhance the storage

modulus of the PLA in the plastic zone, while the S-CNWs also enhanced the storage modulus of the PLA/s elastic zone.

Bondeson and Oksman [26] proposed a different approach because they treated CNWs with Polyvinyl alcohol (PVOH) as a compatibilizer, to improve their dispersion into the PLA. The TEM analysis showed that there was no homogeneous dispersion of the CNWs in the polymer matrix and the whiskers were better dispersed in the PVOH than the PLA phase, resulting in very small improvements in terms of mechanical properties. Thus, CNWs acted as reinforcement for PVOH phase but not to the PLA.

Microcrystalline Cellulose (MCC) has been used as reinforcement in order to produce biocomposites intended for 3D-printing [33]. Murphy and Collins decided to modify the MCC with a titanate coupling agent to obtain a better interaction between MCC and PLA. The addition of 3% w/w titanate modified MCC guaranteed the dispersion in the PLA matrix and the production of the filament. Moreover, the composite characterisation showed that the addition of MCC caused an increase in crystallinity and in the storage modulus. The treatment with the titanate coupling agent reduces the cellulose hydrophilicity, while the biocomposites can absorb a higher quantity of water from the environment.

Besides CNCs, CNWs and MCC, Cellulose Nanofibers (CNFs) are also used with the purpose to reinforce polymer matrices. The major problem with the use of the nanocellulose is the difficulty to disperse them since they tend to aggregate when dried because of their high surface area; a possible solution to solve this drawback is to perform a preliminary treatment of the CNFs. Among the different chemical agents used for that purpose, the 2,2,6,6-Tetramethylpiperidine 1-oxyl (TEMPO)-oxidation of the bacterial cellulose is the method chosen by Li et al. [34]. The use of TEMPO is a highly studied method to improve the dispersion of the CNFs in the polymer matrices, like the PLA, but also to provide a shear-thinning behaviour to the composites and to enhance their printability [35] (Figure 3). Li et al. produced a biodegradable TEMPO-oxidized bacterial cellulose (TOBC)/PLA composite starting froma homogeneous dispersion of TOBC around the microspheres of PLA and by producing the filament for 3D-printing with a single screw extruder [34]. The advantage in the use of bacterial cellulose is that it is a raw material considered as ‘purified cellulose’ because it lacks hemicellulose and lignin, elements that are often responsible of unequal distribution of the cellulose in the polymer matrix. The characterization of the composites showed an improvement in mechanical properties with the addition of TOBC: there was an increasing in tensile strength (+9.2%),

elongation at break (+202%), bending strength (+45%) and elastic modulus (+49%) in the PLA-1.5% w/w TOBC nanocomposites.

The work of Jonoobi et al. studied the reinforcement of the PLA with Cellulose Nanofibers (CNFs) obtained by the Kenaf pulp (*Hibiscus cannabinus L.*) [36]. A good dispersion was obtained with 1% and 3% w/w of CNFs in the PLA matrix and only with 5% w/w of CNFs. From a mechanical point of view, the tensile properties increased with the increased amount of CNFs: tensile modulus and strength in the composites were higher that the pure PLA, 24% and 21%, respectively, with the addition of 5% w/w CNFs. It was also observed that there was a large standard deviation that suggested the unequal dispersion of the CNFs in the matrix.

A recent study conducted by Dong et al. evaluated the influence of the annealing treatment on the flexural properties of the biocomposites of PLA and PLA grafted cellulose nanofibers (PLA-g-CNFs) [37] [38]. A preliminary addition of CNFs to the PLA via ring-opening polymerization resulted in the PLA-g-CNFs. This product is then added to pure PLA in chloroform and then dried in order to proceed through extrusion and then 3D-printing the composite. The analysis carried out showed an increased crystallinity of the composites (between 6% and 12%) and this led to better mechanical properties in the glass state, like the storage modulus and tensile modulus. A subsequent study [37] involves the same PLA/PLA-g-CNFs composites, and the mechanical tests confirmed the improvement in elastic and viscous properties and the reinforcement effect due to the action of PLA-g-CNFs in restricting the mobility of PLA. The annealing treatment was performed above the glass transition temperature (T_g) of PLA. The 3-point bending test at 70 °C showed a better performance in the annealed sample that maintained the original structure layer by layer; on the contrary the unannealed samples were partially damaged. The flexural modulus was 90 times higher than the unannealed samples. The authors concluded that the annealing treatment coupled with the reinforcement given by the PLA-g-CNFs gave to the polymer a good resistance to temperature and an enhancement in flexural and mechanical properties.

An interesting point of view is offered by the study of Tekinalp et al. in which the authors suggested that the role of the CNFs was similar to a microsponge, when added to a polymer like PLA and intended for 3D-printing [39]. Even if there was not a homogeneous dispersion of the CNFs into the PLA matrix, it was still possible to observe the microsponge effect of the nanofibers. Indeed, the CNFs stayed in fiber bundles and the PLA matrix penetrated through the bundles to keep in contact with the cellulose,

creating the effect of a ‘microsponge’. This peculiar distribution contributed to marked improvements in mechanical properties of the composite, in particular the increasing of the tensile strength (+80%), the elastic modulus (+200%), the strain at break (+76%) and the toughness (+220%) compared to the pure PLA resin; all those accomplishments in the manufacturing process suggested that it is possible to use such composite for 3D-printing. In conclusion, the wide availability of the cellulose in nature, the low cost of the raw material and the promising studied carried out on different form of the cellulose (nanofibers, nanowhiskers, microcrystalline cellulose, nanocrystals) configure this material an excellent candidate for the reinforcement of polymer matrices intended for 3D-printing application in biomedicine, food packaging, pharmaceutical and many other fields.

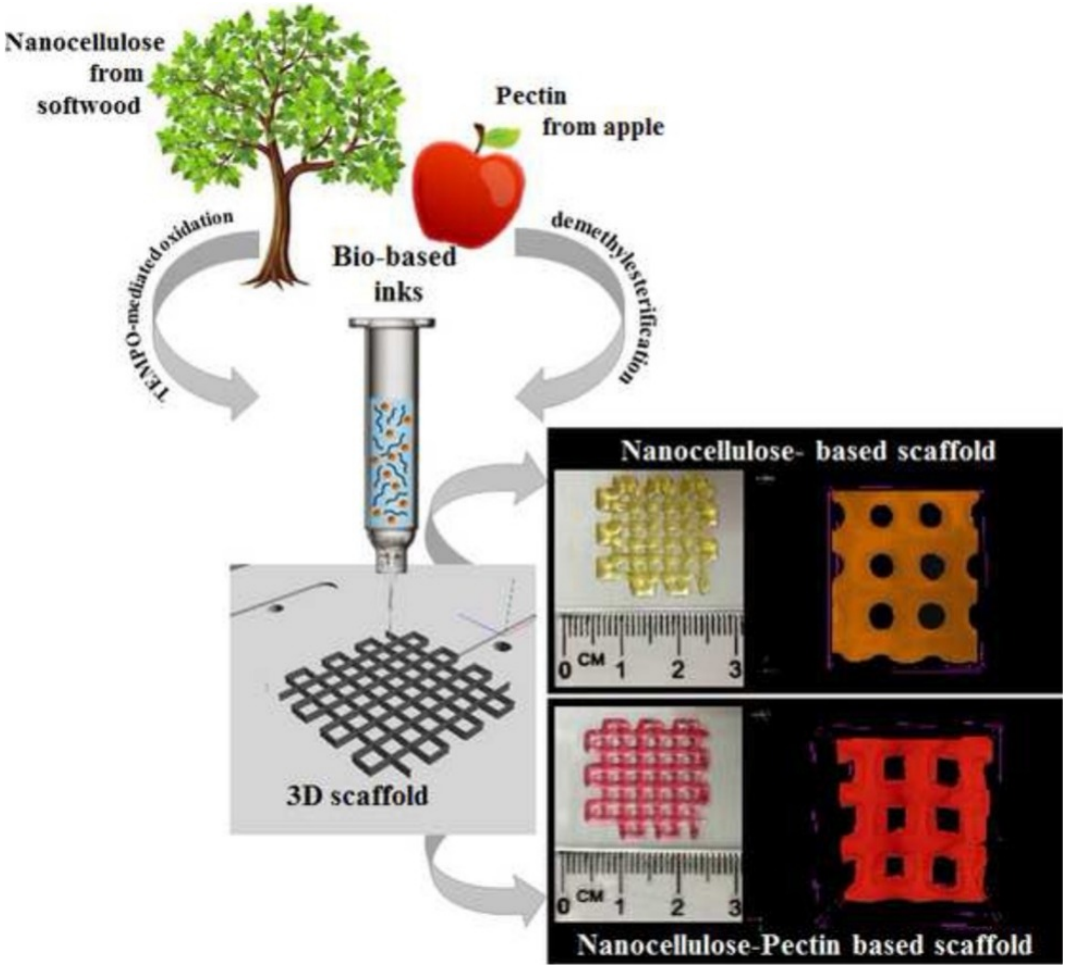

Figure 3 *Pectin reinforced with the carboxylated cellulose nanofibrils for the production of bio-based inks for 3D printing of scaffolds. Reproduced from [35].*

Hemicellulose

Hemicellulose is a type of hetero-polysaccharides found in the plant cell wall together with cellulose. It is formed by liner or branched chains of pentose (e.g. xylose) or hexose sugar (e.g. mannose, galactose), which provide different kind of hemicellulose polymers known as xylans, glucomannans, arabinans, galactans and glucans. Hemicellulose has a lower molecular weight than cellulose since it consists of 50–3000 sugar units (cellulose has instead 7000–15,000 glucose molecules) [40] [41]. Since 2018, the application for 3-D printing of hemicellulose was explored both mixed with cellulose nanofibers or cellulose nanocrystals [42] [43] and alone [44] (Figure 4). However, these polysaccharides has lower properties in terms of mechanical reinforcement in comparison to cellulose, lignin and wood fibers, and they have not employed as filler except in the work of Xu et al. in which the elastic modulus of the composite filament was increased by the addition of 25% w/w of hemicellulose [45].

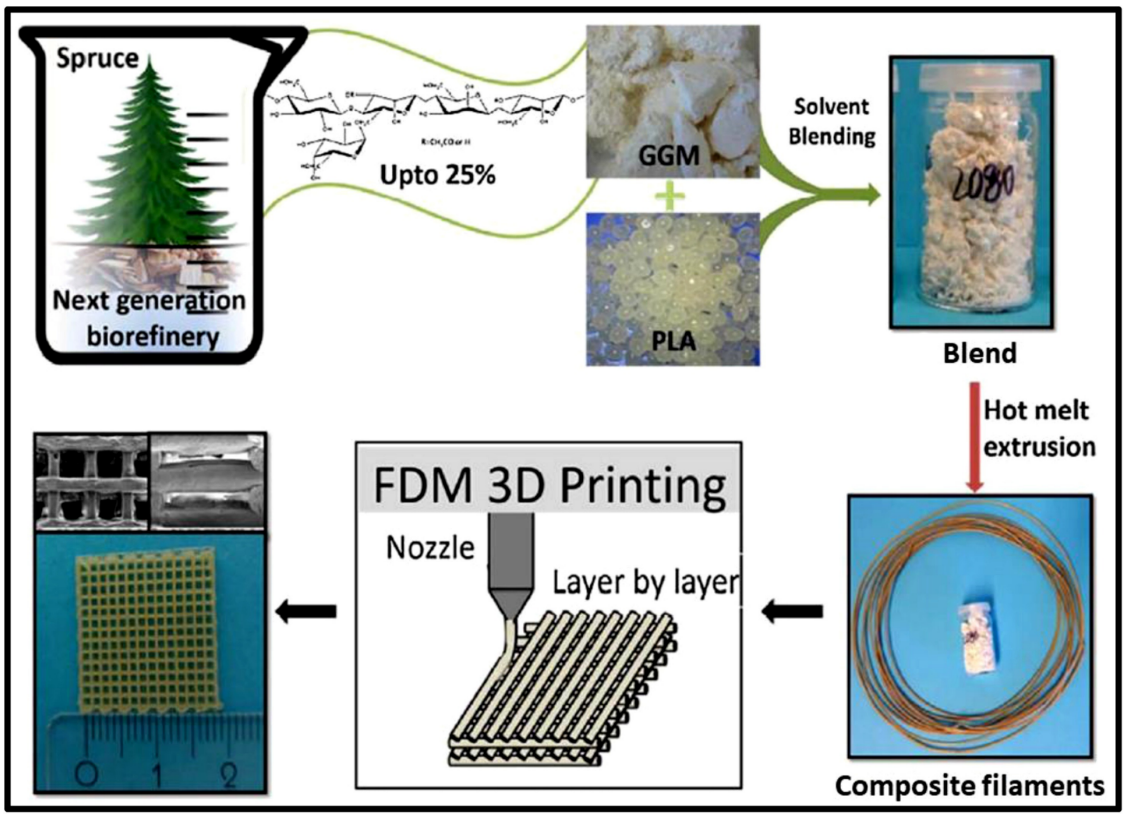

Figure 4 *Preparation of 3D printed scaffolds using fused deposition method (FDM) from galactomannan/PLA composite filaments. Reproduced from [45].*

Lignin

Lignin is the second most abundant biopolymer after cellulose on earth, mainly derived from plants. Chemically, it is a hetero-polymer derived from the cross-linking of three different substituted phenols (lignols): coniferyl, sinapyl, and p-coumaryl alcohols. From wood pulping three types of industrial lignin can be obtained such as kraft lignin, oganosolv lignin and lignosulfonate, which are materials exploited for different applications, including 3D printing [46]. The interest about lignin has been growing in the last years since its availability has been markedly increased as a consequence of the development of more efficient processes for isolation and purification at an industrial scale. Therefore, nowadays lignin can be obtained from different biomasses with a high yield and at a low cost [47]. Thanks to its abundance, biodegradability, high carbon content, aromaticity and low cost, lignin is widely used as a reinforcement agent for manufacturing composites [48]. Moreover, its intrinsic antioxidant, antibacterial and antimutagenic properties, related to the polyphenol structure, can also confer biological properties to the composite [49].

Only recently, lignin has been investigated as an additive for 3D printing, however, its properties and potential use in the production of biocomposites is known so far. Indeed, lignin can be employed without or with modification (e.g. acetylation), despite the best performances in terms of improved material properties have been achieved in its acetylated form [50].

Nguyen, Bowland and Naskar for the first time reported the use of lignin with acrylonitrile-butadiene rubber and acrylonitrile-butadiene-styrene (ABS) polymer for the preparation of materials with an improved 3D printability. Physical and chemical crosslinks can form between lignin and acrylonitrile-butadiene rubber allowing a lignin loading up to 40% w/w with an excellent printability and the obtained 3D printed composites showed mechanical properties comparable to those obtained with a petroleum-based thermoplastics (discontinuous carbon fibers) [51].

The performances of the different types of technical lignin such as Kraft lignin, organosolv lignin,

and lignosulfonate in PLA 3D printed bars using FDM technique were evaluated without the addition of any compatibilizer. This study highlighted the high compatibility of organosolv lignin and lignosulfonate for PLA, resulting in lower mechanical properties of the composites prepared with kraft lignin [52].

In another study, up to 20% w/w of organosolv lignin were incorporated in PLA filaments intended for 3D printing by FDM. Because of the poor mechanical properties of the obtained composite filament, a plasticizer as polyethylene glycol-(PEG) 2000 was added (0.25-5% w/w). The addition of PEG-2000 at a concentration of 2% w/w resulted in an enhancing of both tensile stress and elongation at maximum load by 19% and 35%, respectively for the filament containing 20% w/w of lignin [53].

To achieve a better adhesion to the PLA matrix and improve the mechanical properties of the composites, a chemically modified lignin with maleic anhydride was prepared. The introduction of carboxyl groups on lignin increases the surface polarity and the hydrogen bonding interaction ability with PLA chains. In this way, a suitable filament for FDM 3D printing was obtained with good thermal and mechanical properties [54].

PLA composites containing lignin displaying antibacterial and antioxidant properties and intended for healthcare applications were prepared by FDM technique. The composite filaments were prepared starting from PLA pellets coated with kraft lignin with the aid of castor oil. This procedure allows the production of the filaments using a single screw extruder, differently from other works in which a double screw extruder was necessary. The obtained 3D printed grid showed good antioxidant properties (the concentration of 2,2-diphenyl-1-picrylhydrazyl was reduced of 80% after 5 h,) despite possessing a lower resistance to fracture [55].

Lignin-coated cellulose nanocrystals (L-CNC) were instead employed as mechanical reinforcement for methacrylate resin to obtain nanocomposites through SLA technique. Specifically, mechanical properties in terms of tensile strength and modulus have enhanced with the addition of 0.1% and 0.5% of L-CNC [56].

3.3 Chitosan

Chitosan, the most abundant natural biopolymer after cellulose and lignin , is a natural polysaccharide obtained by deacetylation of chitin and it consists of glucosamine and N-acetyl-glucosamine monomers linked through β(1-4) glycosidic bonds. It is nontoxic, biodegradable and biocompatible and it has important activities such as antimicrobial, anti-inflammatory and antioxidant effect. Chitosan has a polymeric structure that improves adhesion, proliferation and differentiation of cells. His production is low-cost and eco-friendly and it is used for applications in biomedical, food, cosmetics and pharmaceutical field [57].

The main application of chitosan biopolymer in 3-D printing is the development of bio-ink suitable for the production of hydrogels or scaffolds, mimicking the extracellular matrix (ECM) of different tissues (bone, cartilage, vascular, skin and neuronal) and supporting cells attachment, proliferation and differentiation for tissue repairing [58]. Despite the favourable biological properties, chitosan has some limitations in terms of mechanical properties, degradation rates and 3D-printability [59].

Three methods have reported for chitosan 3D printing such as extrusion-based, fused-deposition and solvent dispensing methodology [60] [61]. For all the techniques, the 3-D printability of chitosan is affected by viscosity that, in most of the cases, requires an adjustment by adding other materials like PEG, pectin and gelatine to assure an easy extrusion, to avoid clogging of the device and retain the shape of the construct before drying.

Pectin has been widely employed since it can form polyelectrolytes by physically crosslinking its carboxylic groups with the amino groups of chitosan at pH 3-6 and, as a function of its concentration, can provide 3-D printable bio-inks with a suitable viscosity (between 400-4000 Pa· s)

Indeed, in some cases, the achievement of a satisfactory printability is not the only factor limiting the use of chitosan for 3-D printing since the obtained specimen have a low stiffness and compressive

Strength. Therefore, shrinkage and collapse of the material can occur after printing. To overcome this issue and assure shape fidelity after printing, other reinforcing materials are used to improve the characteristics of composites based on chitosan. One example is offered by the use of rigid particles as filler material, to improve mechanical properties. For this purpose, milled silk particles (SP) were investigated to prepared mixed 3-D printable composites with chitosan. The addition of SP ameliorated not only the

mechanical strength of the hydrogel but also support cell adhesion and growth by provide a rough surface. Overall, the presence of SP gives a greater stability to the bioink. [58] [62].

About the fabrication of PLA/chitosan scaffold, chitosan is at first dried in vacuum and then mixed with PLA. The mixtures are extruded using a twin-screw extruder, so it is possible to produce composite polymeric filaments. The mechanical analysis shows a decrease in tensile strength due to an increase of chitosan content because a higher amount causes discontinuities in polymeric chains. Instead, higher infill density leads to increased tensile strength. The further addition of more chitosan increases the density of the composite material so that the compressive strength increased. The study of these parameters make possible to fabricate chitosan reinforced PLA scaffold using fused filament fabrication (FFF) 3D printed technology [63].

3.4 Wood fibers/ flour

Several experimental studies were conducted using unpurified materials from plant wood as reinforcement, generally referred as wood fibers or wood flour. They can be obtained from the raw materials through grinding processes able to reduce the size in the micrometric range without further purification.

Wood flour is lightweight, renewable, and widely available. The effect of the wood on composite properties depends on several factors: wood particle properties, size distribution and compatibility with the matrix. A particle size of ≤ 100 μm is necessary to avoid debonding of wood particles from the polymeric matrix and the possible fracture of the composites.

Recently, poplar wood flour (1–10 % w/w) was employed to reinforce composites based on metacrylated prepared using SLA 3D printing. This is the first work reporting the ability of wood flour at a low concentration to improve the mechanical properties of plastic prepared by SLA technique [64].

At a low concentration (up to 10% w/w), wood flour is also a good reinforcing agent for FDM 3D printing [65].

Specifically, wood flour has been claimed to be an environmental-friendly and a low cost filler, even compared to the other natural material available, therefore reducing the production costs of 3D printed composites [66] [67].

As for pure cellulose, one of the main limitations in using wood flours as filler is its scarce adhesion to the polymeric matrix, which negatively affects its ability to impart improved mechanical properties. To overcome this issue, one possibility is to functionalise the polymer to increase the interfacial adhesion with wood flour [68].

In a study, PLA was modified using a silane coupling agent and then teak wood flour was added at two different particles sizes in the micrometric range to produce by FMD composite filaments with improved mechanical strength [69].

Other reactive coupling agents as N, N-(1,3-phenylene dimaleimide) (BMI) and 1,1-(methylenedi-4,1-phenylene)bismaleimide (DBMI) can be also employed to ameliorate the interfacial adhesion between PLA and wood flour for the preparation of 3D printed composites. The mechanical properties of the composites were improved in terms of stiffness, strength and deformability. DBMI resulted to be a more efficient coupling agent than BMI because of the flexibility of the molecule [70].

The presence of wood flour worsens the mechanical properties of the composites prepared from unmodified PLA. Therefore, it is necessary to add a compatibilizer or modifier. For

the FDM process, generally thermoplastic polymers are used as compatibilizers and toughening agents such as polyurethane (TPU), polycaprolactone (PCL) and poly (ethylene-co-octene) (POE). Among these, TPU is the most commonly employed as toughening agents for PLA-based composites. TPU has a great influence on the performances of the composites, in fact, it increases the impact strength, the tensile and flexural strength, and the viscosity, favourable for the extrusion process [67]. Moreover, TPU can be also used as polymeric matrix in the presence of wood flour to fabricate composites with good tensile properties without any further surface treatment or addition of a compatibilizer [66].

3.6 Flax/Bamboo

Flax and bamboo are largely known natural fibers used as a cheap alternative to wood. They have been used both alone or in combination to prepare new biodegradable composites because such fibers are abundant in nature and they have mechanical properties similar to that of the wood, without needing many years to grow and be ready for the use [71].

Among the different natural fibers, flax and bamboo are the most used because of their good properties; bamboo is characterized by a low density, good mechanical properties, abundance in nature (particularly in some areas of the world like Asia) and low cost (Figure 5) [72].

The flax fiber (*Linum usitassisimum L.*) is chosen because of its tensile properties that are among the best in the natural fiber variety [73], and its ease of availability. A flax fiber stem is divided in two different layers: the inner layer contains lignin and pectin, and the secondary layer is made up of cellulose microfibrils intercalated by pectin and hemicellulose [74].

Numerous studies were performed in order to enhance the binding between the polymer and the reinforcement fibers, most of which involved the preliminary treatment with alkali, but other treatments were also performed to obtain a better polymer-fiber adhesion. As such, Qian and Sheng [75] carried out a study in which the bamboo cellulose nanowhiskers (BCNW) was treated with a coupling agent, (3-mercaptopropyl)trimethoxysilane (A-189), at five different concentrations. The SEM observation of the silane-treated BCNW indicated that the proper amount of coupling agent is 4% w/w because a minor quantity did not cover all the surface area and a higher quantity led to a self-polycondensation of the coupling agent itself. This quantity also led to a better adhesion between BCNW and PLA and this is demonstrated by the FT-IR analysis. Tensile strength and tensile modulus of the BCNW-PLA composites were lower when the fibers received the preliminary treatment with the coupling agent and reached the best performance with 4 % w/w of A-189. Another relevant parameter is the elongation at break, which represent the capacity of the natural fibers to resist without breaking to a change of shape [76]. Despite generally the addition of a natural fiber to a thermoplastic material causes the reduction of the elongation at break, Qian and Sheng found that the addition of the silane treated BNCW to the PLA led to a huge increase, from 12.35% of the untreated fibers to 250.8% of the treated fibers with 4% of coupling agents. Furthermore, the SEM images showed the typical brittle fracture of the pure PLA,

demonstrating its high tensile strength. The addition of BCNW to the PLA without preliminary treatment increased the toughness of the composites but the best performance was offered by the addition of the silane treated BCNW to the PLA.

Numerous studies involved the only use of Flax fiber as reinforcement for biocomposites. Despite most of these studies in the literature focused on discontinuous fibers (i.d. fibers with short aspect ratios), Le Duigou et al. conducted a study with the novel use of continuous flax fibers/PLA for the manufacturing of biocomposites for 3D-printing [73]. The preparation of the continuous fibers was made by selecting flax fiber yarns and coating them with a PLA polymer matrix. The observation of the biocomposites revealed irregularities on the surface and a larger diameter of the filament respect to the commercial ones. It was also observed an irregular dispersion of the flax fibers in the matrix and a low adhesion between polymer and fibers, represented by the presence of numerous pull-outs of flax fibers. About the tensile mechanical properties, an increasing of stiffness and strength of the flax/PLA composites respect to the pure PLA was observed, probably due to the higher content of the fibers (> 30% w/w), Mechanical properties were also comparable to those of the synthetic fibers (e.g., carbon or glass fibers).

Another study focuses on the feasibility of continuous flax fibers-reinforced plastic (CFFRP) for 3D-printing [77]. The filament was produced as follows: firstly, the pure PLA filament was heated and extruded through a single screw extruder, then the flax fiber was added, and the final composite filament was collected into rolls. The tensile tests did not show a reinforcing effect like that of the synthetic carbon fibers, but there are numerous advantages in the use of the CFFRP because it is biodegradable, environment-friendly and it has low costs. For all these reasons, the use of CFFRP gives a better performance respect to the pure PLA but more investigations shall be carried out to improve its use as a substitute for synthetic fibers.

Badouard et al. [78] published a promising work concerning the production of flax biocomposites with three different biodegradable polymer matrices: Poly-(L-lactide) (PLLA), Poly-(butyl-adipate-terephthalate) (PBAT) and Poly-(butylene-succinate) (PBS). The addition of flax fibers caused an increase in Young's modulus, independently from the polymeric matric used. It was also studied the influence of the fiber content (maximum concentration of 30% for PBAT composites) and the use of flax shives, which have a shorter length than fibers, have been evaluated since they can have some

advantages in terms of better distribution in the polymer matrix during the extrusion of the filament.

The scientific literature concerning natural fibers reinforcement mostly refers to the Polylactic acid (PLA) or the polyolefins plastics, but there are also some studies involving the use of flax fibers to reinforce plastics like Nylon 6 (also called PA6 or Polyamide 6) and Polybutylene terephthalate (PBT) [79]. The reinforcement of this kind of polymers represents a challenge because PA6 and PBT need a higher melting temperature, 230 °C and 250 °C respectively, that can bring to the degradation of hemicellulose and cellulose of the fibers. Flax fibers were chosen because of their thermal stability, in fact, they have lost at 225 °C only 2% of their weight and a loss weight of 4% occurs at 250 °C. For the preparation of composites, the flax fibers were treated with a preliminary alkalinization to prepare the surface for the adhesion to the polymer. The mechanical tensile strength of the obtained filament was 20% higher and the elastic modulus was almost three time higher in the presence of a fiber concentration of 40-50% wt.

The authors concluded that is possible to produce a composite made by mixing plastics and flax fibers by keeping the processing temperature lower than the melting point of the material.

A comparison study was also conducted in which Polylactic acid (PLA) was reinforced with bamboo or flax fibers and two different plasticizers [80].The aim of the work was to understand the influence of length and diameter of the fibers on the composite properties. Two plasticizers were used, cPLA1 and cPLA2, with the aim of reducing the brittleness of the PLA. Four different composites were reinforced with bamboo (B1, B2, B3 and B4) and two composites with flax fibers (F1 and F2). Tensile tests were conducted, and it was found that, among the two plasticizers, the cPLA1 has only 30% of the pure PLA stiffness, while cPLA2 has 19%, suggesting that the first one has to be preferred. Furthermore, the best performance as reinforcement is attributed to the longer bamboo fibers with an increasing of 215% of modulus respect to the short bamboo (only 39%) and the flax fibers. More studies are needed to obtain complete information about the use of Flax and Bamboo fibers as reinforcement, although at the moment they are already used and a great deal of research is being carried out on them.

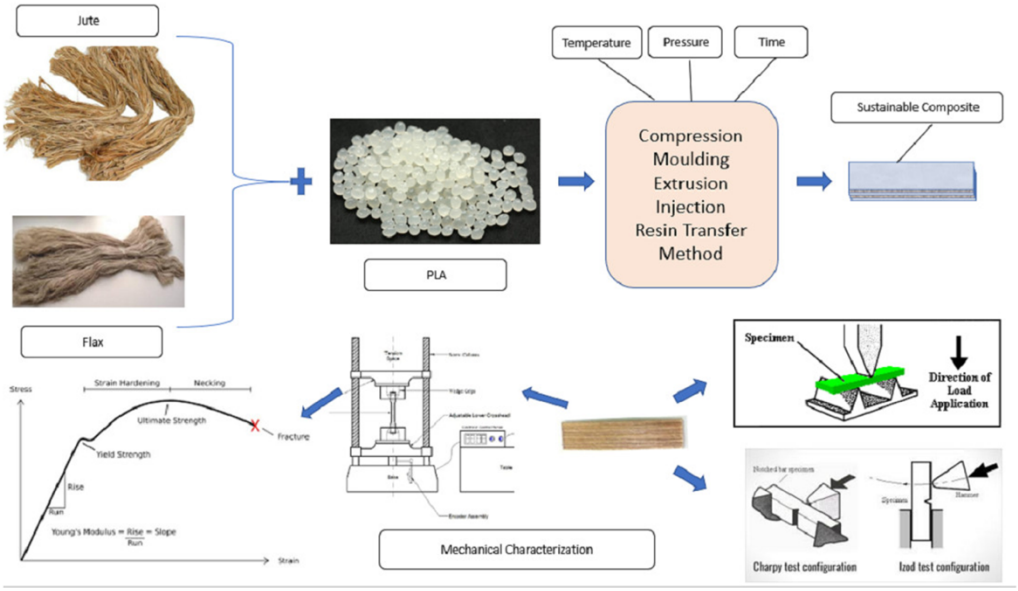

Figure 5 *Schematic illustration of preparation and characterization of sustainable composites produced from PLA and flax/jute fibers. Reproduced from [81].*

3.8 Hemp

Hemp (*Cannabis Sativa L.*) is one of the oldest plants used from the Neolithic age to our days for many applications in different fields such as pharmaceutical, agri-food, cosmetic, textile, paper and building construction but also for its recreational properties [82]. The *Cannabis Sativa L.* plant can easily grow in every climate, and it offers a variety of raw sources (leaves, flowers, stem, plant fiber and fruit - also known as 'achene') that can be used for many applications, from oil and soap to building materials [83]. The growing interest in hemp has led to explore a possible application as reinforcement for the polymeric matrices in 3D-printing in accordance with the need to have "green" and fully biodegradable materials.

In the study conducted by Coppola et al., the powder obtained from hemp shives was employed, at increasing volume percentages (i.e. 1%, 3%, 5% w/w), for the preparation of different blends with polylactic acid (PLA) [84]. The Hemp powder was derived from the waste product of hemp fibers extraction and is mainly composed of cellulose, lignin and pectin. The mixing of hemp powder and PLA is carried out without any previous chemical or physical treatment to improve the adhesion and homogeneity of the final blend and Hemp/PLA composites filaments were obtained by extrusion at 160-180 °C. The DMA analysis on composite filaments shows that the blends with 1% and 3% of hemp have a low storage modulus than the pure PLA, because of the low adhesion between PLA and hemp powder, while the blend containing 5% of hemp powder shows a higher storage modulus. The production of specimens from the different blends with a 3D printer using FDM techniques demonstrates an advantage in the PLA/Hemp composite materials in terms of elastic modulus and tensile strength. Coppola et al. concluded that hemp powder is suitable as reinforcing for polymers in 3D-printing, but further studies are required to understand if some chemical or thermal treatments could result in an enhanced bond between PLA and hemp powder.

In a subsequent study, the possibility of using preliminary treatments to improve the interaction between hemp fibers with PLA was evaluated. Among all, the most common involves the treatment of hemp with alkali to obtain a better interface between fibers and polymer, and to remove, at the same time, lignin, hemicellulose, waxes and oils. Sometimes, this process is not sufficient despite alkali treatment helps in exposing the hydroxyl groups of cellulose in the fibers. Mazzanti et al. carried out a study using a percentage of hemp fiber of 3% and 6% w/w in PLA. The observation with the SEM microscopy shows that the fiber-polymer interface is only slightly affected by the alkali

treatment Anyway, a larger increase of stiffness and strength that results in a lower ductility of the composites is achieved by adding alkali treated hemp fibers with the respect to the untreated ones. The author's conclusion is that the major difference made by the alkali treatment involves the fibers morphology and the better mechanical performances are related to the reduction of the amount of fiber bundles in the composite and the consequent more distributed isolated elementary fibers [85]. Another application in the 3D-printing field involves the use of Hemp Hurd (HH) which is the inner core of the plant stem, containing cellulose, hemicellulose and lignin. Xiao et al. prepared HH/PLA biocomposites to evaluate the Hemp use as filler for FDM 3D-printing. In this case, the blend was prepared by mixing via melt-compounding the PLA with poly (butylene adipate-co-terephthalate (PBAT) as toughening agent and ethylene-methyl acrylate-glycidyl methacrylate terpolymer EGMA as interfacial compatibilizer. Four different blends with increasing percentages of HH (10-40 % w/w) were prepared. The addition of hemp did not affect the thermal behaviour of the biocomposites, but it increased their crystallinity. Despite a slight decrease in tensile and flexural strength occurs by increasing HH concentration related to the high porosity and low interfacial bonding between PLA and HH. Anyway FDM printed specimens shows a greater dimensional accuracy by increasing HH loading [86].

Not only PLA but also silicone was reinforced with Hemp fibers. Among the different treatments proposed in the literature, Koushki et al. decided to compare the untreated hemp fibers with NaOH treated fibers and NaOH-Silane treated fibers. All the tests confirmed that the treatment improved the adhesion between fibers and polymer since treated fibers have a more availability of functional groups that can easily bond with the polymer. Both the tensile strength and the modulus increased of 27% and 54%, respectively, compared to the values of untreated fibers. with a 15% w/w loading of hemp, assuring a good printability by direct ink writing (DIW) [87]. The treatment with coupling agents like maleic anhydride grafted polypropylene (MAPP) and maleic anhydride grafted Poly(ethylene octane) (MAPOE) leads to a better resistance to temperature and also to an improvement in interfacial bonding. The higher content of short hemp fibers improved the higher mechanical properties (e.g., storage modulus) [88]. In conclusion, the use of hemp fibers can be helpful for the production of more convenient 3D-printed specimens, despite as for the other natural fiber more experimental studies are necessary [89].

3.4 Soybean

Soybean (*Glycine max*) is a crop plant original from China, but now widely spread and cultivated in different areas of the world [90]. Soybean represents an important source of seed protein, oil and hull fibers and its importance from a food and technological point of view has increased over time, also thanks to numerous studies that demonstrated its real value. The soybean seed contains 40% of proteins and 20% of oil, both used in different fields, such as food, industry and technology [91].

The increasing attention to the green economy and the reuse of waste materials led the scientific community to carry out numerous researches to give a second life to industrial production waste, as in the case of oils and fibers derived from soybean. Indeed, numerous works were recently carried out to study the feasibility of exploiting epoxidized soybean oil (ESO) as a reactive compatibilizer [92] or plasticizing agent for PLA-based materials intended for 3D printing [93]. Moreover, ESO can be also employed for the preparation of temperature or UV-curable resins for SLA 3-D printing or digital light processing (DLP) [94]. cui et al developed a hybrid resin based on ESO and acrylates for SLA 3D printing. After printing, the thermal curing at 100 °C promoted the formation of interpenetrating networks, leading in the improvement of the mechanical strength of the printed object without affecting its flexural properties and the surface finishing [95].

Voet and coworkers prepared UV-curable resins based on meta-acrylate oligomers functionalized with ESO. Specifically, photoresins were generated when 80% of the photosensitive oligomers were mixed with biobased diluents and a photoinitiator. The authors demonstrated the applicability of their resin in SLA 3D printing and the maintaining of suitable mechanical properties of the 3D printed objects in comparison of using a fossil-based commercial resin, with the advantage of a bio-based product, thereby reducing the environmental impact [96].

Soybean Hull Fibers (SHF) are instead largely investigated as reinforcement agents for thermoplastic polymers mainly intended for FDM 3-D printing. Balla et al. conducted a study to understand the feasibility of the soybean hull fiber as reinforcement for a thermoplastic co-polyester (TPC) to manufacture composites intended for 3D-printing [97]. A preliminary study was carried out to prepare and characterise different composites mixed with chemically treated soybean hull fibers (CT-SHF) and untreated fibers (UT-SHF) [98]. UT-SHF were crushed to reduce their size and then they were added to the TPC, on the contrary, CT-SHF have been subjected to single or double acid chemical treatment, then washed, dried, reduced to fine powder and at the end added to the TPC.

The SEM observation revealed that the treated hull fibers were more porous and had a smaller size after the acid treatment, probably due to the removal of superficial impurities, waxes and hemicellulose, but no morphological differences were found between the fibers treated with single or double acid hydrolysis. The soybean hull fibers were well distributed in the TPC matrix and the mechanical analysis showed that the tensile modulus increased up to 90% with the double chemical treatment, but there was no significant improvement in strength. The addition of CT-SHF also exhibited a toughness 29% higher than the UT-SHF and the analysis of the interface adhesion confirmed that the chemical treatment allows an improved bonding between TPC and soybean fibers. For all these reasons, this work demonstrates the promising use of soybean hull fibers as reinforcement for the production of TPC composites, for 3D-printing, using Fused Deposition Modelling (FDM) technique [97].

In conclusion, these studies demonstrate that the application of soybean hull fibers as reinforcement for matrices intended for 3D-printing is possible, even if some chemical and physical treatments are necessary to obtain their best performance in terms of mechanical properties and printability. The application of soybean hull fiber as reinforcement is still novel and further studies are needed to improve their use and avoid some common problems with FDM 3D-printing process, like nozzle clogging, agglomeration of fibers (due to the non-homogeneous distribution in the composite) and variation of viscosity after the addition of soybean hull fibers.

Coffee waste

Coffee is one of the most important food commodities in the world. The coffee industry generates a large amount of residues, among which the most used are spent coffee grounds (SCG) and coffee silver skin (CS). Particularly, SCG is the residual material obtained during the treatment of coffee powder with hot water or steam for the instant coffee preparation. SCG consists of carbohydrates, proteins, mineral and almost 30% of cellulose fibers [99]. CS, instead, is a thin tegument of coffee that is removed during the roasting, representing the main by-product. It is mainly composed of dietary fibers and other polysaccharides or sugars [100]. Thanks to their abundance, biodegradability and almost zero cost, there is an increasing interest in the used of SCG and CS as natural fillers in polymer matrices in order to develop a series of economic and functional bio-composites for application in various fields, in particular for 3D-printing [101].

Despite coffee waste has been used in the last years as an effective reinforcement filler in bio-composites prepared with different polymers (polylactic acid-PLA, polyhydroxybutyrate-PHB) [102] [103] [104] [105], very few works were performed on 3D printed materials.

Chang et al prepared a 3D printable PLA filament containing up to 20% w/w of oil-extracted spent coffee (Os-SCG). The obtained 3D printed composites show a 418.7% increase in impact toughness compared to the pure PLA with a potential use for high-impact applications, such as personalized prosthesis [106].

Li et al. prepared 3D printed specimens from composited formed by PLA and decolorized SCG. When the content of decolorized SCG was up to 10% w/w, the specimens maintained a tensile and flexural strength comparable to those of pure PLA. On the other side, the melt flow properties of the composite filament were better than pure PLA. The decolorized SCG can be further pigmented for the production of a series of coloured 3D printed specimens [107].

Actually, there is a scarcity of information about the effective use of spent coffee ground for 3D printing However, recent studies have claimed that it is an effective natural filler in polymeric bio-composites produced with other techniques (e.g. twin screw extruder), since it improves the mechanical properties, while being biodegradable and at a low cost. The interaction with other additives (e.g. compatibilizers, coupling agents) in different polymeric matrices should be deepened in further studies in order to develop better bio-composites for different application [108] [109] [110].

3.2 Keratin

Keratin is a fibrous protein and one of the most abundant biopolymers. It is obtained from different common natural sources (wool, chicken feathers and horn) and it has numerous and favourable properties including biocompatibility, biodegradability together with mechanical endurance [111].

C. G. Flores-Hernandez et al. used ground rabbit hair [112] and the rachis of chicken feathers [113] to reinforce PLA-based composites. Both ground rabbit hair and rachis were pre-treated with NaOH 0.1M (to improve interaction between fibres and matrix) and extruded with PLA to obtain a filament for the FDM 3D-printing processing. A different mechanical behaviour of the obtained composites was observed. Thermo-mechanical analyses showed a lower storage modulus (E') for composites prepared with pre-treated keratin from rabbit hair than pure PLA. On the contrary, a large increment in E' with the respect to pure PLA (195%) was observed for composites prepared with 1% of keratin from treated ground rachis. The authors explained such a difference by considering that rabbit hair is predominantly composed of α-keratin, while feathers of β-keratin, provides more flexibility to the composites. The presence of α-keratin fibres determines an increase in the movement of polymeric chains, thereby providing more flexibility and resulting in a decrease of E' modulus on the other side, β-keratin promotes rigidity in the prepared composites.

PLA Composites have been produced using not only keratin alone but also with the addition of chitosan. In L. E. Rojas-Martínez *et al.* work, the effect of keratin configuration (mainly α-helix for keratin from hair or β-sheet for keratin from feather) in the presence of chitosan and the morphology and size of the added reinforcement mixture (fiber-type with a size <1 mm and particle-type with a size <0.7 μm) was investigated. The storage modulus of PLA composites with reinforcement of chitosan and keratin as fibers decreases with the respect of that pure PLA, indicating a more plastic behaviour of the materials. On the contrary, an increase in the storage modulus of around 15% with the respect to pure PLA occurred in composites prepared with the particle-type reinforcement, determining an increase in the rigidity of the composite. Particle-type reinforcement improves fibroblast growth and adhesion more than fibres with a moderate swelling ratio of the obtained scaffold both in water and in simulate body fluid (Figure 6) [114].

Keratin is also mixed with lignin in order to form novel copolymer materials intended for additive manufacturing. In W.J. Grigsby, et al. keratin is complexed with lignin at 4:1 ratio, and suitable filaments for FDM 3D printing were produced [115].

Keratin and keratin/polymer combinations were also processed by SLS technique. Keratin composites prepared with polyamide and polyethylene were considered as to be suitable for SLS processing, without improving relevantly the mechanical properties of the composites [116].

All these studies show that keratin can be a versatile reinforcement agent for 3D printing and it can be used in association with polymer or other materials to develop scaffolds, which can be used for several applications, such as 3D printing and tissue engineering.

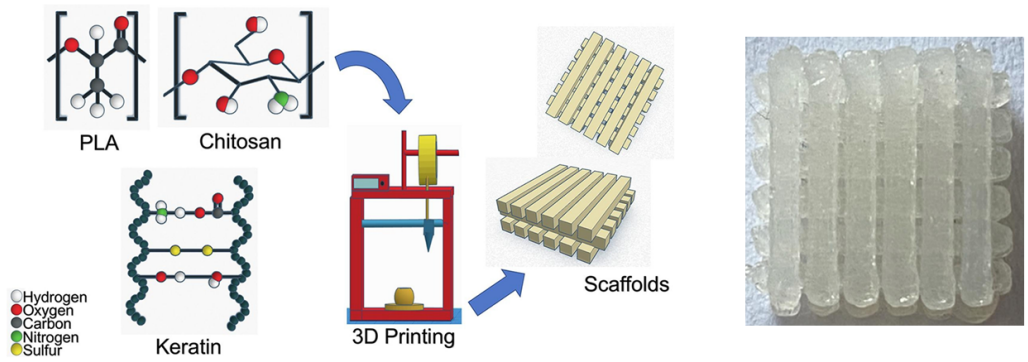

Figure 6 *3D printing of PLA composites scaffolds reinforced with keratin and chitosan. Adapted from [114].*

Silk

Silk is a natural protein fiber, mainly composed of fibroin and produced by different insect larvae. Recently, it has been employed as reinforcement for both synthetic (e.g. polycaprolactone [117]) or natural polymers (e.g. chitosan [118] [119], keratin [120]). In a recent study, silk particles, microfibers and nanofibers were evaluated as reinforcement for a chitosan-based bio-ink for 3D printing. All investigated silk-based reinforcements improved the printability of the bio ink in terms of rheology, printing accuracy and shape fidelity. However, the different geometry (particles, micro- or nano-fibers) markedly affects the mechanical properties of the obtained scaffolds. Indeed, nanofibers were the most effective in increasing the stiffness of the scaffolds, evaluated in terms of compressive strength [119].

Gelatin

Gelatin is a water-soluble functional protein, generally produced from skin or bone collagen by acid or alkali treatment. Gelatin is biodegradable and has high biocompatibility, thereby mimicking the extracellular matrix (ECM) and enabling cell adhesion with a poor antigenicity. For this reason, gelatin is one of the most used biopolymer for 3D printing of scaffolds or hydrogels for tissue engineering [121]. However, gelatin-based printed objects have weak mechanical properties and gelatin is generally used in association with other compounds, such as alginate/carbon nanofibers [122], polyvinyl alcohol (PVA) [123], poly (N-acryloyl 2-glycine) (PACG) [124], poly(lactic-co-glycolic) acid (PLGA) [125] to overcome these limitations. According to the available literature, gelatin is a biopolymer not suitable as reinforcement for polymeric matrix, despite it has been extensively processed for 3D printing.

Conclusions

The employment of natural polymers derived from plants or biomasses as reinforcement agents represents a flourishing field of investigation in 3D printing processes, since it helps cutting the costs of the final printed objects, by making, at the same time, a "greener choice" in terms of producing more biodegradable and lower environmental impact materials. Moreover, the technological approach of improving the thermo-mechanical properties of polymeric printed specimens using natural products promotes the re-use and provides a "second-life" to many agricultural and industrial wastes. Research is still ongoing and more studies are required to define better which are the functionality of each biopolymer and its area of applicability.

References

1. Wang, Q.; Sun, J.; Yao, Q.; Ji, C.; Liu, J.; Zhu, Q. 3D Printing with Cellulose Materials. *Cellulose* **2018**, *25*, 4275–4301, doi:10.1007/s10570-018-1888-y.
2. Park, B.J.; Choi, H.J.; Moon, S.J.; Kim, S.J.; Bajracharya, R.; Min, J.Y.; Han, H.-K. Pharmaceutical Applications of 3D Printing Technology: Current Understanding and Future Perspectives. *J. Pharm. Investig.* **2018**, doi:10.1007/s40005-018-00414-y.
3. Jiménez, M.; Romero, L.; Domínguez, I.A.; Espinosa, M. del M.; Domínguez, M. Additive Manufacturing Technologies: An Overview about 3D Printing Methods and Future Prospects. *Complexity* **2019**, *2019*, 1–30, doi:10.1155/2019/9656938.
4. Liu, Z.; Zhang, M.; Bhandari, B.; Wang, Y. 3D Printing: Printing Precision and Application in Food Sector. *Trends Food Sci. Technol.* **2017**, *69*, 83–94, doi:10.1016/j.tifs.2017.08.018.
5. Godoi, F.C.; Prakash, S.; Bhandari, B.R. 3d Printing Technologies Applied for Food Design: Status and Prospects. *J. Food Eng.* **2016**, *179*, 44–54, doi:10.1016/j.jfoodeng.2016.01.025.
6. Aimar, A.; Palermo, A.; Innocenti, B. The Role of 3D Printing in Medical Applications: A State of the Art. *J. Healthc. Eng.* **2019**, *2019*, 1–10, doi:10.1155/2019/5340616.
7. Li, N.; Qiao, D.; Zhao, S.; Lin, Q.; Zhang, B.; Xie, F. 3D Printing to Innovate Biopolymer Materials for Demanding Applications: A Review. *Mater. Today Chem.* **2021**, *20*, 100459, doi:10.1016/j.mtchem.2021.100459.
8. Ligon, S.C.; Liska, R.; Stampfl, J.; Gurr, M.; Mülhaupt, R. Polymers for 3D Printing and Customized Additive Manufacturing. *Chem. Rev.* **2017**, *117*, 10212–10290, doi:10.1021/acs.chemrev.7b00074.
9. Ligon, S.C.; Liska, R.; Stampfl, J.; Gurr, M.; Mülhaupt, R. Polymers for 3D Printing and Customized Additive Manufacturing. *Chem. Rev.* **2017**, *117*, 10212–10290, doi:10.1021/acs.chemrev.7b00074.
10. Melchels, F.P.W.; Feijen, J.; Grijpma, D.W. A Review on Stereolithography and Its Applications in Biomedical Engineering. *Biomaterials* **2010**, *31*, 6121–6130, doi:10.1016/j.biomaterials.2010.04.050.
11. Melocchi, A.; Uboldi, M.; Maroni, A.; Foppoli, A.; Palugan, L.; Zema, L.; Gazzaniga, A. 3D Printing by Fused Deposition Modeling of Single- and Multi-Compartment Hollow Systems for Oral Delivery – A Review. *Int. J. Pharm.* **2020**, *579*, 119155, doi:10.1016/j.ijpharm.2020.119155.

12. Mazzanti, V.; Malagutti, L.; Mollica, F. FDM 3D Printing of Polymers Containing Natural Fillers: A Review of Their Mechanical Properties. *Polymers* **2019**, *11*, 1094, doi:10.3390/polym11071094.
13. Ghilan, A.; Chiriac, A.P.; Nita, L.E.; Rusu, A.G.; Neamtu, I.; Chiriac, V.M. Trends in 3D Printing Processes for Biomedical Field: Opportunities and Challenges. *J. Polym. Environ.* **2020**, *28*, 1345–1367, doi:10.1007/s10924-020-01722-x.
14. Malhotra, S.K.; Goda, K.; Sreekala, M.S. Part One Introduction to Polymer Composites. *Polym. Compos.* **2012**, *1*, 16.
15. Wang, X.; Jiang, M.; Zhou, Z.; Gou, J.; Hui, D. 3D Printing of Polymer Matrix Composites: A Review and Prospective. *Compos. Part B Eng.* **2017**, *110*, 442–458, doi:10.1016/j.compositesb.2016.11.034.
16. Sudamrao Getme, A.; Patel, B. A Review: Bio-Fiber's as Reinforcement in Composites of Polylactic Acid (PLA). *Mater. Today Proc.* **2020**, *26*, 2116–2122, doi:10.1016/j.matpr.2020.02.457.
17. Deb, D.; Jafferson, J.M. Natural Fibers Reinforced FDM 3D Printing Filaments. *Mater. Today Proc.* **2021**, S2214785321015170, doi:10.1016/j.matpr.2021.02.397.
18. Li, N.; Qiao, D.; Zhao, S.; Lin, Q.; Zhang, B.; Xie, F. 3D Printing to Innovate Biopolymer Materials for Demanding Applications: A Review. *Mater. Today Chem.* **2021**, *20*, 100459, doi:10.1016/j.mtchem.2021.100459.
19. Nehete, J.Y.; Bhambar, R.S.; Narkhede, M.R.; Gawali, S.R. Natural Proteins: Sources, Isolation, Characterization and Applications. *Pharmacogn. Rev.* **2013**, *7*, 107–116, doi:10.4103/0973-7847.120508.
20. Mirzaei, M.; Okoro, O.V.; Nie, L.; Petri, D.F.S.; Shavandi, A. Protein-Based 3D Biofabrication of Biomaterials. *Bioengineering* **2021**, *8*, 48, doi:10.3390/bioengineering8040048.
21. Marchessault, R.H.; Sundararajan, P.R. Cellulose. In *The Polysaccharides*; Elsevier, 1983; pp. 11–95 ISBN 978-0-12-065602-8.
22. Raquez, J.-M.; Habibi, Y.; Murariu, M.; Dubois, P. Polylactide (PLA)-Based Nanocomposites. *Prog. Polym. Sci.* **2013**, *38*, 1504–1542, doi:10.1016/j.progpolymsci.2013.05.014.
23. Habibi, Y.; Lucia, L.A.; Rojas, O.J. Cellulose Nanocrystals: Chemistry, Self-Assembly, and Applications. *Chem. Rev.* **2010**, *110*, 3479–3500, doi:10.1021/cr900339w.
24. Wang, B.; Ding, G.; Chen, K.; Jia, S.; Wei, J.; Wang, Y.; He, R.; Shao, Z. A

Physical and Chemical Double Enhancement Strategy for 3D Printing of Cellulose Reinforced Nanocomposite. *J. Appl. Polym. Sci.* **2020**, *137*, 49164, doi:10.1002/app.49164.

25. Shariatnia, S.; Veldanda, A.; Obeidat, S.; Jarrahbashi, D.; Asadi, A. Atomization of Cellulose Nanocrystals Aqueous Suspensions in Fused Deposition Modeling: A Scalable Technique to Improve the Strength of 3D Printed Polymers. *Compos. Part B Eng.* **2019**, *177*, 107291, doi:10.1016/j.compositesb.2019.107291.

26. Bondeson, D.; Oksman, K. Polylactic Acid/Cellulose Whisker Nanocomposites Modified by Polyvinyl Alcohol. *Compos. Part Appl. Sci. Manuf.* **2007**, *38*, 2486–2492, doi:10.1016/j.compositesa.2007.08.001.

27. Bitinis, N.; Verdejo, R.; Bras, J.; Fortunati, E.; Kenny, J.M.; Torre, L.; López-Manchado, M.A. Poly(Lactic Acid)/Natural Rubber/Cellulose Nanocrystal Bionanocomposites Part I. Processing and Morphology. *Carbohydr. Polym.* **2013**, *96*, 611–620, doi:10.1016/j.carbpol.2013.02.068.

28. Petersson, L.; Kvien, I.; Oksman, K. Structure and Thermal Properties of Poly(Lactic Acid)/Cellulose Whiskers Nanocomposite Materials. *Compos. Sci. Technol.* **2007**, *67*, 2535–2544, doi:10.1016/j.compscitech.2006.12.012.

29. Goussé, C.; Chanzy, H.; Excoffier, G.; Soubeyrand, L.; Fleury, E. Stable Suspensions of Partially Silylated Cellulose Whiskers Dispersed in Organic Solvents. *Polymer* **2002**, *43*, 2645–2651, doi:10.1016/S0032-3861(02)00051-4.

30. Kim, D.-Y.; Nishiyama, Y.; Kuga, S. Surface Acetylation of Bacterial Cellulose. 8.

31. Heux, L.; Chauve, G.; Bonini, C. Nonflocculating and Chiral-Nematic Self-Ordering of Cellulose Microcrystals Suspensions in Nonpolar Solvents. *Langmuir* **2000**, *16*, 8210–8212, doi:10.1021/la9913957.

32. Araki, J.; Wada, M.; Kuga, S. Steric Stabilization of a Cellulose Microcrystal Suspension by Poly(Ethylene Glycol) Grafting. *Langmuir* **2001**, *17*, 21–27, doi:10.1021/la001070m.

33. Murphy, C.A.; Collins, M.N. Microcrystalline Cellulose Reinforced Polylactic Acid Biocomposite Filaments for 3D Printing. *Polym. Compos.* **2018**, *39*, 1311–1320, doi:10.1002/pc.24069.

34. Li, L.; Chen, Y.; Yu, T.; Wang, N.; Wang, C.; Wang, H. Preparation of Polylactic Acid/TEMPO-Oxidized Bacterial Cellulose Nanocomposites for 3D Printing via Pickering Emulsion Approach. *Compos. Commun.* **2019**, *16*, 162–167,

doi:10.1016/j.coco.2019.10.004.

35. Cernencu, A.I.; Lungu, A.; Stancu, I.-C.; Serafim, A.; Heggset, E.; Syverud, K.; Iovu, H. Bioinspired 3D Printable Pectin-Nanocellulose Ink Formulations. *Carbohydr. Polym.* **2019**, *220*, 12–21, doi:10.1016/j.carbpol.2019.05.026.

36. Jonoobi, M.; Harun, J.; Mathew, A.P.; Oksman, K. Mechanical Properties of Cellulose Nanofiber (CNF) Reinforced Polylactic Acid (PLA) Prepared by Twin Screw Extrusion. *Compos. Sci. Technol.* **2010**, *70*, 1742–1747, doi:10.1016/j.compscitech.2010.07.005.

37. Dong, J.; Mei, C.; Han, J.; Lee, S.; Wu, Q. 3D Printed Poly(Lactic Acid) Composites with Grafted Cellulose Nanofibers: Effect of Nanofiber and Post-Fabrication Annealing Treatment on Composite Flexural Properties. *Addit. Manuf.* **2019**, *28*, 621–628, doi:10.1016/j.addma.2019.06.004.

38. Dong, J.; Li, M.; Zhou, L.; Lee, S.; Mei, C.; Xu, X.; Wu, Q. The Influence of Grafted Cellulose Nanofibers and Postextrusion Annealing Treatment on Selected Properties of Poly(Lactic Acid) Filaments for 3D Printing. *J. Polym. Sci. Part B Polym. Phys.* **2017**, *55*, 847–855, doi:10.1002/polb.24333.

39. Tekinalp, H.L.; Meng, X.; Lu, Y.; Kunc, V.; Love, L.J.; Peter, W.H.; Ozcan, S. High Modulus Biocomposites via Additive Manufacturing: Cellulose Nanofibril Networks as "Microsponges." *Compos. Part B Eng.* **2019**, *173*, 106817, doi:10.1016/j.compositesb.2019.05.028.

40. Shavandi, A.; Hosseini, S.; Okoro, O.V.; Nie, L.; Eghbali Babadi, F.; Melchels, F. 3D Bioprinting of Lignocellulosic Biomaterials. *Adv. Healthc. Mater.* **2020**, *9*, 2001472, doi:10.1002/adhm.202001472.

41. Yang, J. Cellulose, Hemicellulose, Lignin, and Their Derivatives as Multi-Components of Bio-Based Feedstocks for 3D Printing. 47.

42. Kam, D.; Chasnitsky, M.; Nowogrodski, C.; Braslavsky, I.; Abitbol, T.; Magdassi, S.; Shoseyov, O. Direct Cryo Writing of Aerogels Via 3D Printing of Aligned Cellulose Nanocrystals Inspired by the Plant Cell Wall. *Colloids Interfaces* **2019**, *3*, 46, doi:10.3390/colloids3020046.

43. Xu, W.; Zhang, X.; Yang, P.; Långvik, O.; Wang, X.; Zhang, Y.; Cheng, F.; Österberg, M.; Willför, S.; Xu, C. Surface Engineered Biomimetic Inks Based on UV Cross-Linkable Wood Biopolymers for 3D Printing. *ACS Appl. Mater. Interfaces* **2019**, *11*, 12389–12400, doi:10.1021/acsami.9b03442.

44. Bahçegül, E.G.; Bahçegül, E.; Özkan, N. 3D Printing of Hemicellulosic

Biopolymers Extracted from Lignocellulosic Agricultural Wastes. *ACS Appl. Polym. Mater.* **2020**, *2*, 2622–2632, doi:10.1021/acsapm.0c00256.

45. Xu, W.; Pranovich, A.; Uppstu, P.; Wang, X.; Kronlund, D.; Hemming, J.; Öblom, H.; Moritz, N.; Preis, M.; Sandler, N.; et al. Novel Biorenewable Composite of Wood Polysaccharide and Polylactic Acid for Three Dimensional Printing. *Carbohydr. Polym.* **2018**, *187*, 51–58, doi:10.1016/j.carbpol.2018.01.069.

46. Ebers, L. -S.; Arya, A.; Bowland, C.C.; Glasser, W.G.; Chmely, S.C.; Naskar, A.K.; Laborie, M. -P. 3D Printing of Lignin: Challenges, Opportunities and Roads Onward. *Biopolymers* **2021**, *112*, doi:10.1002/bip.23431.

47. Watkins, D.; Nuruddin, Md.; Hosur, M.; Tcherbi-Narteh, A.; Jeelani, S. Extraction and Characterization of Lignin from Different Biomass Resources. *J. Mater. Res. Technol.* **2015**, *4*, 26–32, doi:10.1016/j.jmrt.2014.10.009.

48. Tanase-Opedal, M.; Espinosa, E.; Rodríguez, A.; Chinga-Carrasco, G. Lignin: A Biopolymer from Forestry Biomass for Biocomposites and 3D Printing. *Materials* **2019**, *12*, 3006, doi:10.3390/ma12183006.

49. Espinoza-Acosta, J.L.; Torres-Chávez, P.I.; Ramírez-Wong, B.; López-Saiz, C.M.; Montaño-Leyva, B. Antioxidant, Antimicrobial, and Antimutagenic Properties of Technical Lignins and Their Applications. 30.

50. Kun, D.; Pukánszky, B. Polymer/Lignin Blends: Interactions, Properties, Applications. *Eur. Polym. J.* **2017**, *93*, 618–641, doi:10.1016/j.eurpolymj.2017.04.035.

51. Nguyen, N.A.; Bowland, C.C.; Naskar, A.K. A General Method to Improve 3D-Printability and Inter-Layer Adhesion in Lignin-Based Composites. *Appl. Mater. Today* **2018**, *12*, 138–152, doi:10.1016/j.apmt.2018.03.009.

52. Mimini, V.; Sykacek, E.; Syed Hashim, S.N.A.; Holzweber, J.; Hettegger, H.; Fackler, K.; Potthast, A.; Mundigler, N.; Rosenau, T. Compatibility of Kraft Lignin, Organosolv Lignin and Lignosulfonate With PLA in 3D Printing. *J. Wood Chem. Technol.* **2019**, *39*, 14–30, doi:10.1080/02773813.2018.1488875.

53. Wasti, S.; Triggs, E.; Farag, R.; Auad, M.; Adhikari, S.; Bajwa, D.; Li, M.; Ragauskas, A.J. Influence of Plasticizers on Thermal and Mechanical Properties of Biocomposite Filaments Made from Lignin and Polylactic Acid for 3D Printing. *Compos. Part B Eng.* **2021**, *205*, 108483, doi:10.1016/j.compositesb.2020.108483.

54. Hong, S.-H.; Park, J.H.; Kim, O.Y.; Hwang, S.-H. Preparation of Chemically Modified Lignin-Reinforced PLA Biocomposites and Their 3D Printing Performance. *Polymers* **2021**, *13*, 667, doi:10.3390/polym13040667.

55. Domínguez-Robles, J.; Martin, N.; Fong, M.; Stewart, S.; Irwin, N.; Rial-Hermida, M.; Donnelly, R.; Larrañeta, E. Antioxidant PLA Composites Containing Lignin for 3D Printing Applications: A Potential Material for Healthcare Applications. *Pharmaceutics* **2019**, *11*, 165, doi:10.3390/pharmaceutics11040165.
56. Feng, X.; Yang, Z.; Chmely, S.; Wang, Q.; Wang, S.; Xie, Y. Lignin-Coated Cellulose Nanocrystal Filled Methacrylate Composites Prepared via 3D Stereolithography Printing: Mechanical Reinforcement and Thermal Stabilization. *Carbohydr. Polym.* **2017**, *169*, 272–281, doi:10.1016/j.carbpol.2017.04.001.
57. Jiménez-Gómez, C.P.; Cecilia, J.A. Chitosan: A Natural Biopolymer with a Wide and Varied Range of Applications. *Molecules* **2020**, *25*, 3981, doi:10.3390/molecules25173981.
58. Zhang, J.; Allardyce, B.J.; Rajkhowa, R.; Zhao, Y.; Dilley, R.J.; Redmond, S.L.; Wang, X.; Liu, X. 3D Printing of Silk Particle-Reinforced Chitosan Hydrogel Structures and Their Properties. *ACS Biomater. Sci. Eng.* **2018**, *4*, 3036–3046, doi:10.1021/acsbiomaterials.8b00804.
59. Wu, Q.; Therriault, D.; Heuzey, M.-C. Processing and Properties of Chitosan Inks for 3D Printing of Hydrogel Microstructures. *ACS Biomater. Sci. Eng.* **2018**, *4*, 2643–2652, doi:10.1021/acsbiomaterials.8b00415.
60. Kalirajan, C.; Dukle, A.; Nathanael, A.J.; Oh, T.-H.; Manivasagam, G. A Critical Review on Polymeric Biomaterials for Biomedical Applications. *Polymers* **2021**, *13*, 3015, doi:10.3390/polym13173015.
61. Pahlevanzadeh, F.; Emadi, R.; Valiani, A.; Kharaziha, M.; Poursamar, S.A.; Bakhsheshi-Rad, H.R.; Ismail, A.F.; RamaKrishna, S.; Berto, F. Three-Dimensional Printing Constructs Based on the Chitosan for Tissue Regeneration: State of the Art, Developing Directions and Prospect Trends. *Materials* **2020**, *13*, 2663, doi:10.3390/ma13112663.
62. Michailidou, G.; Terzopoulou, Z.; Kehagia, A.; Michopoulou, A.; Bikiaris, D.N. Preliminary Evaluation of 3D Printed Chitosan/Pectin Constructs for Biomedical Applications. *Mar. Drugs* **2021**, *19*, 36, doi:10.3390/md19010036.
63. Singh, S.; Singh, G.; Prakash, C.; Ramakrishna, S.; Lamberti, L.; Pruncu, C.I. 3D Printed Biodegradable Composites: An Insight into Mechanical Properties of PLA/Chitosan Scaffold. *Polym. Test.* **2020**, *89*, 106722, doi:10.1016/j.polymertesting.2020.106722.
64. Zhang, S.; Bhagia, S.; Li, M.; Meng, X.; Ragauskas, A.J. Wood-Reinforced

Composites by Stereolithography with the Stress Whitening Behavior. *Mater. Des.* **2021**, *206*, 109773, doi:10.1016/j.matdes.2021.109773.

65. Kariz, M.; Sernek, M.; Obućina, M.; Kuzman, M.K. Effect of Wood Content in FDM Filament on Properties of 3D Printed Parts. *Mater. Today Commun.* **2018**, *14*, 135–140, doi:10.1016/j.mtcomm.2017.12.016.

66. Bi, H.; Ren, Z.; Guo, R.; Xu, M.; Song, Y. Fabrication of Flexible Wood Flour/Thermoplastic Polyurethane Elastomer Composites Using Fused Deposition Molding. *Ind. Crops Prod.* **2018**, *122*, 76–84, doi:10.1016/j.indcrop.2018.05.059.

67. Guo, R.; Ren, Z.; Bi, H.; Song, Y.; Xu, M. Effect of Toughening Agents on the Properties of Poplar Wood Flour/Poly (Lactic Acid) Composites Fabricated with Fused Deposition Modeling. *Eur. Polym. J.* **2018**, *107*, 34–45, doi:10.1016/j.eurpolymj.2018.07.035.

68. Le Duigou, A.; Castro, M.; Bevan, R.; Martin, N. 3D Printing of Wood Fibre Biocomposites: From Mechanical to Actuation Functionality. *Mater. Des.* **2016**, *96*, 106–114, doi:10.1016/j.matdes.2016.02.018.

69. Petchwattana, N.; Channuan, W.; Naknaen, P.; Narupai, B. 3D Printing Filaments Prepared from Modified Poly(Lactic Acid)/Teak Wood Flour Composites: An Investigation on the Particle Size Effects and Silane Coupling Agent Compatibilisation. *J. Phys. Sci.* **2019**, *30*, 169–188, doi:10.21315/jps2019.30.2.10.

70. Faludi, G.; Dora, G.; Renner, K.; Móczó, J.; Pukánszky, B. Improving Interfacial Adhesion in Pla/Wood Biocomposites. *Compos. Sci. Technol.* **2013**, *89*, 77–82, doi:10.1016/j.compscitech.2013.09.009.

71. Chen, X.; Guo, Q.; Mi, Y. Bamboo Fiber-reinforced Polypropylene Composites: A Study of the Mechanical Properties. 9.

72. Pozo Morales, A.; Güemes, A.; Fernandez-Lopez, A.; Carcelen Valero, V.; De La Rosa Llano, S. Bamboo–Polylactic Acid (PLA) Composite Material for Structural Applications. *Materials* **2017**, *10*, 1286, doi:10.3390/ma10111286.

73. Le Duigou, A.; Barbé, A.; Guillou, E.; Castro, M. 3D Printing of Continuous Flax Fibre Reinforced Biocomposites for Structural Applications. *Mater. Des.* **2019**, *180*, 107884, doi:10.1016/j.matdes.2019.107884.

74. Charlet, K.; Jernot, J.P.; Gomina, M.; Bréard, J.; Morvan, C.; Baley, C. Influence of an Agatha Flax Fibre Location in a Stem on Its Mechanical, Chemical and Morphological Properties. *Compos. Sci. Technol.* **2009**, *69*, 1399–1403, doi:10.1016/j.compscitech.2008.09.002.

75. Qian, S.; Sheng, K. PLA Toughened by Bamboo Cellulose Nanowhiskers: Role of Silane Compatibilization on the PLA Bionanocomposite Properties. *Compos. Sci. Technol.* **2017**, *148*, 59–69, doi:10.1016/j.compscitech.2017.05.020.
76. Djafari Petroudy, S.R. Physical and mechanical properties of natural fibers. In *Advanced High Strength Natural Fibre Composites in Construction*; Elsevier, 2017; pp. 59–83 ISBN 978-0-08-100411-1.
77. Zhang, H.; Liu, D.; Huang, T.; Hu, Q.; Lammer, H. Three-Dimensional Printing of Continuous Flax Fiber-Reinforced Thermoplastic Composites by Five-Axis Machine. *Materials* **2020**, *13*, 1678, doi:10.3390/ma13071678.
78. Badouard, C.; Traon, F.; Denoual, C.; Mayer-Laigle, C.; Paës, G.; Bourmaud, A. Exploring Mechanical Properties of Fully Compostable Flax Reinforced Composite Filaments for 3D Printing Applications. *Ind. Crops Prod.* **2019**, *135*, 246–250, doi:10.1016/j.indcrop.2019.04.049.
79. El-Sabbagh, A.; Steuernagel, L.; Ziegmann, G.; Meiners, D.; Toepfer, O. Processing Parameters and Characterisation of Flax Fibre Reinforced Engineering Plastic Composites with Flame Retardant Fillers. *Compos. Part B Eng.* **2014**, *62*, 12–18, doi:10.1016/j.compositesb.2014.02.009.
80. Depuydt, D.; Balthazar, M.; Hendrickx, K.; Six, W.; Ferraris, E.; Desplentere, F.; Ivens, J.; Van Vuure, A.W. Production and Characterization of Bamboo and Flax Fiber Reinforced Polylactic Acid Filaments for Fused Deposition Modeling (FDM). *Polym. Compos.* **2019**, *40*, 1951–1963, doi:10.1002/pc.24971.
81. Sanivada, U.K.; Mármol, G.; Brito, F.P.; Fangueiro, R. PLA Composites Reinforced with Flax and Jute Fibers—A Review of Recent Trends, Processing Parameters and Mechanical Properties. *Polymers* **2020**, *12*, 2373, doi:10.3390/polym12102373.
82. Karche, T.; Singh, M.R. The Application of Hemp (Cannabis Sativa L.) for a Green Economy: A Review. *Turk J Bot* 14.
83. Sorrentino, G. Introduction to Emerging Industrial Applications of Cannabis (Cannabis Sativa L.). *Rendiconti Lincei Sci. Fis. E Nat.* **2021**, *32*, 233–243, doi:10.1007/s12210-021-00979-1.
84. Coppola, B.; Garofalo, E.; Di Maio, L.; Scarfato, P.; Incarnato, L. Investigation on the Use of PLA/Hemp Composites for the Fused Deposition Modelling (FDM) 3D Printing.; Ischia, Italy, 2018; p. 020086.
85. Mazzanti, V.; Pariante, R.; Bonanno, A.; Ruiz de Ballesteros, O.; Mollica, F.;

Filippone, G. Reinforcing Mechanisms of Natural Fibers in Green Composites: Role of Fibers Morphology in a PLA/Hemp Model System. *Compos. Sci. Technol.* **2019**, *180*, 51–59, doi:10.1016/j.compscitech.2019.05.015.

86. Xiao, X.; Chevali, V.S.; Song, P.; He, D.; Wang, H. Polylactide/Hemp Hurd Biocomposites as Sustainable 3D Printing Feedstock. *Compos. Sci. Technol.* **2019**, *184*, 107887, doi:10.1016/j.compscitech.2019.107887.

87. Koushki, P.; Kwok, T.-H.; Hof, L.; Wuthrich, R. Reinforcing Silicone with Hemp Fiber for Additive Manufacturing. *Compos. Sci. Technol.* **2020**, *194*, 108139, doi:10.1016/j.compscitech.2020.108139.

88. Etaati, A.; Pather, S.; Fang, Z.; Wang, H. The Study of Fibre/Matrix Bond Strength in Short Hemp Polypropylene Composites from Dynamic Mechanical Analysis. *Compos. Part B Eng.* **2014**, *62*, 19–28, doi:10.1016/j.compositesb.2014.02.011.

89. Deb, D.; Jafferson, J.M. Natural Fibers Reinforced FDM 3D Printing Filaments. *Mater. Today Proc.* **2021**, *46*, 1308–1318, doi:10.1016/j.matpr.2021.02.397.

90. Walter R. Fehr Soybean. In *Hybridization of Crop Plants*; Walter R. Fehr, Henry H. Hadley, 1980; pp. 589–599.

91. Jegadeesan, S.; Yu, K. Food Grade Soybean Breeding, Current Status and Future Directions. In; 2020.

92. Zhao, L.; Cheng, S.; Liu, S.; Gao, X. Improvement of the Addition Amount and Dispersion of Hydroxyapatite in the Poly(Lactic Acid) Matrix by the Compatibilizer-Epoxidized Soybean Oil. *J. Mater. Res.* **2020**, *35*, 1523–1530, doi:10.1557/jmr.2020.116.

93. Zhu, G.; Zhang, J.; Huang, J.; Yu, X.; Cheng, J.; Shang, Q.; Hu, Y.; Liu, C.; Hu, L.; Zhou, Y. High-Performance 3D Printing UV-Curable Resins Derived from Soybean Oil and Gallic Acid. *Green Chem.* **2021**, *23*, 5911–5923, doi:10.1039/D1GC01934A.

94. Fernández-Francos, X.; Konuray, O.; Ramis, X.; Serra, À.; De la Flor, S. Enhancement of 3D-Printable Materials by Dual-Curing Procedures. *Materials* **2021**, *14*, 107, doi:10.3390/ma14010107.

95. Cui, Y.; Yang, J.; Lei, D.; Su, J. 3D Printing of a Dual-Curing Resin with Cationic Curable Vegetable Oil. *Ind. Eng. Chem. Res.* **2020**, *59*, 11381–11388, doi:10.1021/acs.iecr.0c01507.

96. Guit, J.; Tavares, M.B.L.; Hul, J.; Ye, C.; Loos, K.; Jager, J.; Folkersma, R.; Voet, V.S.D. Photopolymer Resins with Biobased Methacrylates Based on Soybean Oil

for Stereolithography. *ACS Appl. Polym. Mater.* **2020**, *2*, 949–957, doi:10.1021/acsapm.9b01143.

97. Balla, V.K.; Tadimeti, J.G.D.; Kate, K.H.; Satyavolu, J. 3D Printing of Modified Soybean Hull Fiber/Polymer Composites. *Mater. Chem. Phys.* **2020**, *254*, 123452, doi:10.1016/j.matchemphys.2020.123452.

98. Balla, V.K.; Tadimeti, J.G.D.; Sudan, K.; Satyavolu, J.; Kate, K.H. First Report on Fabrication and Characterization of Soybean Hull Fiber: Polymer Composite Filaments for Fused Filament Fabrication. *Prog. Addit. Manuf.* **2021**, *6*, 39–52, doi:10.1007/s40964-020-00138-2.

99. Kovalcik, A.; Obruca, S.; Marova, I. Valorization of Spent Coffee Grounds: A Review. *Food Bioprod. Process.* **2018**, *110*, 104–119, doi:10.1016/j.fbp.2018.05.002.

100. Narita, Y.; Inouye, K. Review on Utilization and Composition of Coffee Silverskin. *Food Res. Int.* **2014**, *61*, 16–22, doi:10.1016/j.foodres.2014.01.023.

101. *Composites for Environmental Engineering- Chapter 10 (Pages: 319-345)*; Ahmed, S., Chaudhry, S.A., Eds.; First edition.; Scrivener Publishing LLC: Hoboken, New Jersey, 2020; ISBN 978-1-119-55535-3.

102. Reis, K.C.; Pereira, L.; Melo, I.C.N.A.; Marconcini, J.M.; Trugilho, P.F.; Tonoli, G.H.D. Particles of Coffee Wastes as Reinforcement in Polyhydroxybutyrate (PHB) Based Composites. *Mater. Res.* **2015**, *18*, 546–552, doi:10.1590/1516-1439.318114.

103. Suaduang, N.; Ross, S.; Ross, G.M.; Pratumshat, S.; Mahasaranon, S. Effect of Spent Coffee Grounds Filler on the Physical and Mechanical Properties of Poly(Lactic Acid) Bio-Composite Films. *Mater. Today Proc.* **2019**, *17*, 2104–2110, doi:10.1016/j.matpr.2019.06.260.

104. Ortiz-Barajas, D.L.; Arévalo-Prada, J.A.; Fenollar, O.; Rueda-Ordóñez, Y.J.; Torres-Giner, S. Torrefaction of Coffee Husk Flour for the Development of Injection-Molded Green Composite Pieces of Polylactide with High Sustainability. *Appl. Sci.* **2020**, *10*, 6468, doi:10.3390/app10186468.

105. Hejna, A.; Barczewski, M.; Kosmela, P.; Mysiukiewicz, O.; Kuzmin, A. Coffee Silverskin as a Multifunctional Waste Filler for High-Density Polyethylene Green Composites. *J. Compos. Sci.* **2021**, *5*, 44, doi:10.3390/jcs5020044.

106. Chang, Y.-C.; Chen, Y.; Ning, J.; Hao, C.; Rock, M.; Amer, M.; Feng, S.; Falahati, M.; Wang, L.-J.; Chen, R.K.; et al. No Such Thing as Trash: A 3D-Printable Polymer Composite Composed of Oil-Extracted Spent Coffee Grounds and Polylactic

Acid with Enhanced Impact Toughness. *ACS Sustain. Chem. Eng.* **2019**, *7*, 15304–15310, doi:10.1021/acssuschemeng.9b02527.
107. Li, S.; Shi, C.; Sun, S.; Chan, H.; Lu, H.; Nilghaz, A.; Tian, J.; Cao, R. From Brown to Colored: Polylactic Acid Composite with Micro/Nano-Structured White Spent Coffee Grounds for Three-Dimensional Printing. *Int. J. Biol. Macromol.* **2021**, *174*, 300–308, doi:10.1016/j.ijbiomac.2021.01.176.
108. Reis, K.C.; Pereira, L.; Melo, I.C.N.A.; Marconcini, J.M.; Trugilho, P.F.; Tonoli, G.H.D. Particles of Coffee Wastes as Reinforcement in Polyhydroxybutyrate (PHB) Based Composites. *Mater. Res.* **2015**, *18*, 546–552, doi:10.1590/1516-1439.318114.
109. Suaduang, N.; Ross, S.; Ross, G.M.; Pratumshat, S.; Mahasaranon, S. Effect of Spent Coffee Grounds Filler on the Physical and Mechanical Properties of Poly(Lactic Acid) Bio-Composite Films. *Mater. Today Proc.* **2019**, *17*, 2104–2110, doi:10.1016/j.matpr.2019.06.260.
110. Hejna, A.; Barczewski, M.; Kosmela, P.; Mysiukiewicz, O.; Kuzmin, A. Coffee Silverskin as a Multifunctional Waste Filler for High-Density Polyethylene Green Composites. *J. Compos. Sci.* **2021**, *5*, 44, doi:10.3390/jcs5020044.
111. Patrucco, A.; Visai, L.; Fassina, L.; Magenes, G.; Tonin, C. Keratin-based matrices from wool fibers and human hair. In *Materials for Biomedical Engineering*; Elsevier, 2019; pp. 375–403 ISBN 978-0-12-816872-1.
112. Flores-Hernandez, C.G.; Velasco-Santos, C.; Rivera-Armenta, J.L.; Gomez-Guzman, O.; Yañez-Limon, J.M.; Olivas-Armendariz, I.; Lopez-Barroso, J.; Martinez-Hernandez, A.L. Additive Manufacturing of Green Composites: Poly (Lactic Acid) Reinforced with Keratin Materials Obtained from Angora Rabbit Hair. *J. Appl. Polym. Sci.* **2021**, *138*, 50321, doi:10.1002/app.50321.
113. Flores-Hernandez, C.G.; Velasco-Santos, C.; Hernandez-Zea, A.L.; Gomez-Guzman, O.; Yañez-Limon, J.M.; Rivera-Armenta, J.L.; Martinez-Hernandez, A.L. Low Concentrations for Significant Improvements in Thermal and Thermomechanical Properties of Poly(Lactic Acid)–Keratin Biocomposites Obtained by Extrusion and 3D Printing. *J. Nat. Fibers* **2020**, 1–14, doi:10.1080/15440478.2020.1788483.
114. Rojas-Martínez, L.E.; Flores-Hernandez, C.G.; López-Marín, L.M.; Martinez-Hernandez, A.L.; Thorat, S.B.; Reyes Vasquez, C.D.; Del Rio-Castillo, A.E.; Velasco-Santos, C. 3D Printing of PLA Composites Scaffolds Reinforced with Keratin and Chitosan: Effect of Geometry and Structure. *Eur. Polym. J.* **2020**, *141*, 110088,

doi:10.1016/j.eurpolymj.2020.110088.
115. Grigsby, W.J.; Scott, S.M.; Plowman-Holmes, M.I.; Middlewood, P.G.; Recabar, K. Combination and Processing Keratin with Lignin as Biocomposite Materials for Additive Manufacturing Technology. *Acta Biomater.* **2020**, *104*, 95–103, doi:10.1016/j.actbio.2019.12.026.
116. Singamneni, S.; Velu, R.; Behera, M.P.; Scott, S.; Brorens, P.; Harland, D.; Gerrard, J. Selective Laser Sintering Responses of Keratin-Based Bio-Polymer Composites. *Mater. Des.* **2019**, *183*, 108087, doi:10.1016/j.matdes.2019.108087.
117. Vyas, C.; Zhang, J.; Øvrebø, Ø.; Huang, B.; Roberts, I.; Setty, M.; Allardyce, B.; Haugen, H.; Rajkhowa, R.; Bartolo, P. 3D Printing of Silk Microparticle Reinforced Polycaprolactone Scaffolds for Tissue Engineering Applications. *Mater. Sci. Eng. C* **2021**, *118*, 111433, doi:10.1016/j.msec.2020.111433.
118. Zhang, J.; Allardyce, B.J.; Rajkhowa, R.; Zhao, Y.; Dilley, R.J.; Redmond, S.L.; Wang, X.; Liu, X. 3D Printing of Silk Particle-Reinforced Chitosan Hydrogel Structures and Their Properties. *ACS Biomater. Sci. Eng.* **2018**, *4*, 3036–3046, doi:10.1021/acsbiomaterials.8b00804.
119. Zhang, J.; Allardyce, B.J.; Rajkhowa, R.; Kalita, S.; Dilley, R.J.; Wang, X.; Liu, X. Silk Particles, Microfibres and Nanofibres: A Comparative Study of Their Functions in 3D Printing Hydrogel Scaffolds. *Mater. Sci. Eng. C* **2019**, *103*, 109784, doi:10.1016/j.msec.2019.109784.
120. Kwak, H.; Shin, S.; Lee, H.; Hyun, J. Formation of a Keratin Layer with Silk Fibroin-Polyethylene Glycol Composite Hydrogel Fabricated by Digital Light Processing 3D Printing. *J. Ind. Eng. Chem.* **2019**, *72*, 232–240, doi:10.1016/j.jiec.2018.12.023.
121. Wang, X.; Ao, Q.; Tian, X.; Fan, J.; Tong, H.; Hou, W.; Bai, S. Gelatin-Based Hydrogels for Organ 3D Bioprinting. *Polymers* **2017**, *9*, 401, doi:10.3390/polym9090401.
122. Serafin, A.; Murphy, C.; Rubio, M.C.; Collins, M.N. Printable Alginate/Gelatin Hydrogel Reinforced with Carbon Nanofibers as Electrically Conductive Scaffolds for Tissue Engineering. *Mater. Sci. Eng. C* **2021**, *122*, 111927, doi:10.1016/j.msec.2021.111927.
123. Kim, H.; Yang, G.H.; Choi, C.; Cho, Y.; Kim, G. Gelatin/PVA Scaffolds Fabricated Using a 3D-Printing Process Employed with a Low-Temperature Plate for Hard Tissue Regeneration: Fabrication and Characterizations. *Int. J. Biol. Macromol.*

2018, *120*, doi:10.1016/j.ijbiomac.2018.07.159.

124. Gao, F.; Xu, Z.; Liang, Q.; Li, H.; Peng, L.; Wu, M.; Zhao, X.; Cui, X.; Ruan, C.; Liu, W. Osteochondral Regeneration with 3D-Printed Biodegradable High-Strength Supramolecular Polymer Reinforced-Gelatin Hydrogel Scaffolds. *Adv. Sci.* **2019**, *6*, 1900867, doi:10.1002/advs.201900867.

125. Ko, Y.-G.; Kwon, O.H. Reinforced Gelatin-Methacrylate Hydrogels Containing Poly(Lactic-Co-Glycolic Acid) Nanofiber Fragments for 3D Bioprinting. *J. Ind. Eng. Chem.* **2020**, *89*, 147–155, doi:10.1016/j.jiec.2020.04.021.